

RIDE MODEL AND SIMULATION OF A BACKHOE-LOADER

A THESIS SUBMITTED TO
THE GRADUATE SCHOOL OF NATURAL AND APPLIED SCIENCES
OF
MIDDLE EAST TECHNICAL UNIVERSITY

BY

DURMUŞ ALİ GÖZTAŞ

IN PARTIAL FULFILLMENT OF THE REQUIREMENTS
FOR
THE DEGREE OF MASTER OF SCIENCE
IN
MECHANICAL ENGINEERING

DECEMBER 2010

Approval of the thesis:

RIDE MODEL AND SIMULATION OF A BACKHOE-LOADER

submitted by **DURMUŞ ALİ GÖZTAŞ** in partial fulfillment of the requirements for the degree of **Master of Science in Mechanical Engineering Department, Middle East Technical University** by,

Prof. Dr. Canan Özgen
Dean, Graduate School of **Natural and Applied Sciences**

Prof. Dr. Suha Oral
Head of Department, **Mechanical Engineering**

Prof. Dr. Mehmet Çalışkan
Supervisor, **Mechanical Engineering Dept., METU**

Prof. Dr. Eres Söylemez
Co-Supervisor, **Mechanical Engineering Dept., METU**

Examining Committee Members:

Prof. Dr. Y. Samim Ünlüsoy
Mechanical Engineering Dept., METU

Prof. Dr. Mehmet Çalışkan
Mechanical Engineering Dept., METU

Prof. Dr. Eres Söylemez
Mechanical Engineering Dept., METU

Asst. Prof. Gökhan Özgen
Mechanical Engineering Dept., METU

Ferhan Fıçıcı, M.Sc.
Team Leader of R&D, Hidromek Inc.

Date:

I hereby declare that all information in this document has been obtained and presented in accordance with academic rules and ethical conduct. I also declare that, as required by these rules and conduct, I have fully cited and referenced all material and results that are not original to this work.

Name, Last name : Durmuş Ali GÖZTAŞ

Signature :

ABSTRACT

RIDE MODEL AND SIMULATION OF A BACKHOE-LOADER

Göztaş, Durmuş Ali

M.S., Department of Mechanical Engineering

Supervisor : Prof. Dr. Mehmet Çalışkan

Co-Supervisor : Prof. Dr. Eres Söylemez

December 2010, 92 pages

The objective of this study is to present a dynamic model of a backhoe-loader including cab dynamics in order to simulate the vibration levels transmitted to the operator. For this purpose, analytical solutions of the cab and the machine are developed by deriving the equations of motion of the system and the state space forms of the solution are implemented in the commercially available simulation software, MATLAB/Simulink. In addition to the analytical solution, a model is developed using the physical modeling toolboxes of MATLAB/SimMechanics. Cab model developed in SimMechanics is extended to simulate whole machine dynamics by inserting machine body and tire parameters. Vibration data is acquired from the machine for experimental validation of the models. Analytical and SimMechanics solution are evaluated by comparing the seat acceleration results for the same inputs. Furthermore, simulation results obtained from the models and the measurement results are found to be in agreement in both time and frequency domain.

Keywords: Backhoe-loader, Ride Dynamics, Dynamic Simulation

ÖZ

KAZICI-YÜKLEYİCİ İŞ MAKİNASININ SÜRÜŞ DİNAMİĞİNİN MODELLENMESİ VE BENZETİMİ

Göztaş, Durmuş Ali

Yüksek Lisans, Makina Mühendisliği Bölümü

Tez Yöneticisi : Prof. Dr. Mehmet Çalışkan

Ortak Tez Yöneticisi : Prof. Dr. Eres Söylemez

Aralık 2010, 92 sayfa

Bu çalışmanın amacı kabin dinamiğini de içeren ve operatöre iletilen titreşim seviyesinin elde edilebileceği dinamik bir kazıcı-yükleyici iş makinası modelini geliştirmektir. Bu sebeple, kabin ve kazıcı-yükleyici için hareket denklemleri yazılarak analitik modeller oluşturulmuş ve oluşturulan modeller uzay durumu formuna getirilerek MATLAB/Simulink benzetim programında çözüm elde edilmiştir. Analitik modele ek olarak, MATLAB/SimMechanics benzetim programının içindeki fiziksel modelleme araçları kullanılarak da bir kabin modeli oluşturulmuştur. SimMechanics kullanılarak elde edilen kabin modeline lastik ve şasi parametreleri eklenerek, kazıcı-yükleyicinin dinamik davranışını yansıtacak bir makina modeli geliştirilmiştir. Elde edilen modellerin deneysel olarak doğrulanması amacıyla makina üzerinden ölçümler alınmıştır. SimMechanics modelinden ve analitik modelden, aynı girdi değerleri için elde edilen koltuk ivme değerleri karşılaştırmalı olarak verilmiştir. Ayrıca, modellerden elde edilen benzetim

sonularının, lm sonuları ile zaman ve frekans ortamında uyum iinde olduėu gsterilmiřtir.

Anahtar kelimeler: Kazıcı-ykleyici, Srř Dinamiėi, Dinamik Benzetim

To My Family

ACKNOWLEDGMENTS

I wish to express my deepest gratitude to my supervisor Prof. Dr. Mehmet ÇALIŞKAN for his guidance, advice, criticism, encouragements and insight throughout the research.

I would like to state my sincere thanks to my co-supervisor Prof. Dr. Eres SÖYLEMEZ for his guidance, motivation, supervision and patience.

I would like to thank my colleagues Ferhan FIÇICI, Cevdet Can UZER, Tarık OLĞAR, Erkal ÖZBAYRAMOĞLU, Boran KILIÇ, Koray Serdar TEKİN and Tuğçe YALÇIN for their suggestions and comments.

I would also like to express my appreciation to Hasan Basri BOZKURT, general manager of Hidromek Inc., for his support.

Finally, I would like to express my thanks to my family for their support and continuous faith in me.

This study is supported by Hidromek Inc.

TABLE OF CONTENTS

ABSTRACT	iv
ACKNOWLEDGMENTS	viii
TABLE OF CONTENTS	viii
LIST OF FIGURES	x
LIST OF SYMBOLS AND ABBREVIATIONS	xiii
CHAPTERS	
1. INTRODUCTION	1
1.1 General	1
1.2 Motivation for the Study	4
1.3 Objective	5
1.4 Thesis Outline	6
2. LITERATURE SURVEY	8
2.1 Multibody System Modeling	8
2.2 Mount Modeling	13
2.3 Seat Modeling	18
3. DEVELOPMENT OF ANALYTICAL AND SIMMECHANICS	
SOLUTIONS	22
3.1 Identification of Stiffness and Damping Properties	26
3.1.1 Identification of Seat Suspension and Mount Properties	26
3.1.2 Identification of Tire Properties	29
3.2 Identification of Inertial Properties	36
3.3 Development of Analytical Solutions	38
3.3.1 Cab Model	38
3.3.2 Extended Machine Model	44
3.4 Development of SimMechanics Solutions	53
3.4.1 Cab Model	53
3.4.2 Extended Machine Model	57

4. EXPERIMENTAL PROCEDURE FOR THE VALIDATION	61
4.1 Instrumentation	62
4.2 Measurement Points	64
4.3 Preliminary Data Processing	67
5. COMPARATIVE EVALUTION OF THE CAB MODELS.....	69
6. RESULTS, DISCUSSION AND CONCLUSIONS.....	76
6.1 Comparison of the Measurement and Simulation Results	76
6.1.1 Comparison for the Cab Model	76
6.1.2 Comparison for the Extended Machine Model	80
6.2 Discussion	83
6.3 Summary and Conclusions.....	86
6.4 Future Work	87
REFERENCES.....	89

LIST OF FIGURES

FIGURES

Figure 1.1 - HMK 102B Energy Series Backhoe-Loader General View.....	2
Figure 1.2 – Location of the Seat and Cab Mounts on the Machine.....	3
Figure 2.1 – The Half-Car Model in SimMechanics [6].....	9
Figure 2.2 – Schematic Illustration of the Model [7].....	10
Figure 2.3 – Model diagram of the tractor [9]	11
Figure 2.4 – Schematic representation of the 44 DOF model [12]	13
Figure 2.5 - Viscoelastic models [13]	14
Figure 2.6 - Generalized viscoplastic models [13].....	14
Figure 2.7 – Rubber component model [15]	16
Figure 2.8 – Bushing model implementation using MATLAB and ADAMS [18] ...	17
Figure 2.9 – Schematic of the lumped parameter model [19].....	18
Figure 2.10 – Schematic of the Bouc-Wen model [19]	19
Figure 2.11 – Seat model with adjustable damper and auxiliary spring [20]	20
Figure 3.1 – Cab Structure and Mount Locations	22
Figure 3.2 – Schematic View of the 2D Planar Cab Model.....	23
Figure 3.3 – Schematic Representation of the Extended Model.....	24
Figure 3.4 – Auxiliary Model Used to Identify Stiffness and Damping Values.....	27
Figure 3.5 – Velocity Input Used for the Identification of Mount Parameters	28
Figure 3.6 – Force vs. Displacement Graph of the Mount.....	28
Figure 3.7 – Schematic Representation of Load-Deflection Experiments.....	30
Figure 3.8 – Location of the Load Cell and Position Transducer	31
Figure 3.9 – Load-Deflection Curve for the Front Tire	32
Figure 3.10 - Load-Deflection Curve for the Rear Tire.....	32
Figure 3.11 - Schematic Representation of the Drop Tests	33

Figure 3.12 - Location of the Position Transducer and Support	35
Figure 3.13 – Drop Tests - Tire Displacement Responses	35
Figure 3.14 – Mass Properties of the Cab Structure	37
Figure 3.15 – Free Body Diagram of the Cab	39
Figure 3.16 – Free Body Diagram of the Seat	39
Figure 3.17 – Implementation of Analytical Solution of the Cab to Simulink	44
Figure 3.18 - Free Body Diagram of the Machine Body	45
Figure 3.19 - Implementation of Analytical Solution of Machine Model to Simulink	53
Figure 3.20 – Definition of the Positions of the Body Coordinate Systems of the Cab	54
Figure 3.21 - Visualization of the Cab Model in SimMechanics.....	56
Figure 3.22 – SimMechanics Solution of the Cab	57
Figure 3.23 – Machine Body Subsystem	58
Figure 3.24 – Visualization of the Machine Model in SimMechanics	59
Figure 3.25 – SimMechanics Solution of the Whole Machine	60
Figure 4.1 – LMS SCADAS Mobile Data Acquisition System.....	63
Figure 4.2 – Crossbow LP Series Triaxial Accelerometer.....	63
Figure 4.3 – Disc Used for Seat Measurements.....	64
Figure 4.4 – Location of the Accelerometer Used on the Front Mount Connection .	65
Figure 4.5 - Location of the Accelerometer Used on the Rear Mount Connection ...	65
Figure 4.6 –Measurement Point for the Seat Acceleration	66
Figure 4.7 – Installation of the Data Acquisition System	67
Figure 5.1 – Velocity Inputs for the First Case.....	70
Figure 5.2 – Comparison of Analytical and SimMechanics Solution - (Seat Acceleration Time Histories for the First Case).....	70
Figure 5.3 – Comparison of Analytical and SimMechanics Solution – (PSD of Seat Acceleration for the First Case).....	71
Figure 5.4 - Velocity Inputs for the Second Case	72
Figure 5.5 - Comparison of Analytical and SimMechanics Solution – (Seat Acceleration Time Histories for the Second Case)	72

Figure 5.6 - Comparison of Analytical and SimMechanics Solution – (PSD of Seat Acceleration for the Second Case)	73
Figure 5.7 - Velocity Inputs for the Third Case	73
Figure 5.8 - Comparison of Analytical and SimMechanics Solution – (Seat Acceleration Time Histories for the Third Case)	74
Figure 5.9 - Comparison of Analytical and SimMechanics Solution – (PSD of Seat Acceleration for the Third Case)	74
Figure 6.1 - Comparison of Measurement and Simulation – (Seat Acceleration Time Histories for the First Case).....	77
Figure 6.2 - Comparison of Measurement and Simulation – (PSD of Seat Acceleration for the First Case).....	77
Figure 6.3 - Comparison of Measurement and Simulation – (Seat Acceleration Time Histories for the Second Case)	78
Figure 6.4 - Comparison of Measurement and Simulation – (PSD of Seat Acceleration for the Second Case)	78
Figure 6.5 - Comparison of Measurement and Simulation – (Seat Acceleration Time Histories for the Third Case).....	79
Figure 6.6 - Comparison of Measurement and Simulation – (PSD of Seat Acceleration for the Third Case).....	79
Figure 6.7 – FFT of the Velocity Inputs for the Third Case	80
Figure 6.8 – Position Input for the Front and Rear Tires	81
Figure 6.9 - Comparison of Measurement and Simulation for the Extended Machine Model – (Seat Acceleration Time Histories for the Bump Test)	82
Figure 6.10 - Comparison of Measurement and Simulation for the Extended Machine Model – (PSD of Seat Acceleration for the Bump Test).....	82
Figure 6.11 - Comparison of Measurement and Simulation for the Extended Machine Model for the Bump Test – (Peak Frequencies of the PSD Estimations)	83
Figure 6.12 - Comparison of Measurement and Simulation for the Cab Model for the Bump Test – (Peak Frequencies of the PSD Estimations)	84
Figure 6.13 – PSD Estimation for the Tire Input	84
Figure 6.14 – Simulated FRF Between Front Tire Input and Seat Acceleration	85

LIST OF SYMBOLS AND ABBREVIATIONS

SYMBOLS

- A : Connection Point of the Front Mount and the Cab
- a : Distance Between the Point A and Point C
- B : Connection Point of the Rear Mount and the Cab
- b : Distance Between the Point A and the Center of Gravity of the Cab
- C : Connection Point of the Seat Suspension and the Cab
- c_{mf} : Front Mount Damping Coefficient
- c_{mr} : Rear Mount Damping Coefficient
- c_s : Seat Suspension Damping Coefficient
- c_{tf} : Front Tire Damping Coefficient
- c_{tr} : Rear Tire Damping Coefficient
- c_{eq} : Equivalent Damping Coefficient
- D : Connection Point of the Front Mount and the Machine Body

- d : Distance Between the Point F and Point D
- d_A : Vertical Displacement of the Point A from the Equilibrium Position
- d_B : Vertical Displacement of the Point B from the Equilibrium Position
- d_C : Vertical Displacement of the Point C from the Equilibrium Position
- d_D : Vertical Displacement of the Point D from the Equilibrium Position
- d_E : Vertical Displacement of the Point E from the Equilibrium Position
- d_F : Vertical Displacement of the Point F from the Equilibrium Position
- d_G : Vertical Displacement of the Point G from the Equilibrium Position
- E : Connection Point of the Rear Mount and the Machine Body
- e : Distance Between the Point F and Point E
- F : Connection Point of the Front Tire and the Machine Body
- F_{har} : Steady-State Harmonic Loading
- F_f : Load Variation of the Front Axle
- F_r : Load Variation of the Rear Axle
- F_{sf} : Front Axle Static Load for the Drop Test
- F_{sr} : Rear Axle Static Load for the Drop Test

- F_{kmf} : Spring Force Generated by the Front Mount for the Cab Model
- F'_{kmf} : Spring Force Generated by Front Mount for Extended Machine Model
- F_{cmf} : Damping Force Generated by the Front Mount for the Cab Model
- F'_{cmf} : Damping Force Generated by Front Mount for Extended Machine Model
- F_{kmr} : Spring Force Generated by the Rear Mount for the Cab Model
- F'_{kmr} : Spring Force Generated by Rear Mount for the Extended Machine Model
- F_{cmr} : Damping Force Generated by the Rear Mount for the Cab Model
- F'_{cmr} : Damping Force Generated by Rear Mount for the Extended Machine Model
- F_{ks} : Spring Force Generated by the Seat Suspension
- F_{cs} : Damping Force Generated by the Seat Suspension
- F_{ktf} : Spring Force Generated by the Front Tire
- F_{ctf} : Damping Force Generated by the Front Tire
- F_{ktr} : Spring Force Generated by the Rear Tire
- F_{ctr} : Damping Force Generated by the Rear Tire
- G : Connection Point of the Rear Tire and the Machine Body
- g : Distance Between Point F and the Center of Gravity of the Machine Body

- H_f : Front Lifting Point for the Load-Deflection Experiment
- H_r : Rear Lifting Point for the Load-Deflection Experiment
- I_c : Moment of Inertia of the Cab with respect to the Lateral Axis
- I_b : Moment of Inertia of the Machine Body with respect to the Lateral Axis
- k_{mf} : Front Mount Stiffness
- k_{mr} : Rear Mount Stiffness
- k_s : Seat Suspension Stiffness
- k_{tf} : Front Tire Stiffness
- k_{tr} : Rear Tire Stiffness
- k_{eq} : Equivalent Stiffness
- L : Distance Between the Point A and Point B
- L_1 : Wheelbase of the Machine
- L_f : Front Lifting Force for the Load-Deflection Experiment
- L_r : Rear Lifting Force for the Load-Deflection Experiment
- m_c : Mass of the Cab
- m_s : Mass of the Seat Body and Operator

- m_b : Mass of the Machine Body
- o : Distance Between the Point S_s and Rear Tire Ground Connection
- p : Distance Between the Point H_f and Front Tire Ground Connection
- q : Distance Between the Point H_r and Rear Tire Ground Connection
- q_f : Vertical Displacement of the Connection of the Front Mount and Chassis
- q_r : Vertical Displacement of the Connection of the Rear Mount and Chassis
- q_{tf} : Vertical Displacement of the Connection of the Front Tire and Road Surface
- q_{tr} : Vertical Displacement of the Connection of the Rear Tire and Road Surface
- r : Distance Between the COG of Machine and Front Tire Ground Connection
- S_b : Front Bucket Support Point for the Drop Test
- S_s : Stabilizer Support Point for the Drop Test
- t : Distance Between the S_b and Front Tire Ground Connection
- w : Excitation Frequency of the Steady-State Harmonic Loading
- W : Weight of the Machine
- x : Response to the Steady-State Harmonic Loading
- x_1 : Amplitude of the First Successive Periods of the Tire Response

- x_2 : Amplitude of the Second Successive Periods of the Tire Response
- X : Magnitude of the Steady-State Harmonic Response
- y_1 : Vertical Displacement of the Center of Gravity of the Cab
- y_2 : Vertical Displacement of the Center of Gravity of the Seat and Operator
- y_3 : Vertical Displacement of the Center of Gravity of the Machine Body
- θ_1 : Angular Displacement of the Cab with respect to the Lateral Axis
- θ_3 : Angular Displacement of the Machine Body with respect to the Lateral Axis
- ζ : Damping Ratio
- ΔW : Dissipated Energy per Cycle

ABBREVIATIONS

3D : Three Dimensional

CAD : Computer Aided Design

COG : Center of Gravity

FEA : Finite Element Analysis

FFT : Fast Fourier Transform

FRF : Frequency Response Function

MSS : Motion Stabilizer System

PSD : Power Spectral Density

STL : Stereolithographic

WBV : Whole Body Vibration

CHAPTER 1

INTRODUCTION

1.1 General

Earth-moving machines are used for engineering projects such as roads, dams, open pit excavation, quarries, trenching, recycling, landscaping and building sites [1]. Among various types of earth-moving machines, backhoe-loader (Figure 1.1) is one of the most commonly used machines. There are two main systems in this machine: loader and backhoe. While the loader system is used for lifting, transporting and dumping the material; backhoe system is used for digging and excavating operations. Loader remains in place when the machine is used as an excavator and vice versa. A backhoe work cycle normally consists of excavating, elevating, swinging and discharging of material. A loader work cycle normally includes filling, elevating, transporting and discharging of material [2].

Backhoe-loader is propelled by an internal combustion engine. A transmission is connected to the engine and two shafts from the transmission are connected to the front and rear axles. The rear axle is attached rigidly to the vehicle body, and the front axle is allowed to oscillate around the longitudinal axis of the machine, thus allowing all wheels to maintain contact with the ground. A cab, which contains the seat and the machine controls, is attached to the chassis from four points via rubber mounts. Attachments are actuated by hydraulic cylinders. A hydraulic pump, which is connected directly to the internal combustion engine, supplies the necessary oil flow for these actuating cylinders. Directional control valves enable the operator to control the direction and amount of the fluid flow into cylinders.

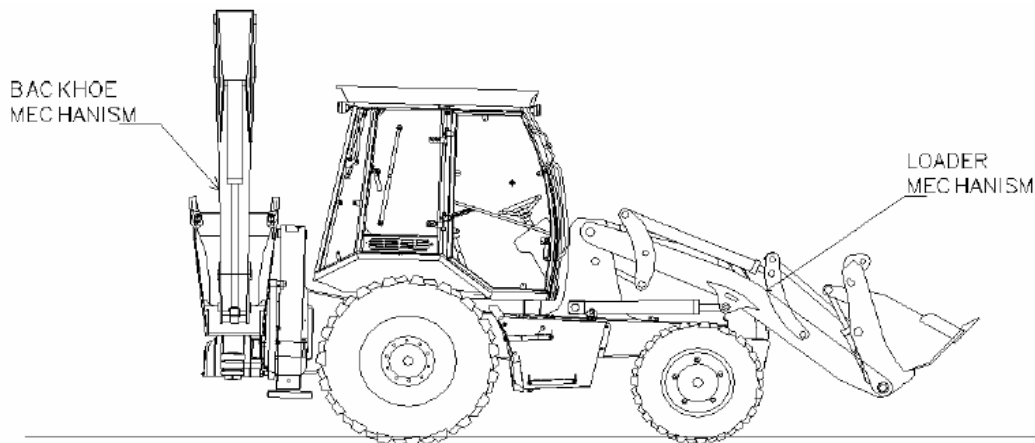


Figure 1.1 - HMK 102B Energy Series Backhoe-Loader General View

In order to satisfy the safe and comfortable driving conditions, vibration isolation is also needed for backhoe-loaders. Vibration isolation of the backhoe-loaders is provided by the combined contributions of various isolators. Main elastic components of the machine that reduce the vibration induced by the ground are typically tires, cab mounts and the operator seat. Other components like axles, chassis and attachments are generally assumed to be rigid and have no isolation effect due to their high stiffness.

Since the backhoe-loaders have unsuspended axles, tires are the primary isolators for the vibrations induced by the road surfaces. Cab mounts and seat suspension are the other isolators between the operator and the road surface. Location of these parts on the machine is shown schematically in Figure 1.2. Cab mounts are used to decrease the vibrations transferred from chassis to the cab and similarly seat suspensions are designed to reduce the vibration between the cab and the driver. Mounts are rubber based components and provides stiffness and viscoelastic damping. They also serve as structure borne noise isolators by preventing metal-to-metal contact. Seat suspensions are usually pneumatic or mechanical type and have adjustable stiffness

and damping values according to the weight of the operator. In addition to cab mounts and seat suspension, some backhoe-loaders are equipped with motion stabilizer system (MSS) to decouple the mass and inertia of the loader mechanism. Lifting cylinders of the loader mechanism are used as damping elements in the MSS.



Figure 1.2 – Location of the Seat and Cab Mounts on the Machine

There are several commercially available multibody simulation programs used for comfort studies of the vehicles. MATLAB[®], used in this work, is a powerful simulation software with various toolboxes embedded inside. One of these toolboxes is Simulink[®], which is an environment for multidomain simulations and model based designs for dynamic systems. By using Simulink, it is possible to design, simulate, and analyze different time-varying systems including the physical systems such as

mechanical systems. After deriving the differential equations of the system, Simulink interface gives opportunity to form the block diagram of the corresponding equations by using basic mathematical blocks and to investigate the results by solving them. Since, it is difficult to obtain the equations of multidomain systems when the number of the components in the system and their complexity are high; it will be impractical to use the Simulink in this way.

Simscape™ , which includes tools and libraries for modeling the physical systems, increases the capabilities of Simulink. Standard mechanical, hydraulic, electrical and thermal component blocks are embedded inside the Simscape libraries; but these blocks use the simplest correlations for simulation.

Among these libraries, SimMechanics™ toolbox is the one used for modeling the mechanical systems. It extends Simscape's mechanical system modeling capabilities by introducing blocks for standard components such as joints, rigid bodies, springs and dampers. These blocks can be used to model dynamic mechanical systems, instead of deriving and solving differential equations.

1.2 Motivation for the Study

Although, less attention has been paid to ride comfort issues, since the development of backhoe-loaders, great effort has been made to increase durability, safety and efficiency. Conventionally, backhoe-loaders have been thought as just earth moving machinery working on harsh environments. So these machines' performance in terms of vehicle dynamics has been seen less important. However, increasing demand for more comfortable machines as well as the high productivity has raised the need for studies on driving dynamics.

Due to the less attention paid to the vehicle dynamics, considerations in the design stage and the rough working conditions of the backhoe-loaders, vibration levels of these machines are relatively high. Consequently, during the course of normal daily operation, drivers of off-road vehicles may well be exposed to high levels of whole body vibration (WBV), causing discomfort and increased risk of lower-back pain [3]. Since, WBV is considered one of the main reasons for the operators' health problems; legislations are developed to restrict the exposure levels. Legislation concerning the exposure of the workers to the risks arising from physical agents (vibration) is published by European Council, called Directive 2002/44/EC [4].

Besides the comfort considerations, developing dynamic models of the backhoe-loaders is essential to design more durable and reliable machines. Designing such machines needs a better understanding of loading conditions of the components in their actual working environment. Since, obtaining dynamic forces by testing the machinery in actual working sites is costly and time consuming; recently design engineers get these forces from dynamic models for use in finite element analysis (FEA) and fatigue analysis.

1.3 Objective

The objective of this study is to present a dynamic model of a backhoe-loader including cab dynamics. As the result of this work, vibration levels transmitted from chassis to the operator and the dynamic forces on the cab will be obtained. Moreover, outcomes of this study will be used for the detailed analysis of backhoe-loader dynamics.

In this study, dynamic models are developed in trial licensed versions of MATLAB/SimMechanics[®]. A modeling methodology that is similar to the approach used in vehicle dynamics analyses is developed for the backhoe-loaders dynamics.

1.4 Thesis Outline

The thesis is composed of six chapters. First chapter gives a brief introduction about the backhoe-loaders and vibration isolation elements used on backhoe-loaders. General properties of the used software in modeling are also explained. Moreover, motivation for the study and the thesis objective are given in the first chapter.

The second chapter is denoted for the literature survey. In this chapter, multibody system modeling studies conducted with SimMechanics software are described besides the cab models of various vehicles like agricultural tractors. Furthermore, material based and experimental based mount modeling techniques and seat models developed are given in the second chapter.

The third chapter describes the development of analytical and SimMechanics solutions. Parameter identification procedures for the stiffness and damping values of the seat suspension, mount and tires are presented. Identification procedure of mass and inertia properties of the rigid bodies are also explained. In addition, development procedure of the analytical and SimMechanics solutions for the cab and the whole machine is defined in the third chapter.

Experimental studies done to validate the models of are explained in the fourth chapter. Instrumentation used in the measurements, measurement points and data processing done on the acquired acceleration values are presented in the fourth chapter.

Comparative evaluation of the analytical and SimMechanics cab solutions is given in the fifth chapter. Velocity inputs obtained from the experimental studies are utilized to simulate the analytical and SimMechanics solutions of the cab and results acquired from the both models are demonstrated.

In the sixth chapter, results obtained from the measurements are compared with the results obtained from the cab and backhoe-loader model to assess the physical test and simulation results. Findings of this study with a brief summary are given. Moreover, possible future work on this subject is discussed.

CHAPTER 2

LITERATURE SURVEY

Results of the literature survey are presented in this chapter. Firstly, some multibody system models related to the topic of this study are given. Then, mount models found in literature are discussed in detail. And then, studies about the seat modeling are explained.

2.1 Multibody System Modeling

Multibody system modeling is a common method to make ride analysis in vehicle dynamics. There are several multibody system models constructed for different ride dynamic applications like passenger vehicles, transportation vehicles, railway vehicles and agricultural tractors. However, specific models for backhoe-loader ride dynamics for this purpose do not exist in literature. In this section, examples of the multibody system models constructed are given and these models including cab dynamics are explained.

Most frequent ride models used to investigate vertical vehicle dynamics are explained theoretically in the study of Rehnberg [5]. Comparison of these ride models is made to study the applicability of the axle suspensions to the wheel loader which is earth moving machinery with the front end loader mechanism. Quarter car model and the half car model are assessed in terms of their success in reflecting the wheel loader dynamics. In another work, Van Boekel [6] presented a report in which a comparison between three multibody packages (Simulink/SimMechanics,

MapleSim and Dymola) is made. As a part of this report, a half-car model structure is constructed by using SimMechanics (Figure 2.1).

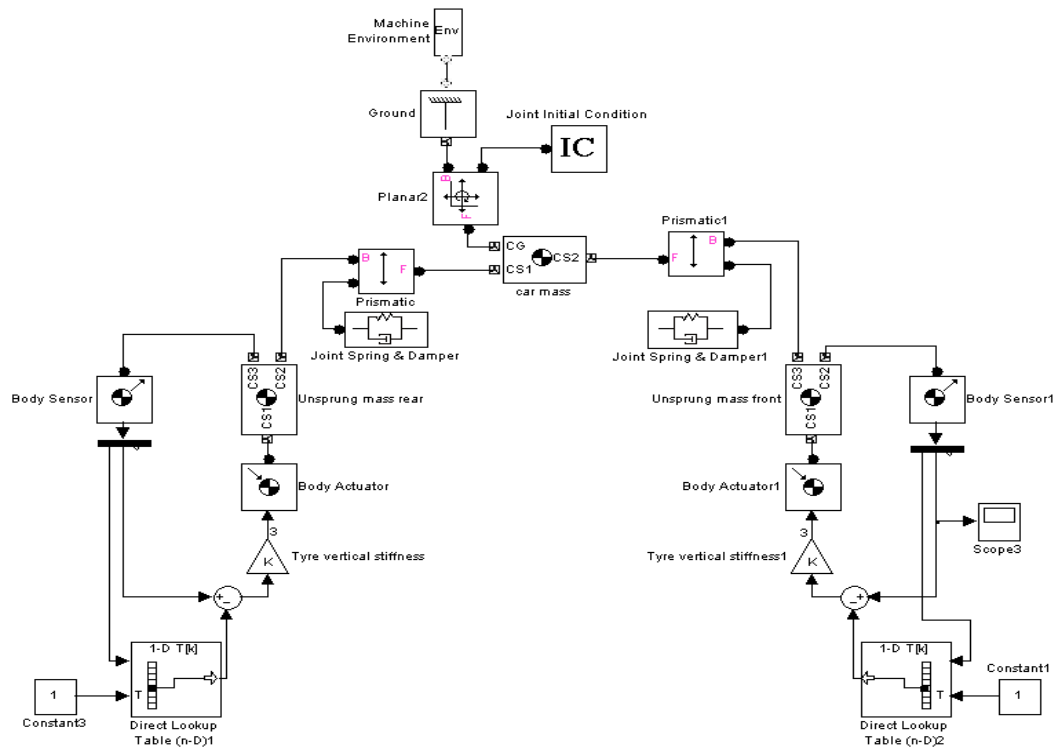


Figure 2.1 – The Half-Car Model in SimMechanics [6]

De Temmerman et al. [7] proposed a linear, 6 degree of freedom (DOF) mathematical model for the cab suspension of a self-propelled agricultural machine (Figure 2.2). Equation of motion of the cab model is based on Lagrange's equation. Kinetic energy of the suspension and the virtual work performed by the suspension on the cab body are calculated to obtain the equation of motion. Model is validated by an experimental test rig for different vibration signals. Test rig is excited in the frequency range between 0.7 Hz to 7 Hz during the validation process.

Eigenfrequencies for each DOF and the frequency response function for the vertical DOF are compared in the stated frequency range. As the second part of this study, the model damping values are optimized using standard comfort parameters [8]. Appropriate damping values are determined by combining the comfort parameters and power spectra interpretation. As a result of the work, it is concluded that lowering the stiffness value would provide even better vibration attenuation performance due to avoidance of the eigenfrequency of the suspension system being positioned in the frequency range most excited with road profiles.

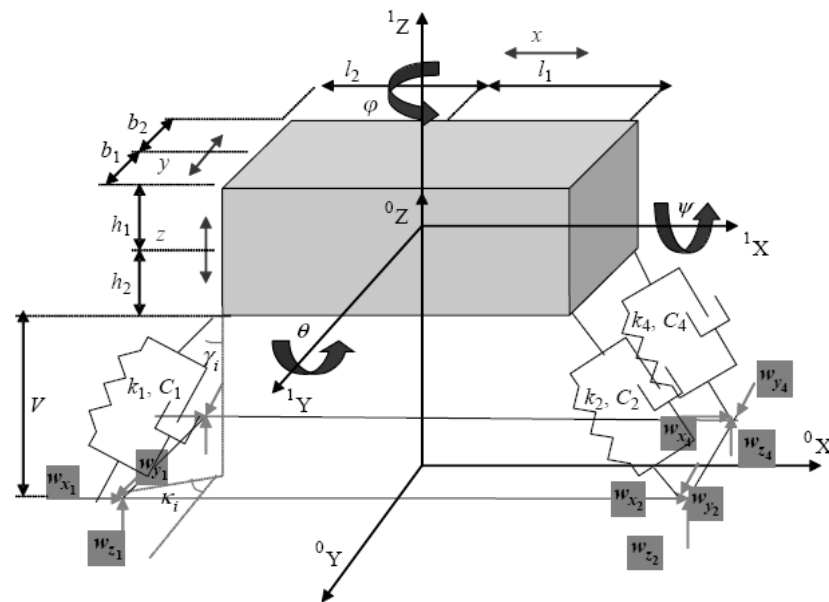


Figure 2.2 – Schematic Illustration of the Model [7]

Spelta et al. [9] studied on the modeling and identification of vertical dynamics of an agricultural machine with suspended cabin. In their work, a semi-physical model, which describes the full vertical dynamics of the tractor, is proposed (Figure 2.3) and

SimMechanics multibody tool is used as the modeling environment. Developed model is regarded as a generalization of the half-car model and three main assumptions are done:

- Yaw and roll dynamics are neglected.
- Vertical excitations do not induce any significant yaw movement.
- Cabin and vehicle pitch angles are comparatively small.

Parameters describing the model are identified in two stages. First, the car and the cabin parameters are identified separately and then, via using the intermediate results as initial conditions, final identification is completed. Model validation is done with experimental study.

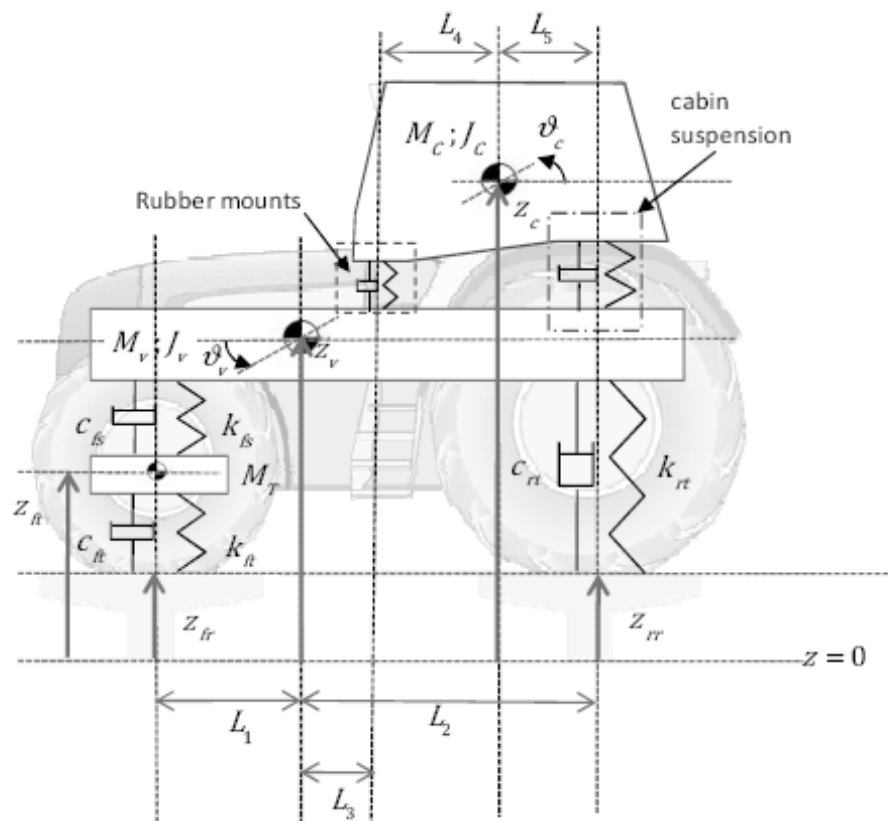


Figure 2.3 – Model diagram of the tractor [9]

An analytical model of an agricultural tractor through the assembly of tire and cab and seat suspension models, in order to predict the vibrations transmitted to the driver's seat is constructed by Ahmed and Goupillon [10]. Three suspended structures, namely, the tractor chassis, the cab, and the seat/driver unit are assumed to be rigid in the dynamic tractor model. Each suspension elements are defined by its stiffness and damping characteristics in the model.

ElMadany [11] presented 9 DOF planar vibrational model of an articulated vehicle with a suspended cab. In this work, the heave, fore-aft and pitch motions of a tractor-semitrailer truck are considered and the evaluation of the statistical performance of the linear and nonlinear passive cab suspension systems are emphasized. In addition, an optimization procedure based on comfort/cab deflection trade-off is developed.

Evers et al. [12] developed a modular truck semi-trailer model in the multi-body toolbox SimMechanics. In this study, SimMechanics is chosen as the multi-body software since the model created is desired to combine control software. In addition, easiness of creating sub-systems for different parts of the vehicle by using various Simulink tools and storing them as modules in a component library is the other reason for the preference of SimMechanics. Several modules including the cabin module are created to develop the truck semi-trailer model. In the study, cabin is modeled as a rigid body and it is fixed with two spring damper in the front and dampers at the rear in lateral direction. In vertical direction suspension elements are modeled as spring damper combinations. Designed 44 DOF model (Figure 2.4) is validated by doing tests on a real truck.

Models explained in this section are mainly includes the cab models and SimMechanics models. It will be concluded from the studies discussed that use of vehicle dynamics concepts in the modeling stage and investigation of low frequency response in the validation step is the common approach. Moreover, in almost all the models discussed, a parameter identification procedure is followed by utilization of

experimental results to estimate the system parameters. Experimental results mostly validate the models in the studies.

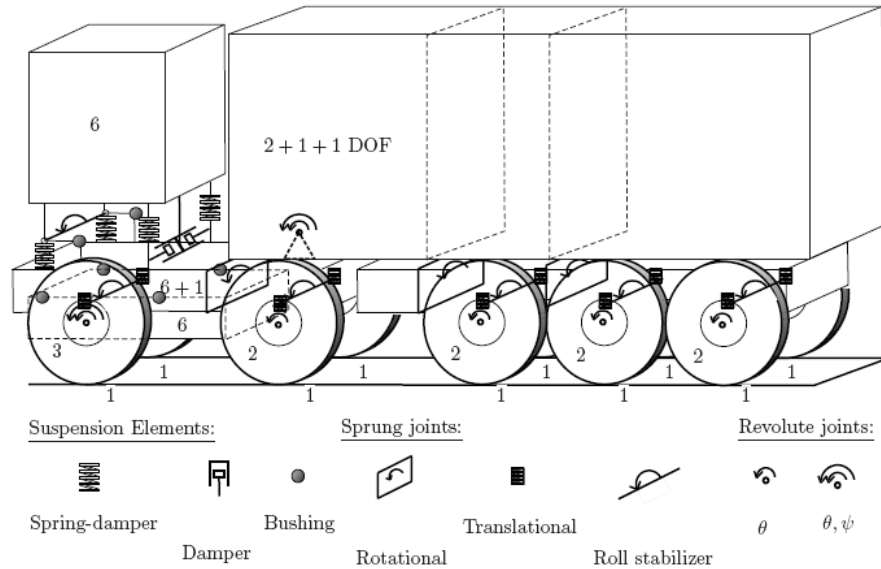


Figure 2.4 – Schematic representation of the 44 DOF model [12]

2.2 Mount Modeling

Mount models used in multibody dynamic simulations are explained in this section. Studies on bushings which have the similar characteristics due to their rubber based nature are also described. Karlsson and Persson [13] developed and studied various bushing models in MATLAB. Viscoelastic models (Figure 2.5) including Kelvin-Voigt, Zener, and Generalized Maxwell, elastoplastic models and generalized viscoplastic (viscoelastic elastoplastic) models (Figure 2.6) are investigated and a parameter identification process is developed by using the results of the physical

component tests. Bushing models are validated against physical test data and it is seen that viscoelastic models (Kelvin-Voigt, Zener, and Generalized Maxwell) represent the behaviour of the components very poorly because of their inability to show amplitude dependence. Moreover, it is inferred that elastoplastic models are able to capture frequency dependence, but generalized viscoplastic (viscoelastic elastoplastic) models resemble the rubber components in a satisfying manner.

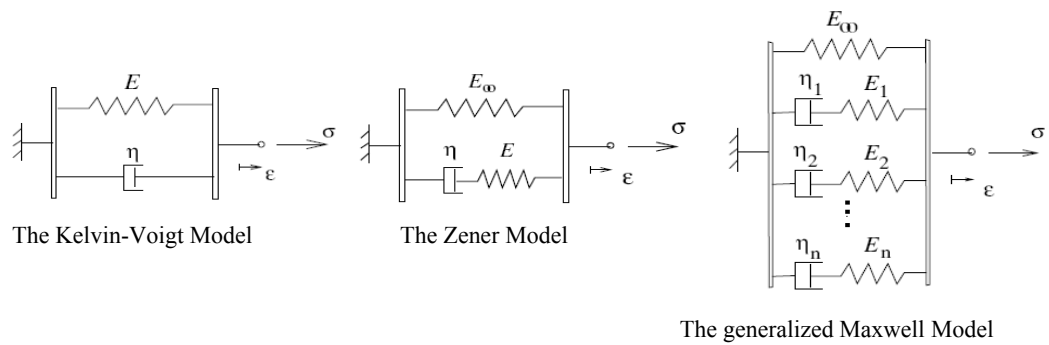


Figure 2.5 - Viscoelastic models [13]

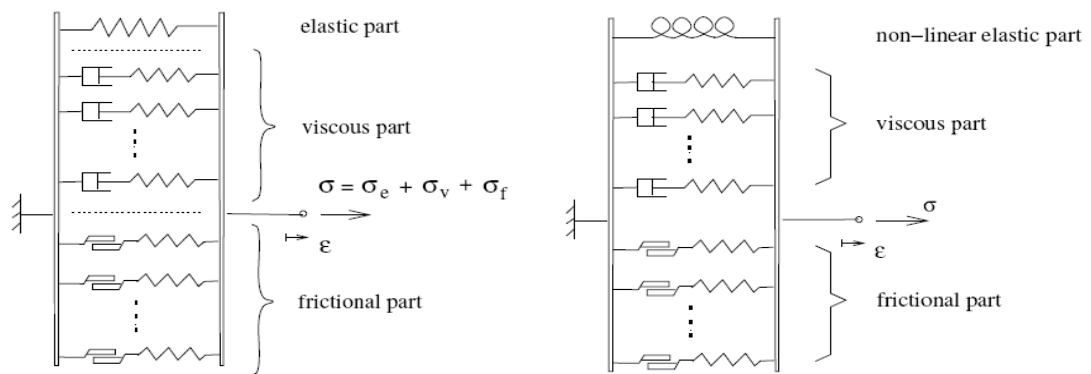


Figure 2.6 - Generalized viscoplastic models [13]

Ledesma et al. [14] presented a formulation in order to introduce nonlinear viscoelastic bushing elements into multibody systems. Nonlinear viscoelastic bushing forces between two elements are described as massless force elements by this formulation. Proposed analytical model is implemented into the general purpose multibody dynamics code ADAMS. Both for nonlinear viscoelastic model and nonlinear elastic model validation are performed by comparing experimental data to simulation results. Better dynamic load and displacement prediction capability of the nonlinear viscoelastic model compared to the nonlinear elastic model is demonstrated.

Sjöberg and Kari [15] modeled frequency dependence of a rubber isolator by a fractional calculus element and amplitude dependence by a frictional component. In their study, frequency dependence is obtained by a fractional Kelvin-Voigt model. This model is realized by replacing the dashpot of the ordinary Kelvin-Voigt model by a spring pot which gives the stress directly proportional to strain and to its time derivative of fractional order. Amplitude dependence is modeled by inserting a friction model into the fractional Kelvin-Voigt model. Friction model used is based on a stick-slip component model of Coulomb type. However, it gives smoother characteristics compared to the stick-slip model. The final proposed rubber component model is composed of a spring-pot and the smooth friction model coupled in parallel with an elastic stiffness (Figure 2.7). In the model, it is approximated that amplitude dependence is independent of frequency and the frequency dependence is independent of amplitude. By this approximation, force components are thought to be uncoupled and parameters of each force components are identified independently.

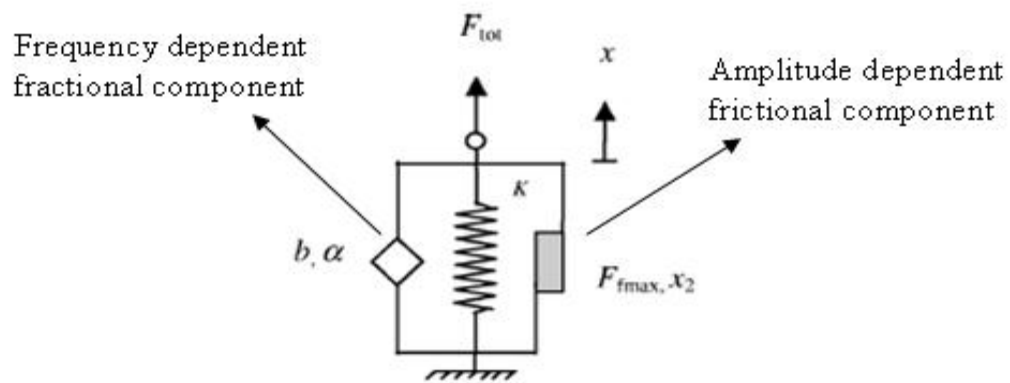


Figure 2.7 – Rubber component model [15]

Simple engineering models for the dynamic stiffness of rubber bushings including amplitude and frequency dependence are presented by Garcia [16]. A material model composed of separable elastic, viscoelastic and friction rubber component model is proposed in the study. Unlike other studies, formulas including the amplitude dependence due to non-homogeneous strain states are included in this work.

Barber [17] explained different methodologies like whitebox and blackbox models used for describing dynamics of nonlinear frequency dependent components and introduced a blackbox technique called Empirical Dynamics Modeling. Systems having only amplitude dependence or only frequency dependence and conventional blackbox methods used to describe these systems are discussed. Inadequacy of the conventional methods to represent the systems that have both amplitude and frequency dependence is also revealed. In the study, features of the proposed Empirical Dynamics Models, which overcome the deficiencies of the conventional methods via use of neural networks, are explained and the capabilities of the proposed model are demonstrated in case studies for shock absorbers and a rubber

bushing. In case studies, benefits and limitations of the Empirical Dynamic Modeling approach are introduced.

Yoo et al. [18] developed a practical automotive bushing component model to improve the accuracy of the vehicle dynamic analysis. In their study, bushing components of a vehicle suspension system are tested to obtain the nonlinear and hysteretic properties of typical rubber bushing elements and based on the acquired results, a new bushing model using artificial neural network algorithm is proposed. MATLAB and Simulink are used to construct the empirical bushing module and an interface module is developed to implement the bushing model with the dynamic analysis programme ADAMS (Figure 2.8). Test rig used to capture the bushing properties is simulated in ADAMS with the new bushing model for the validation.

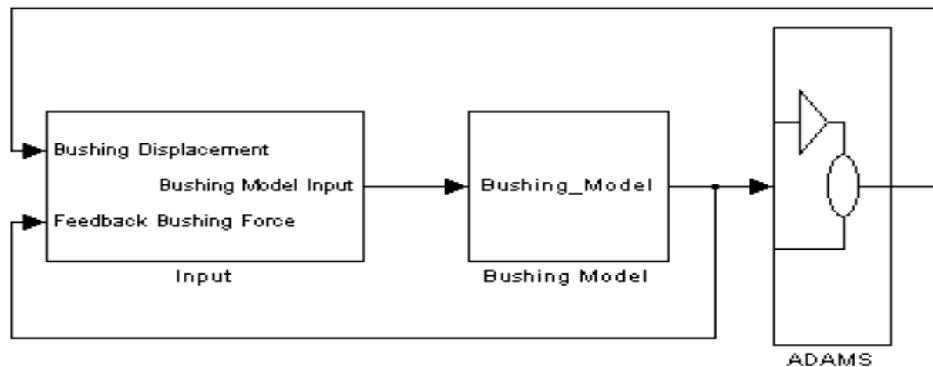


Figure 2.8 – Bushing model implementation using MATLAB and ADAMS [18]

Mount models described in this section are mainly developed by using two techniques. First approach is constructing the model by mathematical investigation of a rubber material model which requires defining the system equations and advanced analytical calculations like fractional derivatives. However, these models are more

adjustable since they are parametric. Second approach is using experimental data to model the complete component. This method is based on forming a relationship between the inputs and outputs using curve fitting technique. It is advantageous to use this approach when the system model requires large number of parameters.

2.3 Seat Modeling

Seat dynamics plays an important role in the transmission of vibration to the operator in earth moving machinery. In this section, studies on seat modeling in the literature are presented. Gunston et al. [19] proposed and compared two alternative methods to model the seat suspensions. A ‘lumped parameter model’ (Figure 2.9) is compared with a global ‘Bouc-Wen model’ (Figure 2.10) in their study. In the lumped parameter approach, non-linear dynamics of the seat suspension is described by coefficients related to the specific component parts and then, solving the resulting equations by numerical integration techniques. The cushion, the suspension linkage and stiffness, the suspension damper and the end-stop buffers parameters are identified by separate dynamic measurements in this approach.

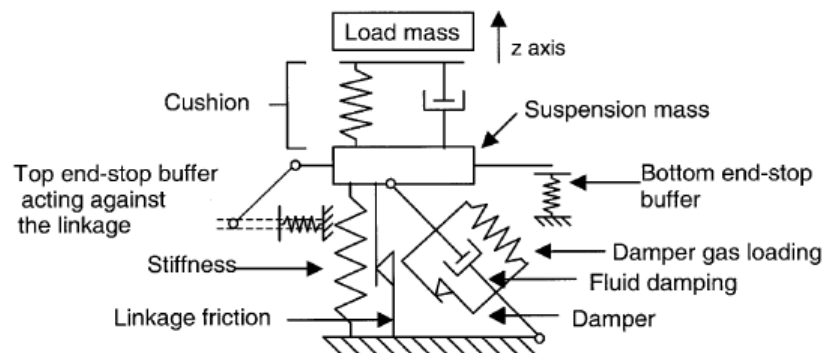


Figure 2.9 – Schematic of the lumped parameter model [19]

In the ‘Bouc-Wen’ model the dynamic characteristics of the seat suspension are represented using a Bouc-Wen formula. In this model, a global approach which is based on the measured input motion at the seat base and the measured output motion on the seat cushion is used. It is concluded in the study that the lumped parameter model may be useful for the design of new seats or the modification of existing seats and the Bouc-Wen model may be the best choice in situations where the seat is a part of a more complex model of the vehicle. It is also seen from the results of the work that both models provide quite good representation of the seat dynamics, but needs further improvements for the extreme motions.

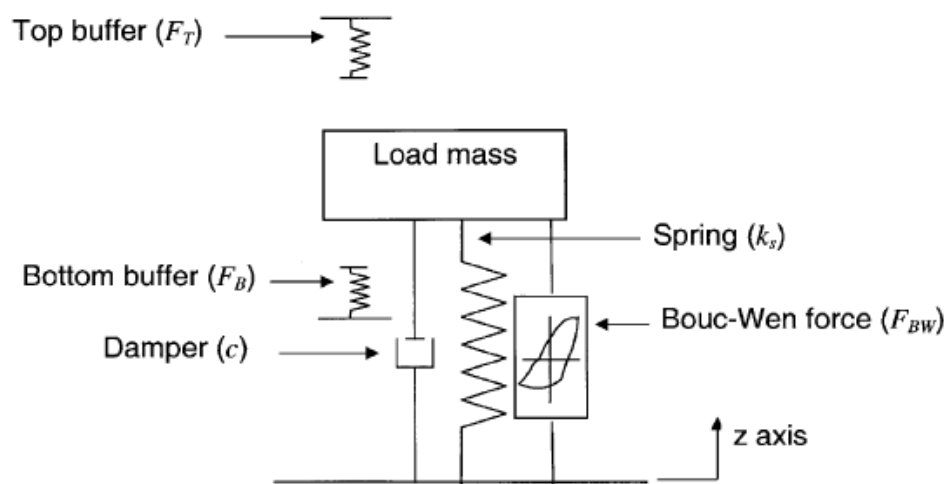


Figure 2.10 – Schematic of the Bouc-Wen model [19]

Stein et al. [20] presented a dynamic seat model based on Zener’s structure for a standard seat fitted into locomotives and showed the insufficiency of single DOF suspension model. The dynamic properties of a vertical seat suspension with an adjustable damper are described by the model in the study. Model is constructed with

a main spring, in parallel with a series combination of a viscous damper and an auxiliary spring (Figure 2.11). Values for these parameters are identified by using the transmissibility curves measured in the frequency range 0.5-8 Hz. Quadratic error function between the frequency response function modulus obtained from the simulation and the measured transmissibility is tried to be minimized. Model is detailed by adding a cushion model to the vertical suspension model and identification is done with field measurements. Enlarged model is optimized in terms of both seat vertical acceleration attenuation and seat vertical displacement. Validation study showed that developed model and parameter identification procedure allows finding a set of parameters of vertical seat suspension model with good accuracy.

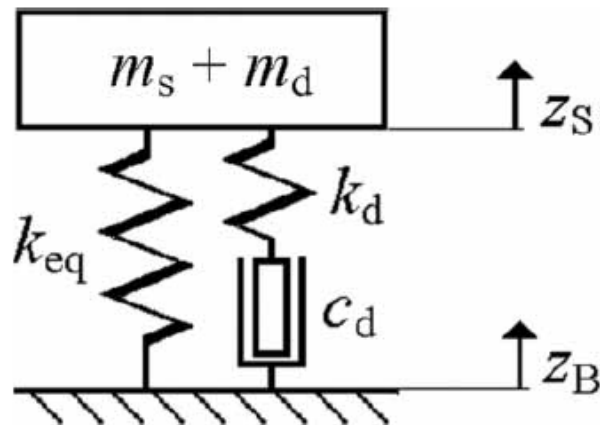


Figure 2.11 – Seat model with adjustable damper and auxiliary spring [20]

Maciejewski et al. [21] proposed a mathematical model for the conventional passive seat suspension. Spring force, damping force, forces from end-stop buffers, overall friction force of suspension system and gravity force are taken into account in the

model. Model parameters are identified by experimental analysis and vibro-isolation properties of the seat suspension are improved by the modification of spring force and damping force. A multi-criteria optimization is done for the improved model. Minimization of absolute acceleration of the loaded seat to protect the driver's health and minimization of relative displacement of seat suspension to ensure the controllability of the working machine are the opposite criteria in the study. As a result of the optimization, vibro-isolating properties of the seat are increased significantly especially at the natural frequency while maintaining the controllability of the machine.

Stein and Mucka [22] used a simple linear cushioned seat and a seated human model with a planar passenger car model. A half-car model with linear human body and vehicle component models are used throughout the study. The combined planar model developed in this work consists of a planar model of a vehicle with two wheels, a single DOF seat model and a linear human body model.

Explained studies in this section shows that seat models developed by identifying each seat component parameters separately and calculating each component force is appropriate for the seat design or modifications. However, for the situations where a seat is an input or output to another system, a description of the global dynamic behaviour of the seat is sufficient. In addition, models explained here mostly assume a rigid connection between the seat cushion and the mass on the seat body. It is also deduced from the literature survey that linear models reflects the seat dynamics quiet good.

CHAPTER 3

DEVELOPMENT OF ANALYTICAL AND SIMMECHANICS SOLUTIONS

Backhoe-loader cab modeled in this study is assembled to the machine body from four points with rubber mounts and includes the suspended seat and machine controls. Cab structure in general terms and location of the mounts are shown in Figure 3.1.

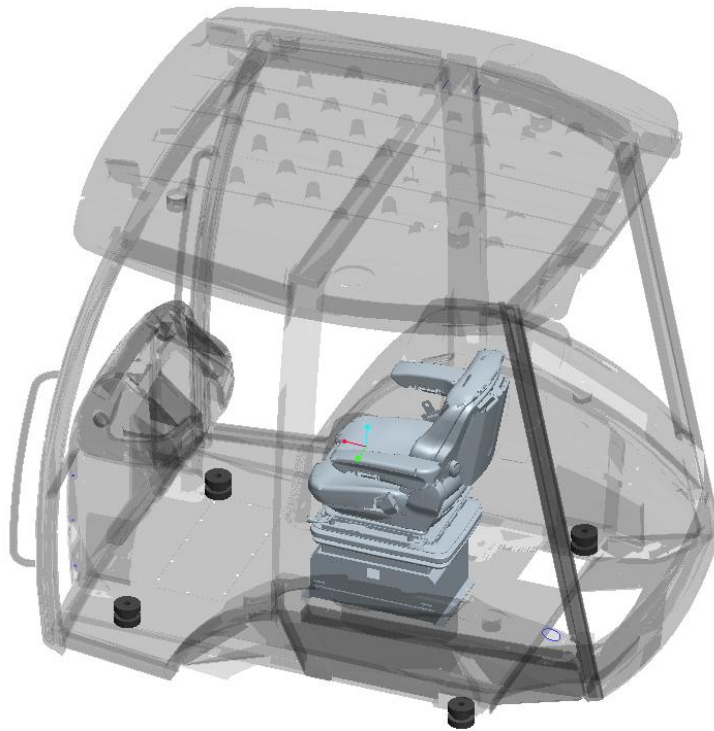


Figure 3.1 – Cab Structure and Mount Locations

Although, the cab is three dimensional, it is modeled as a planar 3 DOF system in this study. Bounce and pitch motions of the cab are considered as the two degrees of freedom and roll motion of the cab is not modeled. The third degree of freedom is taken as the vertical motion of the seat and operator. Schematic view of the developed cab model is given in Figure 3.2.

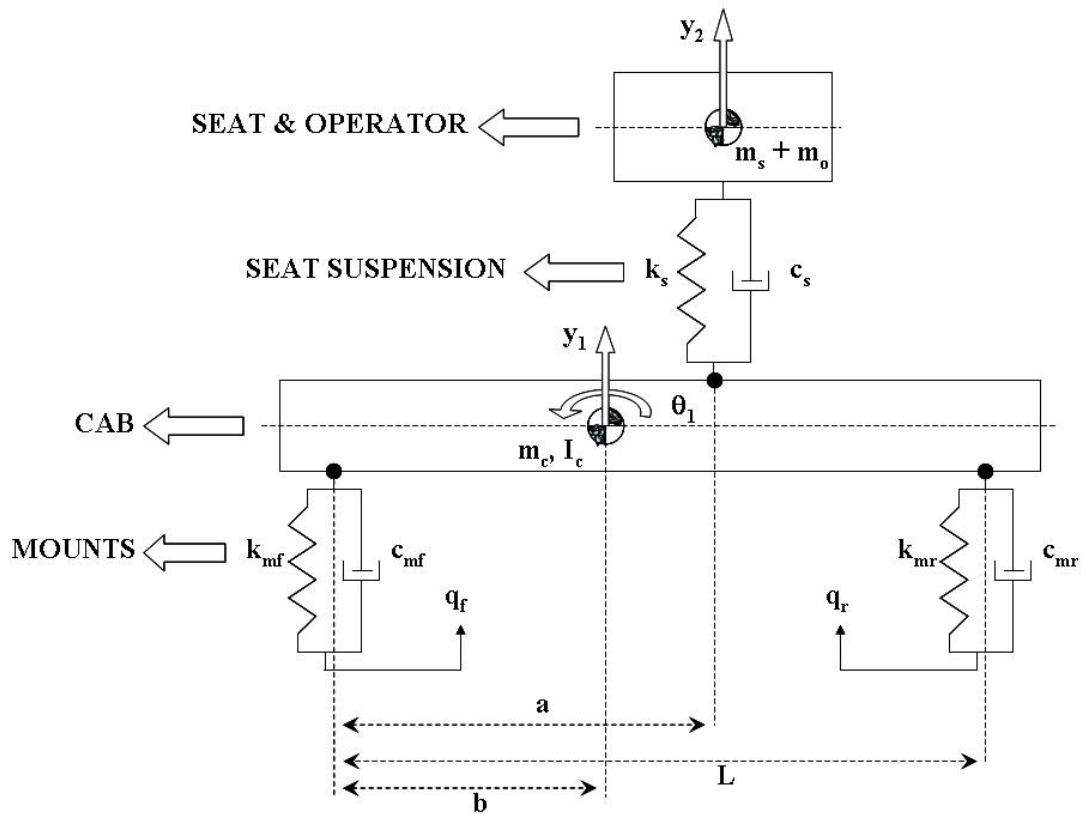


Figure 3.2 – Schematic View of the 2D Planar Cab Model

In addition to the cab model, an extended ride model for the whole machine is also developed. In the extended model, tires and the machine body are also modeled and degrees of freedom of the model are increased to five. One of the additional degrees

of freedom comes from the pitch motion of the machine body and the other one comes from the bounce motion of this part. Schematic representation of the extended model is shown in Figure 3.3.

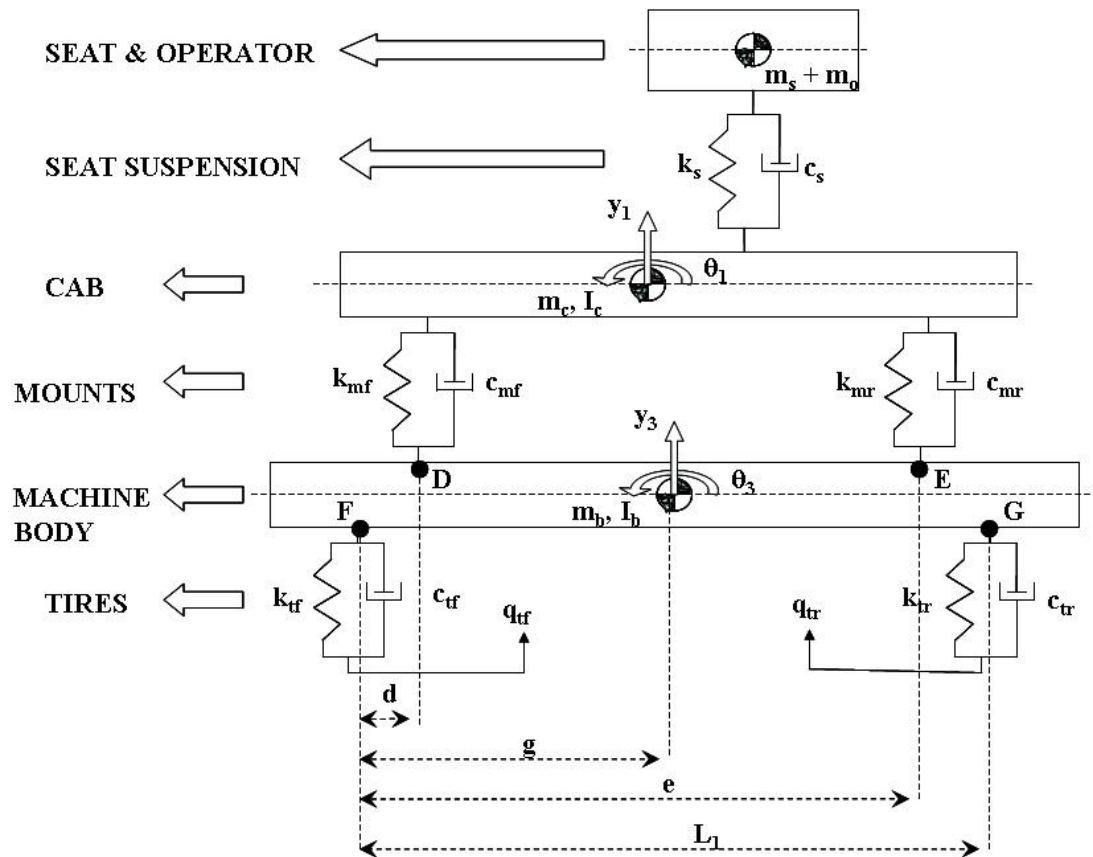


Figure 3.3 – Schematic Representation of the Extended Model

Seat suspension, mounts and tires are the elastic parts and they are modeled with linear spring and dashpot units. Spring resembles the stiffness and dashpot resembles the damping of these parts. Since backhoe-loader has no suspension elements between the chassis and axles, damping of the tires are considered in the extended

model. Cab, seat and machine body are the parts that are defined as rigid bodies in the models. Operator is also assumed to be a body that is rigidly connected to the seat.

Seat suspension, mounts and tires are actually the elastic parts with non-linear dynamic characteristics at the end points of the deflection limits. When the deflection of these parts approaches to the non-linear region, it causes the operator to move relative to the seat surface, which is a situation that is not modeled in this study. Therefore, relative displacement of the seat suspension, mounts and tires are assumed to be within the linear region of the deflection limits and these parts are modeled with linear spring and dashpot units. Validity of this assumption is checked with the simulation results obtained for the three measurement cases described in Chapter 3.

Front and rear mounts are placed symmetrically with respect to the longitudinal axis of the machine. Therefore, front and rear mounts are modeled with single mounts and placed on the intersection points of the longitudinal axis of the machine and the lines that are connecting the front and rear mounts. Since there are two mounts in parallel both in the front and at the rear in actual cab connection, mount stiffness and damping coefficient values are multiplied by two in the model. Similarly, front and rear tires are also placed symmetrically with respect to the longitudinal axis of the machine. Therefore, placement of tires, stiffness and damping values are defined in the same way with the mounts in the extended machine model. Center of gravities (COG) of the seat, cab and the machine body are also assumed to be on the longitudinal axis of the machine.

First part of the chapter is dedicated to explain the procedure to estimate stiffness and damping characteristics of the seat suspension, mounts and tires. Determination of the mass and inertia properties of the rigid parts are explained in the second part. In the third part, analytical solutions of the cab and whole machine are developed by using the differential equations which describes the behaviour of the each system.

Models constructed with physical blocks of the SimMechanics for the cab and the whole machine is presented in the last section.

3.1 Identification of Stiffness and Damping Properties

3.1.1 Identification of Seat Suspension and Mount Properties

Force-displacement behaviour of the seat suspension and mounts obtained at a certain velocity are used to determine the stiffness and damping coefficients of these parts. Force-displacement graphs have two important characteristics that provide information about the dynamics of the part. First one is the backbone curve which is directly related to the stiffness and the second one is the hysteresis around the backbone curve which is directly related to the damping of the component. By using this information, parameters of the seat suspension and mounts are identified in this study. Slope of the backbone curve is used to identify the stiffness values and the width of the hysteresis is employed to identify the damping coefficients.

An auxiliary model is developed in SimMechanics for the identification process of the damping and stiffness values. This model is used for identification of both mount and seat suspension parameters and the model structure is presented in Figure 3.4. In the model, physical modeling blocks of the SimMechanics and SimScape Foundation library are used.

A dummy mass is connected to the ground with two translational joints to create a single DOF mass-spring-damper system. “Translational Damper” and “Translational Spring” blocks from the Simscape Foundation library, a one dimensional modeling environment, are used to represent the stiffness and damping properties. Connection between these one-dimensional elements and the 3D SimMechanics elements is obtained by a “Prismatic Translational Interface” block. This block feeds force from

the spring and damper through one of the prismatic joint to the mass and feeds the relative motion of the mass with respect to the ground to the spring and damper side. The second prismatic joint is used to give the velocity input that is specified in the test data supplied by the manufacturer. Velocity input given to the auxiliary model for the identification of mount parameters is demonstrated in Figure 3.5. In this velocity profile, starting portion of the loading, transition from loading to unloading and the final part of the unloading are defined with ramp functions.

Displacement and reaction force from the translational joint that is connected to the spring and damper is measured and force vs. displacement graph is plotted. Hysteresis curve supplied by the manufacturer and obtained from the model is compared for the mount in Figure 3.6.

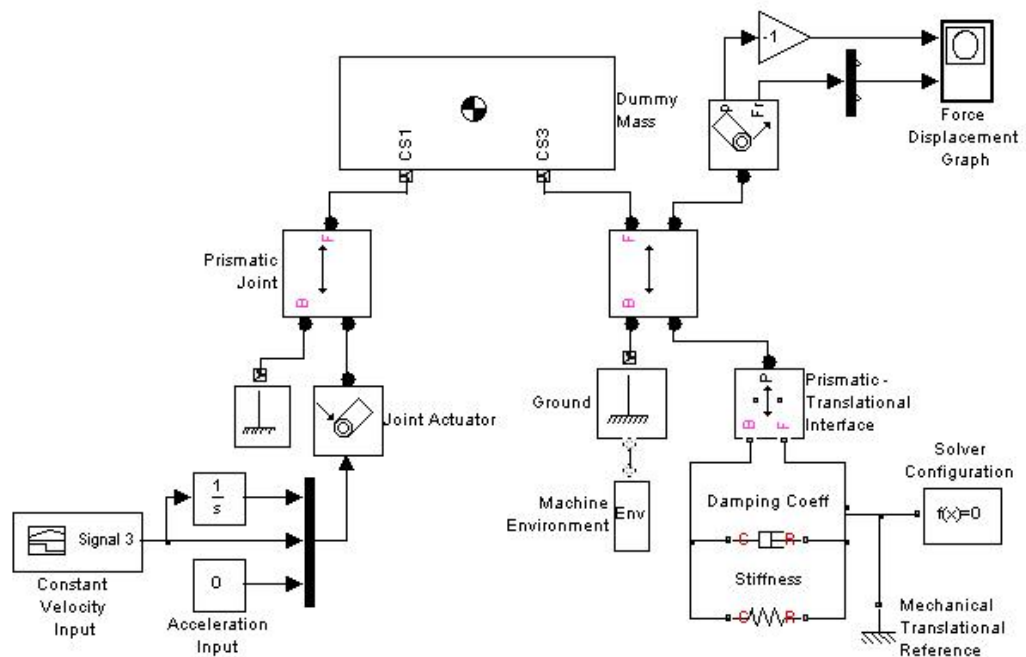


Figure 3.4 – Auxiliary Model Used to Identify Stiffness and Damping Values

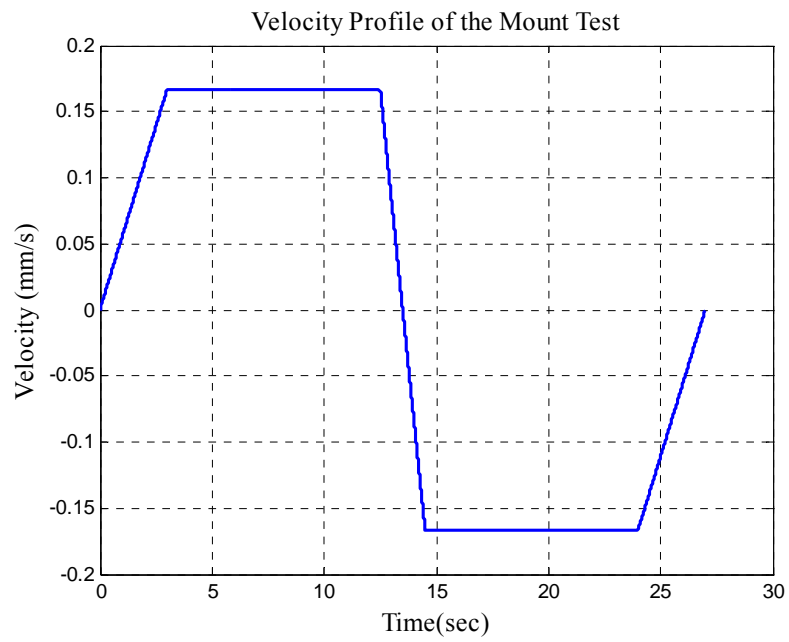


Figure 3.5 – Velocity Input Used for the Identification of Mount Parameters

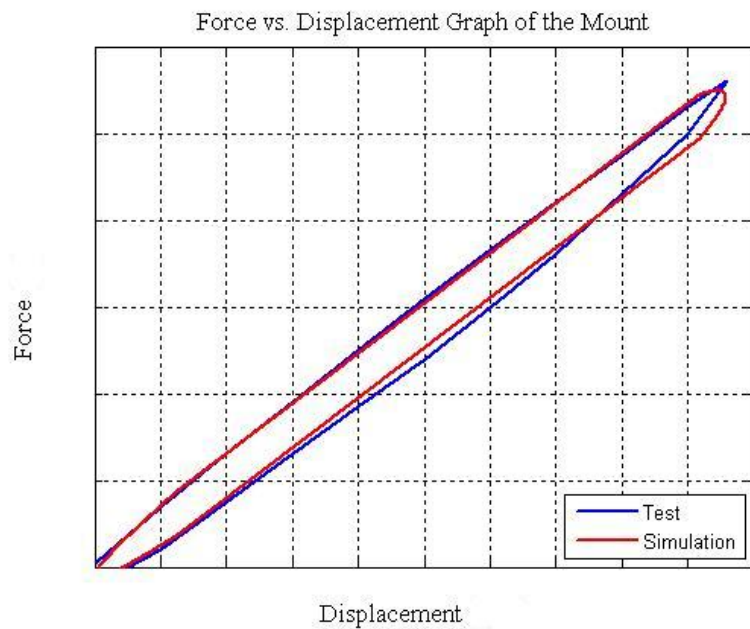


Figure 3.6 – Force vs. Displacement Graph of the Mount

In addition to the results obtained from the auxiliary SimMechanics model, equivalent damping coefficient is also investigated by using the area of the hysteresis loop which denotes the energy loss in one loading and unloading cycle. To do this, it is assumed that the force-displacement curve supplied by the manufacturer is obtained for a steady-state harmonic loading which is defined in equation (3.1), and the corresponding response is given in equation (3.2).

$$F_{har}(t) = (-ic_{eq}\omega + k_{eq})x \quad (3.1)$$

$$x = Xe^{-i\omega t} \quad (3.2)$$

Then, the equation (3.3) is gives the energy dissipated per cycle which is the area of the hysteresis loop.

$$\Delta W = \pi\omega c_{eq} X^2 \quad (3.3)$$

The area of the hysteresis loop of the mount, ΔW , calculated by numeric integration and the equivalent damping coefficient value, c_{eq} , identified by using the auxiliary model are put into equation (3.3). Then, the corresponding harmonic excitation frequency, ω , is approximated as 0.02 Hz, which will be assumed to be almost static.

3.1.2 Identification of Tire Properties

Load-deflection experiments are conducted for both front and rear tires to obtain the tire stiffness values. In these tests, actual machine is used and tire pressures are adjusted to their nominal values. Load on the front axle is increased by lifting the machine a point just above the stabilizers and it is increased for the rear axle by lifting the machine from the front bucket. Front and rear lifting points are shown as

H_f and H_r , respectively in Figure 3.7. Throughout these tests, the lifting force is measured with a load cell and tire deflection is measured with a wire potentiometric position transducer simultaneously. Locations of the load cell and the position transducer are illustrated in Figure 3.8. Load distribution of the front and rear axles are calculated by using equations (3.4) and (3.5), respectively. Calculated load values for the axles are divided by two to obtain the single tire load variation and plotted with respect to measured tire deflection. Stiffness values of the front and rear tires are determined from the slope of the linear regression lines fitted to the load-deflection curves displayed in Figure 3.9 and Figure 3.10.

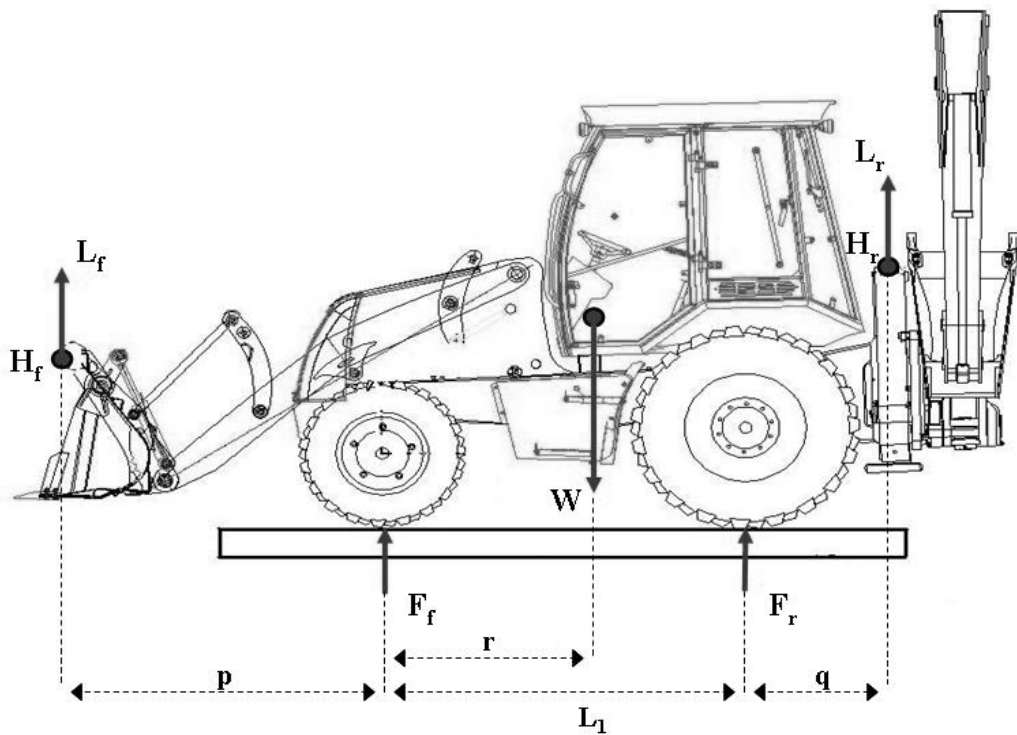


Figure 3.7 – Schematic Representation of Load-Deflection Experiments



Figure 3.8 – Location of the Load Cell and Position Transducer

$$F_f = \frac{L_r q + W(L_1 - r)}{L_1} \quad (3.4)$$

$$F_r = \frac{L_f p + W r}{L_1} \quad (3.5)$$

Load cell used in the measurements is a compression type load cell with a 0.1 kg resolution and 35000 kg maximum rated force. This load cell is insensitive to excentrical loads.

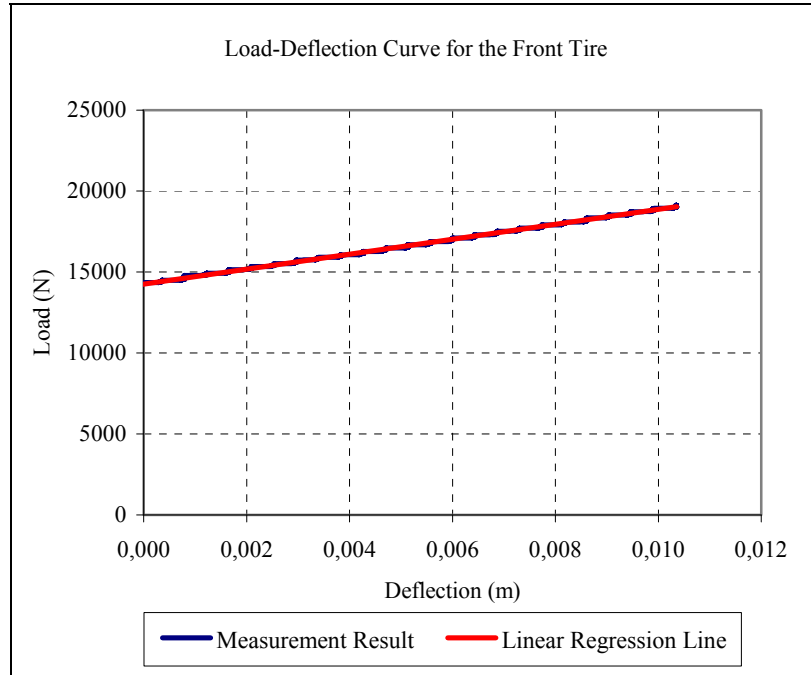


Figure 3.9 – Load-Deflection Curve for the Front Tire

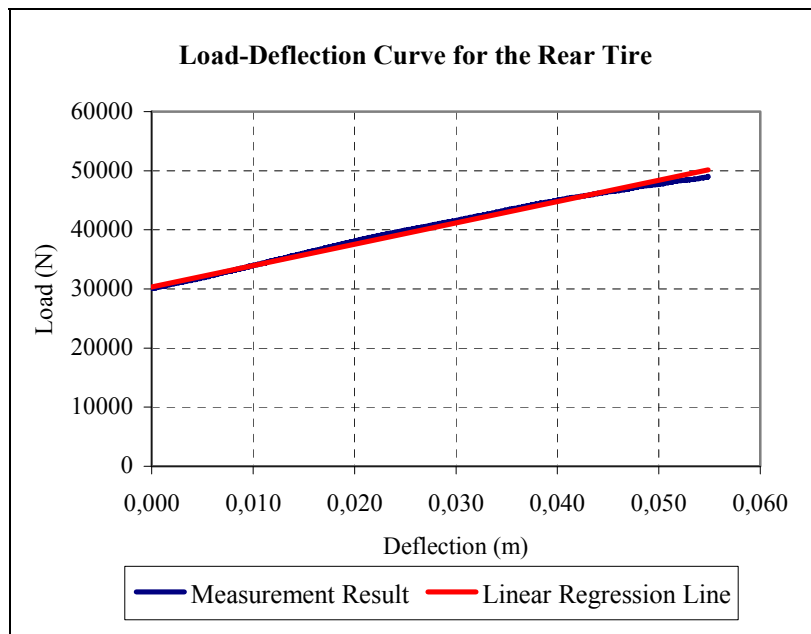


Figure 3.10 - Load-Deflection Curve for the Rear Tire

Drop test is employed to identify the damping coefficients of the front and rear tires. These tests are also repeated with actual machine and nominal tire pressures. As the first step, static loads both on the front and rear axles are estimated. Front axle static load is calculated according to the equation (3.6) when the rear axle is raised on the stabilizer support point shown with S_s in Figure 3.11. The rear axle static load is calculated according to the equation (3.7) when the front axle is raised on the front bucket support point shown with S_b in Figure 3.11. Calculated static load values for the axles are divided by two to obtain the single tire static load values assuming even distribution of the load between two wheels.

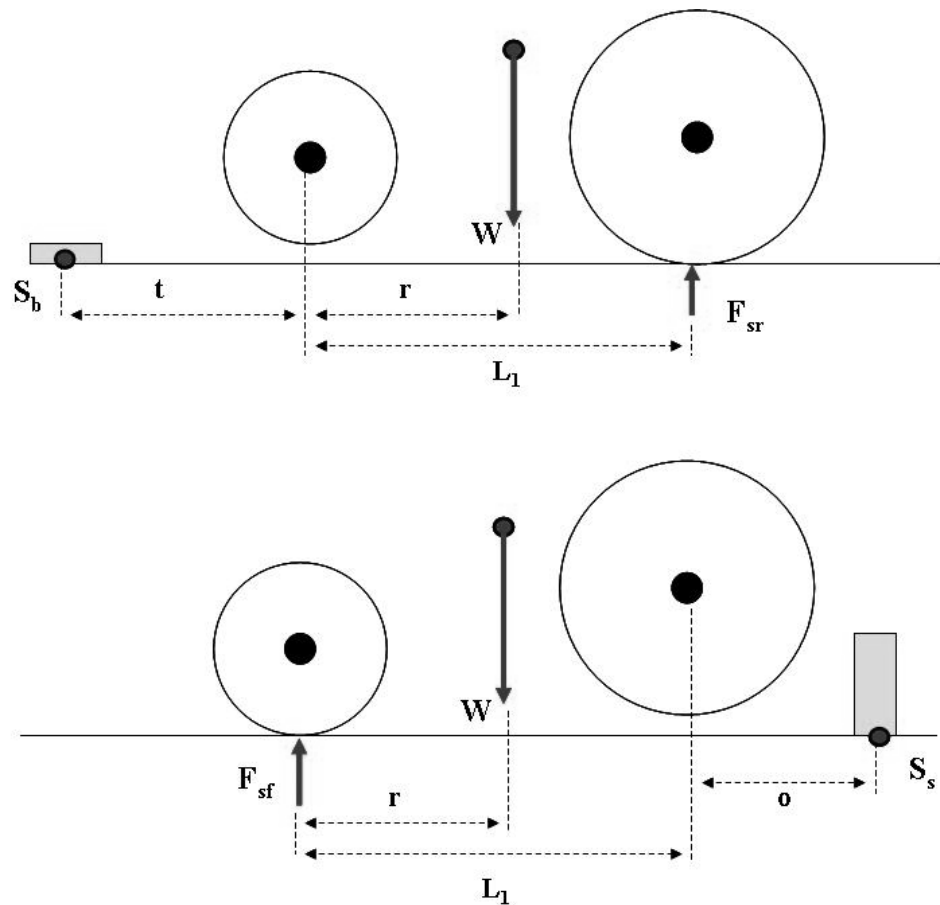


Figure 3.11 - Schematic Representation of the Drop Tests

$$F_{sf} = \frac{W(L_1 - r + o)}{(L_1 + o)} \quad (3.6)$$

$$F_{sr} = \frac{W(r + t)}{(L_1 + t)} \quad (3.7)$$

In the performance of the drop test for the front tire, the front axle of the machine is lifted by a support in such a way that the front tires are just in contact with the ground. Then the front axle is set free by removing the support suddenly and allowed to deform statically under the static tire load. Similar operation is repeated to perform the rear tire drop test. However, in this case the rear axle is lifted on a support and allowed to deform statically under the tire load.

Throughout the drop tests, a wire potentiometric position transducer is mounted on the axles to measure tire displacement response. Location of the position transducer and the support used to lift the front axle are demonstrated in Figure 3.12. Position transducer readings for both front and rear tires are illustrated in Figure 3.13. Using the amplitudes of successive periods of the response, x_1 and x_2 are employed in the logarithmic decrement equation, the damping ratios of front and rear tire, ζ , are found according to

$$\ln \frac{x_1}{x_2} = \frac{2\pi\zeta}{\sqrt{1-\zeta^2}} \quad (3.8)$$

Then, damping coefficients of the front tire, c_{tf} , and rear tire, c_{tr} , are estimated by using the damping ratios, tire stiffness values and static tire loads.

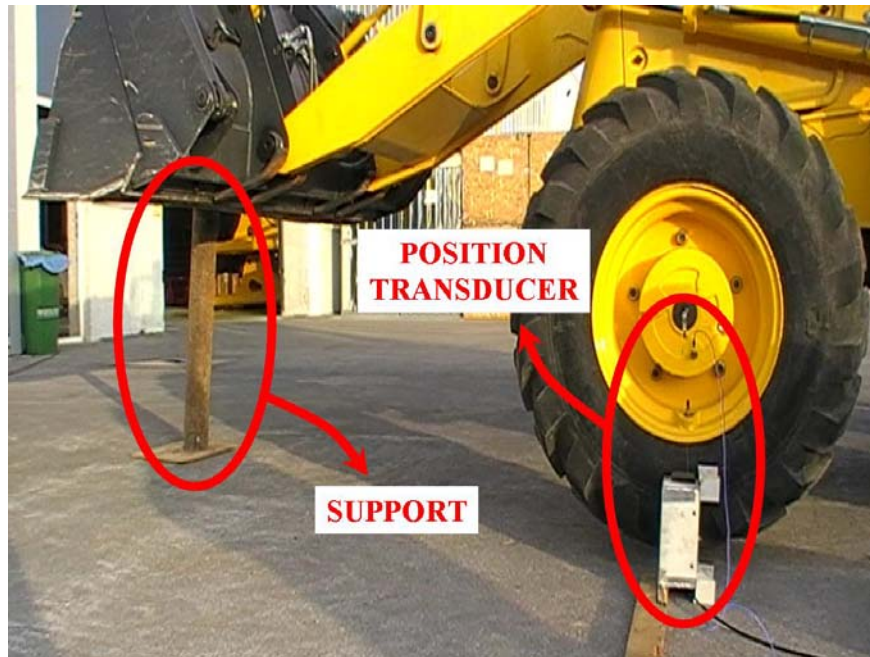


Figure 3.12 - Location of the Position Transducer and Support

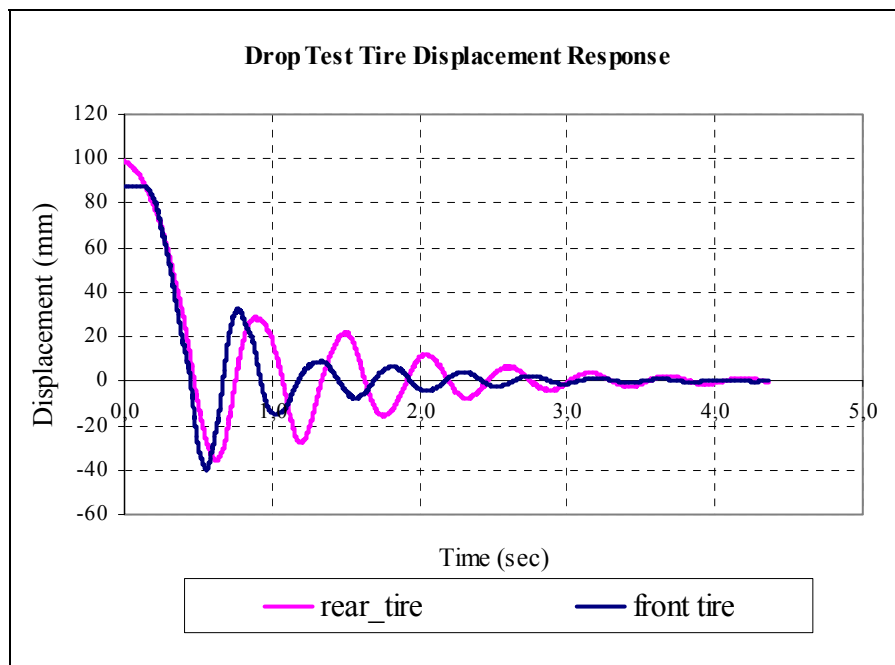


Figure 3.13 – Drop Tests - Tire Displacement Responses

3.2 Identification of Inertial Properties

Inertial parameters that are required to be identified are the mass values, COG positions and the inertia tensor of the cab structure. Mass values are measured easily but it is difficult to acquire the inertia tensor and to locate the center of gravities with measurements. However, use of a 3D computer-aided drawing software gives opportunity to the user to estimate mass and inertia related properties with respect to a selected coordinate system. For this reason, 3D drawings of the rigid parts are generated in Pro/ENGINEER[®] which is a commercial CAD program.

Another reason for the 3D drawings is the SimMechanics' capability of importing 3D body geometries for the visualization of the model. This property of the SimMechanics is a useful tool to represent each body with a 3D geometry and to see whether the initial positions of the bodies with respect to each other are appropriate or not in the simulation environment. However, in order to obtain an accurate model, orientations of the COG coordinate systems in SimMechanics and Pro/ENGINEER should coincide with each other. Moreover, inertia tensor of each part should be defined with respect to the coordinate system located at the COG in SimMechanics.

In order to obtain the mass and inertia properties of a part in Pro/ENGINEER[®], densities of all the components composing that part should be specified. However, it is a very time consuming process to draw all the parts and specify all the densities for complicated assemblies. Therefore, simplified drawings of the cab, seat and operator are used to identify the mass and inertia properties. Operator model is drawn according to the ISO 3164 [23] standard which gives the dimensions of the orthogonal approximation of a large, seated, male operator. In this section, the procedure for obtaining the mass and inertia properties of the simplified cab structure is described as an example. The same procedure is followed for the other rigid bodies

First, location of the COG of the simplified cab structure is found according to the default coordinate system that is generated at an arbitrary position by

Pro/ENGINEER®. Secondly, a new coordinate system is set to the located COG position. Then, a line that is parallel to the longitudinal axis of the cab is drawn on the rear mount –chassis connection point. X axis of the coordinate system located at the COG is aligned with this line. Another line that is perpendicular to the first one is drawn and Z axis of the coordinate system is aligned with this second line while keeping the position of the coordinate system fixed. Thus, the position and orientation of the COG coordinate system are adjusted as shown in Figure 3.14.

Density of the structure is found by dividing the measured mass value to the volume calculated by Pro/ENGINEER. This means that the mass of the whole cab is distributed to the simplified structure homogeneously. Calculated density is entered as a material property and the inertia tensor with respect to the COG coordinate system is obtained from Pro/ENGINEER.

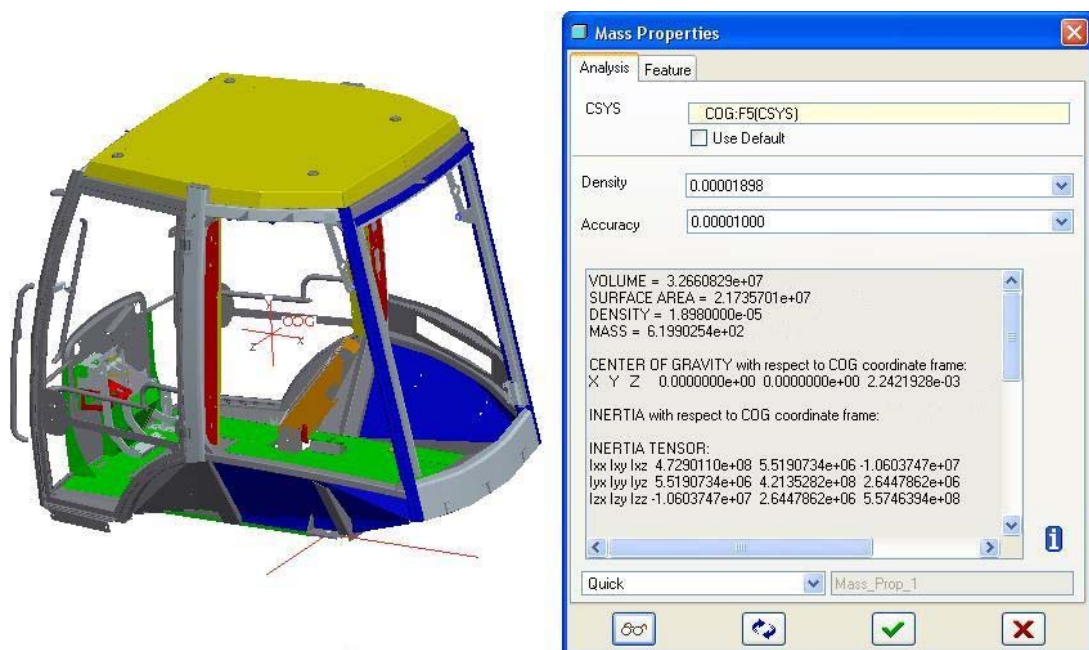


Figure 3.14 – Mass Properties of the Cab Structure

3.3 Development of Analytical Solutions

3.3.1 Cab Model

An approximate analytical solution is developed to describe cab's dynamic behaviour on the basis of the 3 DOF planar model shown in Figure 3.2. Bounce of the cab, pitch of the cab and vertical motion of the seat are represented with three independent coordinates. Vertical and angular displacement of the cab with respect to the longitudinal axis of the cab are defined as y_1 and θ_1 , respectively. Vertical displacement of the seat and operator is defined as y_2 . Positive directions for y_1 and y_2 are taken as the upward direction whereas the counter clockwise direction for θ_1 is taken as positive.

Vertical displacements of the mount-chassis connection points are the inputs to the model. Front mount vertical displacement is named as q_f and rear mount vertical displacement is named as q_r .

Differential equations describing the system behaviour are derived from the equilibrium conditions of the free body diagrams of the cab and seat. Free body diagrams of the cab and the seat are shown in Figure 3.15 and Figure 3.16, respectively. The cab is assumed to be moved from the first position to the second position. In addition, in order to linearize the model, rotation of the cab is assumed to be small that it satisfies the equation $\sin \theta_1 \cong \theta_1$. Then, owing to the linearity assumption vertical displacements of the points A, B, and C can be written as follows:

$$d_A = y_1 - b\theta_1 \quad (3.9)$$

$$d_B = y_1 + (L - b)\theta_1 \quad (3.10)$$

$$d_c = y_1 - (b - a)\theta_1 \quad (3.11)$$

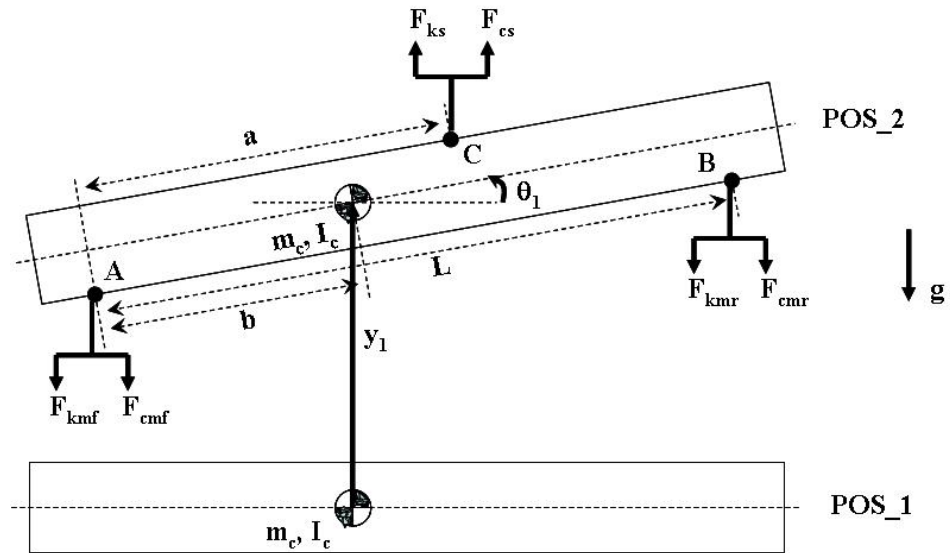


Figure 3.15 – Free Body Diagram of the Cab

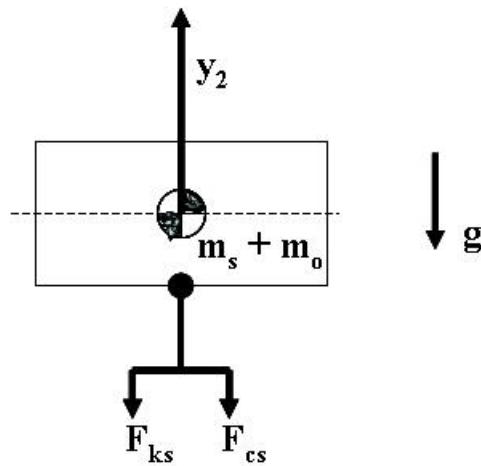


Figure 3.16 – Free Body Diagram of the Seat

Forces developed in the mounts and seat suspension are also demonstrated in the free body diagrams. It is assumed that $d_A > q_f$, $d_B > q_r$ and $y_2 > d_C$, then directions of the forces are drawn accordingly. Spring and dashpot forces are calculated with the following equations:

$$F_{kmf} = k_{mf}(y_1 - b\theta_1 - q_f) \quad (3.12)$$

$$F_{cmf} = c_{mf}(\dot{y}_1 - b\dot{\theta}_1 - \dot{q}_f) \quad (3.13)$$

$$F_{kmr} = k_{mr}(y_1 + (L-b)\theta_1 - q_r) \quad (3.14)$$

$$F_{cmr} = c_{mr}(\dot{y}_1 + (L-b)\dot{\theta}_1 - \dot{q}_r) \quad (3.15)$$

$$F_{ks} = k_s(y_2 - y_1 + (b-a)\theta_1) \quad (3.16)$$

$$F_{cs} = c_s(\dot{y}_2 - \dot{y}_1 + (b-a)\dot{\theta}_1) \quad (3.17)$$

Force and moment balance equations for the cab are given as:

$$m_c \ddot{y}_1 + F_{kmf} + F_{cmf} + F_{kmr} + F_{cmr} - F_{ks} - F_{cs} = 0 \quad (3.18)$$

$$I_c \ddot{\theta}_1 + (F_{kmr} + F_{cmr})(L-b) + (F_{ks} + F_{cs})(b-a) - (F_{kmf} + F_{cmf})b = 0 \quad (3.19)$$

Force balance equation for the seat and operator is expressed as:

$$m_s \ddot{y}_2 + F_{ks} + F_{cs} = 0 \quad (3.20)$$

Equations (3.18), (3.19) and (3.20) are the simplest representation of the differential equations that define the mathematical model. These equations are converted into the

following form by inserting equations (3.12), (3.13), (3.14), (3.15), (3.16) and (3.17) into these equations.

$$\begin{aligned}
\ddot{y}_1 = & -\left(\frac{k_{mf} + k_{mr} + k_s}{m_c}\right)y_1 - \left(\frac{-bk_{mf} + (L-b)k_{mr} - k_s(b-a)}{m_c}\right)\theta_1 + \left(\frac{k_s}{m_c}\right)y_2 \\
& -\left(\frac{c_{mf} + c_{mr} + c_s}{m_c}\right)\dot{y}_1 - \left(\frac{-bc_{mf} + (L-b)c_{mr} - c_s(b-a)}{m_c}\right)\dot{\theta}_1 + \left(\frac{c_s}{m_c}\right)\dot{y}_2 \\
& + \left(\frac{k_{mf}}{m_c}\right)q_f + \left(\frac{k_{mr}}{m_c}\right)q_r + \left(\frac{c_{mf}}{m_c}\right)\dot{q}_f + \left(\frac{c_{mr}}{m_c}\right)\dot{q}_r
\end{aligned} \tag{3.21}$$

$$\begin{aligned}
\ddot{\theta}_1 = & -\left(\frac{k_{mr}(L-b) - k_{mf}b - k_s(b-a)}{I_c}\right)y_1 - \left(\frac{k_{mr}(L-b)^2 + k_{mf}b^2 + k_s(b-a)^2}{I_c}\right)\theta_1 \\
& -\left(\frac{c_{mr}(L-b) - c_{mf}b - c_s(b-a)}{I_c}\right)\dot{y}_1 - \left(\frac{c_{mr}(L-b)^2 + c_{mf}b^2 + c_s(b-a)^2}{I_c}\right)\dot{\theta}_1 \\
& -\left(\frac{k_s(b-a)}{I_c}\right)y_2 - \left(\frac{c_s(b-a)}{I_c}\right)\dot{y}_2 - \left(\frac{k_{mf}b}{I_c}\right)q_f + \left(\frac{k_{mr}(L-b)}{I_c}\right)q_r \\
& -\left(\frac{c_{mf}b}{I_c}\right)\dot{q}_f + \left(\frac{c_{mr}(L-b)}{I_c}\right)\dot{q}_r
\end{aligned} \tag{3.22}$$

$$\begin{aligned}
\ddot{y}_2 = & \left(\frac{k_s}{m_s}\right)y_1 - \left(\frac{k_s(b-a)}{m_s}\right)\theta_1 + \left(\frac{c_s}{m_s}\right)\dot{y}_1 - \left(\frac{c_s(b-a)}{m_s}\right)\dot{\theta}_1 - \left(\frac{k_s}{m_s}\right)y_2 \\
& -\left(\frac{c_s}{m_s}\right)\dot{y}_2
\end{aligned} \tag{3.23}$$

Equations (3.21), (3.22) and (3.23) can be written in the form:

$$[M]\{\ddot{x}\} + [C]\{\dot{x}\} + [K]\{x\} = [F]\{q\} \tag{3.24}$$

where $\{x\} = [y_1 \quad \theta_1 \quad y_2]^T$, $\{q\} = [q_f \quad q_r \quad \dot{q}_f \quad \dot{q}_r]^T$

$$[M] = \begin{bmatrix} m_c & 0 & 0 \\ 0 & I_c & 0 \\ 0 & 0 & m_s \end{bmatrix}$$

$$[C] = \begin{bmatrix} (c_{mf} + c_{mr} + c_s) & (-bc_{mf} + (L-b)c_{mr} - c_s(b-a)) & (-c_s) \\ (c_{mr}(L-b) - c_{mf}b - c_s(b-a)) & (c_{mr}(L-b)^2 + c_{mf}b^2 + c_s(b-a)^2) & (c_s(b-a)) \\ (-c_s) & (c_s(b-a)) & (c_s) \end{bmatrix}$$

$$[K] = \begin{bmatrix} (k_{mf} + k_{mr} + k_s) & (-bk_{mf} + (L-b)k_{mr} - k_s(b-a)) & (-k_s) \\ (k_{mr}(L-b) - k_{mf}b - k_s(b-a)) & (k_{mr}(L-b)^2 + k_{mf}b^2 + k_s(b-a)^2) & (k_s(b-a)) \\ (-k_s) & (k_s(b-a)) & (k_s) \end{bmatrix}$$

$$[F] = \begin{bmatrix} (k_{mf}) & (k_{mr}) & (c_{mf}) & (c_{mr}) \\ (-k_{mf}b) & (k_{mr}(L-b)) & (-c_{mf}b) & (c_{mr}(L-b)) \\ 0 & 0 & 0 & 0 \end{bmatrix}$$

“State-Space” block is utilized for the analytical solution as shown in Figure 3.17. This block makes implementation of the system to the Simulink easier. However, for the use of “State-Space” block, system should be expressed in the following form:

$$\begin{aligned} \{\dot{x}\} &= [A]\{x\} + [B]\{u\} \\ \{y\} &= [C]\{x\} + [D]\{u\} \end{aligned} \quad (3.25)$$

where $\{x\}$ is the state vector, $\{u\}$ is the input vector, and $\{y\}$ is the output vector. For the solution, equation (3.24) is converted into the state space form by using the state vector $\{x\} = [y_1 \quad \dot{y}_1 \quad \theta_1 \quad \dot{\theta}_1 \quad y_2 \quad \dot{y}_2]^T$ and input vector $\{u\} = [q_f \quad \dot{q}_f \quad q_r \quad \dot{q}_r]^T$. $[C]$ is taken as 6x6 identity matrix and $[D]$ is taken as 6x4 zero matrix. $[A]$ is written in the form $[A]_{6 \times 6} = [[T]_{6 \times 3} [U]_{6 \times 3}]$. Then, $[T]$, $[U]$ and $[B]$ is given as:

$$[T] = \begin{bmatrix} 0 & 1 & 0 \\ -\left(\frac{k_{mf} + k_{mr} + k_s}{m_c}\right) & -\left(\frac{c_{mf} + c_{mr} + c_s}{m_c}\right) & -\left(\frac{-bk_{mf} + (L-b)k_{mr} - k_s(b-a)}{m_c}\right) \\ 0 & 0 & 0 \\ -\left(\frac{k_{mr}(L-b) - k_{mf}b - k_s(b-a)}{I_c}\right) & -\left(\frac{c_{mr}(L-b) - c_{mf}b - c_s(b-a)}{I_c}\right) & -\left(\frac{k_{mr}(L-b)^2 + k_{mf}b^2 + k_s(b-a)^2}{I_c}\right) \\ 0 & 0 & 0 \\ \left(\frac{k_s}{m_s}\right) & \left(\frac{c_s}{m_s}\right) & -\left(\frac{k_s(b-a)}{m_s}\right) \end{bmatrix}$$

$$[U] = \begin{bmatrix} 0 & 0 & 0 \\ -\left(\frac{-bk_{mf} + (L-b)c_{mr} - c_s(b-a)}{m_c}\right) & \left(\frac{k_s}{m_c}\right) & \left(\frac{c_s}{m_c}\right) \\ 1 & 0 & 0 \\ -\left(\frac{c_{mr}(L-b)^2 + c_{mf}b^2 + c_s(b-a)^2}{I_c}\right) & -\left(\frac{k_s(b-a)}{I_c}\right) & -\left(\frac{c_s(b-a)}{I_c}\right) \\ 0 & 0 & 1 \\ -\left(\frac{c_s(b-a)}{m_s}\right) & -\left(\frac{k_s}{m_s}\right) & -\left(\frac{c_s}{m_s}\right) \end{bmatrix}$$

$$[B] = \begin{bmatrix} 0 & 0 & 0 & 0 \\ \left(\frac{k_{mf}}{m_c}\right) & \left(\frac{c_{mf}}{m_c}\right) & \left(\frac{k_{mr}}{m_c}\right) & \left(\frac{c_{mr}}{m_c}\right) \\ 0 & 0 & 0 & 0 \\ -\left(\frac{k_{mf} \cdot b}{I_c}\right) & -\left(\frac{c_{mf}b}{I_c}\right) & \left(\frac{k_{mr}(L-b)}{I_c}\right) & \left(\frac{c_{mr}(L-b)}{I_c}\right) \\ 0 & 0 & 0 & 0 \\ 0 & 0 & 0 & 0 \end{bmatrix}$$

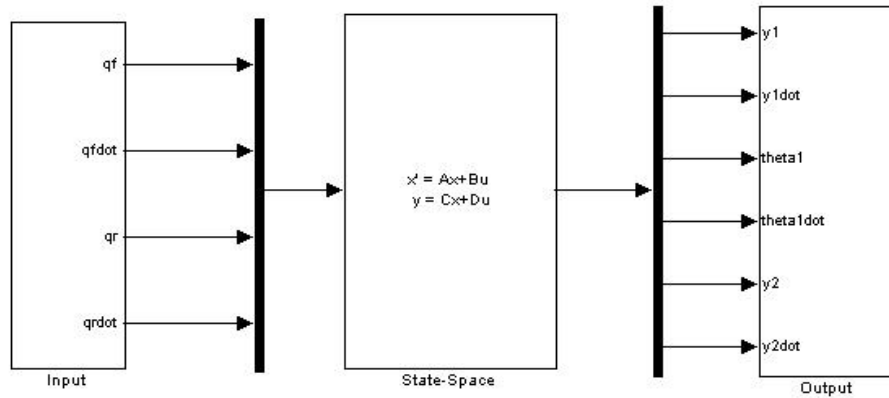


Figure 3.17 – Implementation of Analytical Solution of the Cab to Simulink

3.3.2 Extended Machine Model

Analytical solution developed for the cab is extended for the whole machine on the basis of the 5 DOF planar model shown in Figure 3.3. In addition to the independent coordinates defined in the cab model, two independent coordinates are presented for the vertical and pitch motion of the machine body. Vertical displacement of the machine body is defined as y_3 , and angular displacement of the machine body with respect to the longitudinal axis of the machine is defined as θ_3 . Positive direction for y_3 is taken as the upward direction whereas the counter clockwise direction for θ_3 is taken as positive.

Inputs to the extended machine model are vertical displacements of the front and rear tires. Vertical displacements of the front and rear tires are named as q_{ff} and q_{rr} , respectively.

Forces developed in the mounts, seat suspension and tires are also demonstrated in the free body diagrams. It is assumed that $d_F > q_{if}$, $d_G > q_{tr}$, $d_A > d_D$, $d_B > d_E$ and $y_2 > d_C$, then directions of the forces are drawn accordingly. Spring and dashpot force generated in the seat suspension are given in equations (3.16) and (3.17), and remains same for the extended model. However, tire and mount forces for the extended model are calculated with the following equations:

$$F'_{kmf} = k_{mf} (y_1 - b\theta_1 - y_3 + (g - d)\theta_3) \quad (3.30)$$

$$F'_{cmf} = c_{mf} (\dot{y}_1 - b\dot{\theta}_1 - \dot{y}_3 + (g - d)\dot{\theta}_3) \quad (3.31)$$

$$F'_{kmr} = k_{mr} (y_1 + (L - b)\theta_1 - y_3 - (e - g)\theta_3) \quad (3.32)$$

$$F'_{cmr} = c_{mr} (\dot{y}_1 + (L - b)\dot{\theta}_1 - \dot{y}_3 - (e - g)\dot{\theta}_3) \quad (3.33)$$

$$F_{k_{if}} = k_{if} (y_3 - g\theta_3 - q_{if}) \quad (3.34)$$

$$F_{c_{if}} = c_{if} (\dot{y}_3 - g\dot{\theta}_3 - \dot{q}_{if}) \quad (3.35)$$

$$F_{k_{tr}} = k_{tr} (y_3 + (L_1 - g)\theta_3 - q_{tr}) \quad (3.36)$$

$$F_{c_{tr}} = c_{tr} (\dot{y}_3 + (L_1 - g)\dot{\theta}_3 - \dot{q}_{tr}) \quad (3.37)$$

Force balance equation of the seat and operator is given in equation (3.20), force and moment balance equations of the cab for the extended model are expressed as:

$$m_c \ddot{y}_1 + F'_{kmf} + F'_{cmf} + F'_{kmr} + F'_{cmr} - F_{ks} - F_{cs} = 0 \quad (3.38)$$

$$I_c \ddot{\theta}_1 + (F'_{kmr} + F'_{cmr})(L-b) + (F_{ks} + F_{cs})(b-a) - (F'_{kmf} + F'_{cmf})b = 0 \quad (3.39)$$

Force and moment balance equations for the machine body are given as:

$$m_b \ddot{y}_3 + F_{ktf} + F_{ctf} + F_{ktr} + F_{ctr} - F'_{kmf} - F'_{cmf} - F'_{kmr} - F'_{cmr} = 0 \quad (3.40)$$

$$I_b \ddot{\theta}_3 - (F_{ktf} + F_{ctf})g + (F'_{kmf} + F'_{cmf})(g-d) - (F'_{kmr} + F'_{cmr})(e-g) + (F_{ktr} + F_{ctr})(L_1 - g) = 0 \quad (3.41)$$

Equations (3.20), (3.38), (3.39), (3.40), and (3.41) are the simplest representation of the differential equations that define the mathematical model of the whole machine ride dynamics. These equations are converted into the following form by inserting equations (3.16), (3.17), (3.30), (3.31), (3.32), (3.33), (3.34), (3.35), (3.36), and (3.37) into these equations.

$$\begin{aligned} \ddot{y}_3 = & \left(\frac{-k_{tf} - k_{tr} - k_{mf} - k_{mr}}{m_b} \right) y_3 + \left(\frac{-c_{tf} - c_{tr} - c_{mf} - c_{mr}}{m_b} \right) \dot{y}_3 + \left(\frac{k_{tf}}{m_b} \right) q_{tf} + \left(\frac{c_{tf}}{m_b} \right) \dot{q}_{tf} \\ & + \left(\frac{k_{tf}g - k_{tr}(L_1 - g) + k_{mf}(g-d) - k_{mr}(e-g)}{m_b} \right) \theta_3 + \left(\frac{-k_{mf}b + k_{mr}(L-b)}{m_b} \right) \theta_1 \\ & + \left(\frac{c_{tf}g - c_{tr}(L_1 - g) + c_{mf}(g-d) - c_{mr}(e-g)}{m_b} \right) \dot{\theta}_3 + \left(\frac{-c_{mf}b + c_{mr}(L-b)}{m_b} \right) \dot{\theta}_1 \\ & + \left(\frac{k_{mf} + k_{mr}}{m_b} \right) y_1 + \left(\frac{c_{mf} + c_{mr}}{m_b} \right) \dot{y}_1 + \left(\frac{k_{tr}}{m_b} \right) q_{tr} + \left(\frac{c_{tr}}{m_b} \right) \dot{q}_{tr} \end{aligned} \quad (3.42)$$

$$\begin{aligned}
\ddot{\theta}_3 = & \left(\frac{k_{tf}g - k_{tr}(L_1 - g) + k_{mf}(g - d) - k_{mr}(e - g)}{I_b} \right) y_3 + \left(\frac{k_{tr}(L_1 - g)}{I_b} \right) q_{tr} \\
& + \left(\frac{c_{tf}g - c_{tr}(L_1 - g) + c_{mf}(g - d) - c_{mr}(e - g)}{I_b} \right) \dot{y}_3 + \left(\frac{c_{tr}(L_1 - g)}{I_b} \right) \dot{q}_{tr} \\
& + \left(\frac{-k_{tf}g^2 - k_{tr}(L_1 - g)^2 - k_{mf}(g - d)^2 - k_{mr}(e - g)^2}{I_b} \right) \theta_3 + \left(\frac{-k_{tf}g}{I_b} \right) q_{tf} \\
& + \left(\frac{-c_{tf}g^2 - c_{tr}(L_1 - g)^2 - c_{mf}(g - d)^2 - c_{mr}(e - g)^2}{I_b} \right) \dot{\theta}_3 + \left(\frac{-c_{tf}g}{I_b} \right) \dot{q}_{tf} \\
& + \left(\frac{k_{mf}b(g - d) + k_{mr}(e - g)(L - b)}{I_b} \right) \theta_1 + \left(\frac{-k_{mf}(g - d) + k_{mr}(e - g)}{I_b} \right) y_1 \\
& + \left(\frac{c_{mf}b(g - d) + c_{mr}(e - g)(L - b)}{I_b} \right) \dot{\theta}_1 + \left(\frac{-c_{mf}(g - d) + c_{mr}(e - g)}{I_b} \right) \dot{y}_1 \quad (3.43)
\end{aligned}$$

$$\begin{aligned}
\ddot{y}_1 = & \left(\frac{k_{mf} + k_{mr}}{m_c} \right) y_3 + \left(\frac{c_{mf} + c_{mr}}{m_c} \right) \dot{y}_3 + \left(\frac{-k_{mf} - k_{mr} - k_s}{m_c} \right) y_1 + \left(\frac{-c_{mf} - c_{mr} - c_s}{m_c} \right) \dot{y}_1 \\
& + \left(\frac{k_{mf}b - k_{mr}(L - b) + k_s(b - a)}{m_c} \right) \theta_1 + \left(\frac{-k_{mf}(g - d) + k_{mr}(e - g)}{m_c} \right) \theta_3 \\
& + \left(\frac{-c_{mf}(g - d) + c_{mr}(e - g)}{m_c} \right) \dot{\theta}_3 + \left(\frac{c_{mf}b - c_{mr}(L - b) + c_s(b - a)}{m_c} \right) \dot{\theta}_1 \\
& + \left(\frac{k_s}{m_c} \right) y_2 + \left(\frac{c_s}{m_c} \right) \dot{y}_2 \quad (3.44)
\end{aligned}$$

$$\begin{aligned}
\ddot{\theta}_1 = & \left(\frac{-k_{mr}(L - b)^2 - k_{mf}b^2 - k_s(b - a)^2}{I_c} \right) \theta_1 + \left(\frac{k_{mr}(L - b) - k_{mf}b}{I_c} \right) y_3 \\
& + \left(\frac{-c_{mr}(L - b)^2 - c_{mf}b^2 - c_s(b - a)^2}{I_c} \right) \dot{\theta}_1 + \left(\frac{c_{mr}(L - b) - c_{mf}b}{I_c} \right) \dot{y}_3 \\
& + \left(\frac{c_{mf}b(g - d) + c_{mr}(e - g)(L - b)}{I_c} \right) \dot{\theta}_3 + \left(\frac{-k_{mr}(L - b) + k_{mf}b + k_s(b - a)}{I_c} \right) y_1 \\
& + \left(\frac{k_{mf}b(g - d) + k_{mr}(e - g)(L - b)}{I_c} \right) \theta_3 + \left(\frac{-c_{mr}(L - b) + c_{mf}b + c_s(b - a)}{I_c} \right) \dot{y}_1 \\
& + \left(\frac{-k_s(b - a)}{I_c} \right) y_2 + \left(\frac{-c_s(b - a)}{I_c} \right) \dot{y}_2 \quad (3.45)
\end{aligned}$$

Equations (3.23), (3.42), (3.43), (3.44) and (3.45) can be written in the form:

$$[M]\{\ddot{x}\} + [C]\{\dot{x}\} + [K]\{x\} = [F]\{q\} \quad (3.46)$$

where $\{x\} = [y_3 \quad \theta_3 \quad y_1 \quad \theta_1 \quad y_2]^T$, $\{q\} = [q_{tf} \quad \dot{q}_{tf} \quad q_{tr} \quad \dot{q}_{tr}]^T$. The damping matrix, $[C]$, is written the form $[C]_{5 \times 5} = [[N]_{5 \times 2} [O]_{5 \times 3}]$ and the stiffness matrix, $[K]$, is written the form $[K]_{5 \times 5} = [[P]_{5 \times 2} [Q]_{5 \times 3}]$. Then, $[M]$, $[N]$, $[O]$, $[P]$, $[Q]$, and $[F]$ are give as:

$$[M] = \begin{bmatrix} m_b & 0 & 0 & 0 & 0 \\ 0 & I_b & 0 & 0 & 0 \\ 0 & 0 & m_c & 0 & 0 \\ 0 & 0 & 0 & I_c & 0 \\ 0 & 0 & 0 & 0 & m_s \end{bmatrix}$$

$$[N] = \begin{bmatrix} -(-c_{jf} - c_{tr} - c_{mf} - c_{mr}) & -(c_{jf}g - c_{tr}(L_1 - g) + c_{mf}(g - d) - c_{mr}(e - g)) \\ -(c_{jf}g - c_{tr}(L_1 - g) + c_{mf}(g - d) - c_{mr}(e - g)) & -(c_{jf}g^2 - c_{tr}(L_1 - g)^2 - c_{mf}(g - d)^2 - c_{mr}(e - g)^2) \\ -(c_{mf} + c_{mr}) & -(-c_{mf}(g - d) + c_{mr}(e - g)) \\ -(c_{mr}(L - b) - c_{mf}b) & -(c_{mf}b(g - d) + c_{mr}(e - g)(L - b)) \\ 0 & 0 \end{bmatrix}$$

$$[O] = \begin{bmatrix} -(c_{mf} + c_{mr}) & -(-c_{mf}b + c_{mr}(L - b)) & 0 \\ -(-c_{mf}(g - d) + c_{mr}(e - g)) & -(c_{mf}b(g - d) + c_{mr}(e - g)(L - b)) & 0 \\ -(-c_{mf} - c_{mr} - c_s) & -(c_{mf}b - c_{mr}(L - b) + c_s(b - a)) & -c_s \\ -(c_{mf}b - c_{mr}(L - b) + c_s(b - a)) & -(c_{mr}(L - b)^2 - c_{mf}b^2 - c_s(b - a)^2) & -(c_s(b - a)) \\ -c_s & -(-c_s(b - a)) & c_s \end{bmatrix}$$

$$[P] = \begin{bmatrix} -(k_{jf} - k_{tr} - k_{mf} - k_{mr}) & -(k_{jf}g - k_{tr}(L_1 - g) + k_{mf}(g - d) - k_{mr}(e - g)) \\ -(k_{jf}g - k_{tr}(L_1 - g) + k_{mf}(g - d) - k_{mr}(e - g)) & -(k_{jf}g^2 - k_{tr}(L_1 - g)^2 - k_{mf}(g - d)^2 - k_{mr}(e - g)^2) \\ -(k_{mf} + k_{mr}) & -(-k_{mf}(g - d) + k_{mr}(e - g)) \\ -(k_{mr}(L - b) - k_{mf}b) & -(k_{mf}b(g - d) + k_{mr}(e - g)(L - b)) \\ 0 & 0 \end{bmatrix}$$

$$[Q] = \begin{bmatrix} -(k_{mf} + k_{mr}) & -(-k_{mf}b + k_{mr}(L-b)) & 0 \\ -(-k_{mf}(g-d) + k_{mr}(e-g)) & -(k_{mf}b(g-d) + k_{mr}(e-g)(L-b)) & 0 \\ -(-k_{mf} - k_{mr} - k_s) & -(k_{mf}b - k_{mr}(L-b) + k_s(b-a)) & -k_s \\ -(k_{mf}b - k_{mr}(L-b) + k_s(b-a)) & -(-k_{mr}(L-b)^2 - k_{mf}b^2 - k_s(b-a)^2) & -(-k_s(b-a)) \\ -k_s & -(-k_s(b-a)) & k_s \end{bmatrix}$$

$$[F] = \begin{bmatrix} k_{if} & c_{if} & k_{ir} & c_{ir} \\ -k_{if}g & -c_{if}g & k_{ir}(L_1 - g) & c_{ir}(L_1 - g) \\ 0 & 0 & 0 & 0 \\ 0 & 0 & 0 & 0 \\ 0 & 0 & 0 & 0 \end{bmatrix}$$

Similar to the cab model, “State-Space” block is utilized for the analytical solution of the extended machine model as shown in Figure 3.19. For the use of “State-Space” block, system is expressed in the following form:

$$\begin{aligned} \{\dot{x}\} &= [A]\{x\} + [B]\{u\} \\ \{y\} &= [C]\{x\} + [D]\{u\} \end{aligned} \quad (3.47)$$

where $\{x\}$ is the state vector, $\{u\}$ is the input vector, and $\{y\}$ is the output vector. For the solution, equation (3.46) is converted into the state space form by using the state vector $\{x\} = [y_3 \quad \dot{y}_3 \quad \theta_3 \quad \dot{\theta}_3 \quad y_1 \quad \dot{y}_1 \quad \theta_1 \quad \dot{\theta}_1 \quad y_2 \quad \dot{y}_2]^T$ and input vector $\{u\} = [q_{if} \quad \dot{q}_{if} \quad q_{ir} \quad \dot{q}_{ir}]^T$. $[C]$ is taken as 10x10 identity matrix and $[D]$ is taken as 10x4 zero matrix. $[A]$ is written in the form $[A]_{10 \times 10} = [[R]_{10 \times 3} [S]_{10 \times 3} [T]_{10 \times 4}]$. Then, $[R]$, $[S]$, $[T]$ and $[B]$ are given as:

$$[R] = \begin{bmatrix} 0 & 1 & 0 \\ \frac{-k_{yf} - k_{yr} - k_{mf} - k_{mr}}{m_b} & \frac{-c_{yf} - c_{yr} - c_{mf} - c_{mr}}{m_b} & \frac{k_{yf}g - k_{yr}(L_1 - g) + k_{mf}(g - d) - k_{mr}(e - g)}{m_b} \\ 0 & 0 & 0 \\ \frac{k_{yf}g - k_{yr}(L_1 - g) + k_{mf}(g - d) - k_{mr}(e - g)}{I_b} & \frac{c_{yf}g - c_{yr}(L_1 - g) + c_{mf}(g - d) - c_{mr}(e - g)}{I_b} & \frac{-k_{yf}g^2 - k_{yr}(L_1 - g)^2 - k_{mf}(g - d)^2 - k_{mr}(e - g)^2}{I_b} \\ 0 & 0 & 0 \\ \frac{k_{mf} + k_{mr}}{m_c} & \frac{c_{mf} + c_{mr}}{m_c} & \frac{-k_{mf}(g - d) + k_{mr}(e - g)}{m_c} \\ 0 & 0 & 0 \\ \frac{k_{mr}(L - b) - k_{mf}b}{I_c} & \frac{c_{mr}(L - b) - c_{mf}b}{I_c} & \frac{k_{mf}b(g - d) + k_{mr}(e - g)(L - b)}{I_c} \\ 0 & 0 & 0 \\ 0 & 0 & 0 \end{bmatrix}$$

$$[S] = \begin{bmatrix} 0 & 0 & 0 \\ \frac{c_{yf}g - c_{yr}(L_1 - g) + c_{mf}(g - d) - c_{mr}(e - g)}{m_b} & \frac{k_{mf} + k_{mr}}{m_b} & \frac{c_{mf} + c_{mr}}{m_b} \\ 1 & 0 & 0 \\ \frac{-c_{yf}g^2 - c_{yr}(L_1 - g)^2 - c_{mf}(g - d)^2 - c_{mr}(e - g)^2}{I_b} & \frac{-k_{mf}(g - d) + k_{mr}(e - g)}{I_b} & \frac{-c_{mf}(g - d) + c_{mr}(e - g)}{I_b} \\ 0 & 0 & 1 \\ \frac{-c_{mf}(g - d) + c_{mr}(e - g)}{m_c} & \frac{-k_{mf} - k_{mr} - k_s}{m_c} & \frac{-c_{mf}(g - d) + c_{mr}(e - g)}{I_b} \\ 0 & 0 & 0 \\ \frac{c_{mf}b(g - d) + c_{mr}(e - g)(L - b)}{I_c} & \frac{-k_{mr}(L - b) + k_{mf}b + k_s(b - a)}{I_c} & \frac{-c_{mr}(L - b) + c_{mf}b + c_s(b - a)}{I_c} \\ 0 & 0 & 0 \\ 0 & \frac{k_s}{m_s} & \frac{c_s}{m_s} \end{bmatrix}$$

$$[T] = \begin{bmatrix} 0 & 0 & 0 & 0 \\ \frac{-k_{mj}b + k_{mr}(L-b)}{m_b} & \frac{-c_{mj}b + c_{mr}(L-b)}{m_b} & 0 & 0 \\ 0 & 0 & 0 & 0 \\ \frac{k_{mj}b(g-d) + k_{mr}(e-g)(L-b)}{I_b} & \frac{c_{mj}b(g-d) + c_{mr}(e-g)(L-b)}{I_b} & 0 & 0 \\ 0 & 0 & 0 & 0 \\ \frac{k_{mj}b - k_{mr}(L-b) + k_s(b-a)}{m_c} & \frac{c_{mj}b - c_{mr}(L-b) + c_s(b-a)}{m_c} & \frac{k_s}{m_c} & \frac{c_s}{m_c} \\ 0 & 1 & 0 & 0 \\ \frac{-k_{mr}(L-b)^2 - k_{mj}b^2 - k_s(b-a)^2}{I_c} & \frac{-c_{mr}(L-b)^2 - c_{mj}b^2 - c_s(b-a)^2}{I_c} & \frac{-k_s(b-a)}{I_c} & \frac{-c_s(b-a)}{I_c} \\ 0 & 0 & 0 & 1 \\ \frac{-k_s(b-a)}{m_s} & \frac{-c_s(b-a)}{m_s} & \frac{-k_s}{m_c} & \frac{-c_s}{m_c} \end{bmatrix}$$

$$[B] = \begin{bmatrix} 0 & 0 & 0 & 0 \\ \frac{k_{jf}}{m_b} & \frac{c_{jf}}{m_b} & \frac{k_{jr}}{m_b} & \frac{c_{jr}}{m_b} \\ 0 & 0 & 0 & 0 \\ \frac{-k_{jf}g}{I_b} & \frac{-c_{jf}g}{I_b} & \frac{k_{jr}(L_1-g)}{I_b} & \frac{c_{jr}(L_1-g)}{I_b} \\ 0 & 0 & 0 & 0 \\ 0 & 0 & 0 & 0 \\ 0 & 0 & 0 & 0 \\ 0 & 0 & 0 & 0 \\ 0 & 0 & 0 & 0 \\ 0 & 0 & 0 & 0 \end{bmatrix}$$

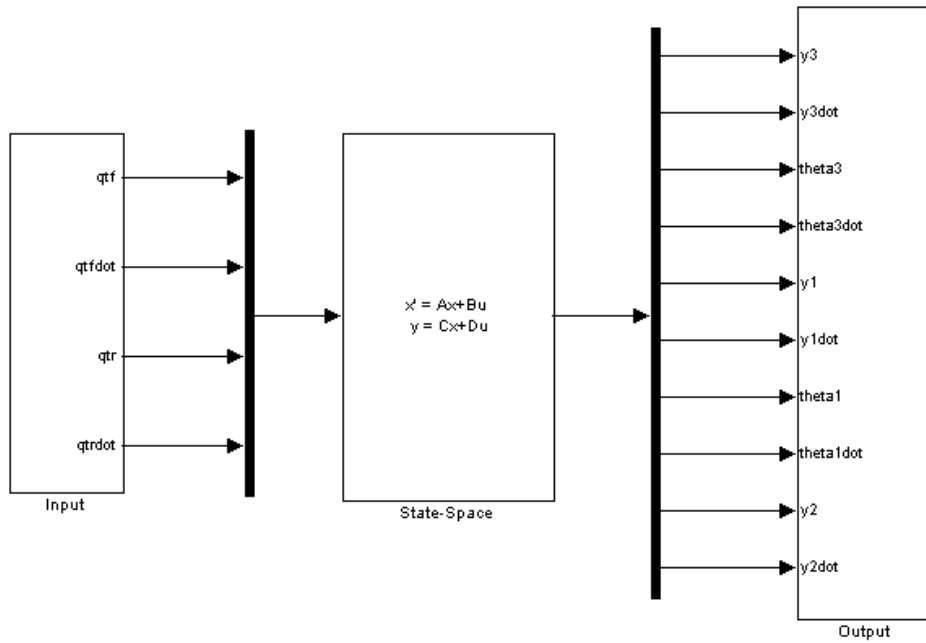


Figure 3.19 - Implementation of Analytical Solution of Machine Model to Simulink

3.4 Development of SimMechanics Solutions

3.4.1 Cab Model

SimMechanics uses an internally defined fixed coordinate system called “World”. This coordinate system is located at the (0,0,0) position and +X axis points right, +Y axis points up as default.

“Body” blocks from the SimMechanics library are used to model the rigid bodies like cab, seat and operator. Connection points to the ground or other rigid bodies are defined by body coordinate systems in each “Body” blocks. Positions and orientations of these coordinate systems will be defined according to the world

coordinate system or another body coordinate system in SimMechanics. In the developed model, orientations of all the body coordinate systems are the same as with the world coordinate system and their positions are measured from the 3D drawings of the rigid parts created in ProEngineer. While measuring the positions, X axis is taken as the longitudinal axis of the machine and Y axis taken as the vertical axis of the machine. Definition of the positions of the body coordinate systems for the cab is given in Figure 3.20 as an example. In addition, mass and inertia properties of the rigid parts are specified for the “Body” blocks.

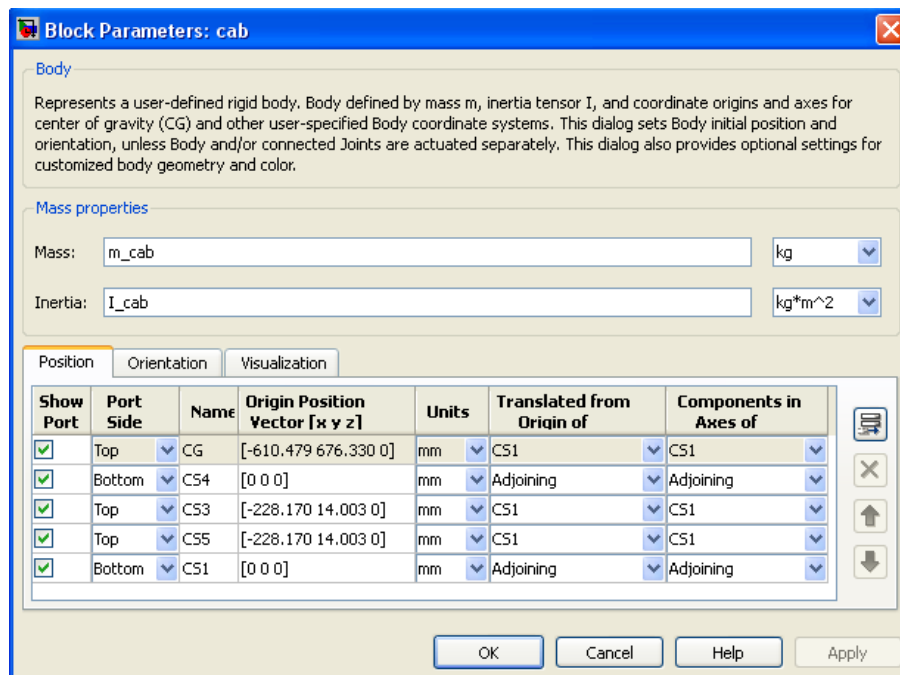


Figure 3.20 – Definition of the Positions of the Body Coordinate Systems of the Cab

Fixed points of a model are represented by “Ground” blocks in SimMechanics and positions of these blocks are specified with respect to “World” coordinate system. Two “Ground” blocks are used in the model. One of them is located at (0,0,0)

position and used to define the chassis point that is connected to the front mount. The other one is located to the (1250.66,10.523,0) position and used to define the chassis point that is connected to the rear mount.

“Ground” blocks representing chassis points are connected to the cab with “Custom Joint” blocks which are user-defined joints with multiple degrees of freedom. “Custom Joint” at the front mount is defined with 3 DOF namely linear translation in the Y axis, linear translation in the X axis and angular rotation with respect to the Z axis. However, “Custom Joint” at the rear mount is defined with 2 DOF which are linear translation in the Y axis and angular rotation with respect to the Z axis. An extra degree of freedom given to the front mount location is necessary to allow the pitch motion of the cab. The seat is connected to the cab with a “Prismatic Joint” block which represents the translational DOF of the seat in the vertical direction. “Weld” block is used to connect the seat and operator. This block has no degrees of freedom. Therefore, it is assumed that seat and operator are rigidly connected with each other throughout the simulation.

Seat suspension and mounts are modeled by generating the elastic and damping forces caused by these elements and supplying them to the joint blocks. For the mount model, displacement and velocity of the mount connection points on the cab side are measured and they are subtracted from the displacement and velocity of the mount connection points of the chassis which are the inputs to the system. In this way, relative displacement and velocity between the cab and the chassis are achieved. In order to obtain the forces developed in the mounts, relative displacement and velocity between the cab and chassis are multiplied with the mount stiffness and damping coefficient values via “Gain” blocks. Then, acquired forces are summed and supplied to the joint between the cab and the chassis in the vertical direction by means of “Joint Actuator” block. A similar subsystem is constructed for the seat suspension. In this case, relative displacement and velocity between the seat and the cab are measured and these values are multiplied with the seat suspension stiffness and damping coefficient values.

Visualization of the system is obtained by importing external graphics files to the SimMechanics. Three-dimensional drawings of the rigid parts are exported into Stereolithographic (STL) file format because it is the only format that is supported by the SimMechanics' custom body visualization option. This option gives the opportunity to realize actual geometries of the parts on the visualization screen. While exporting the STL files, coordinate systems located at the COG in ProEngineer is selected and these graphic files are attached to the COG coordinate systems defined in SimMechanics. In this way, accurate model visualization is acquired. Visualization of the model in SimMechanics that shows the body geometries, location of center of gravities and body coordinate systems are illustrated in Figure 3.21 and the developed SimMechanics solution is demonstrated in Figure 3.22.

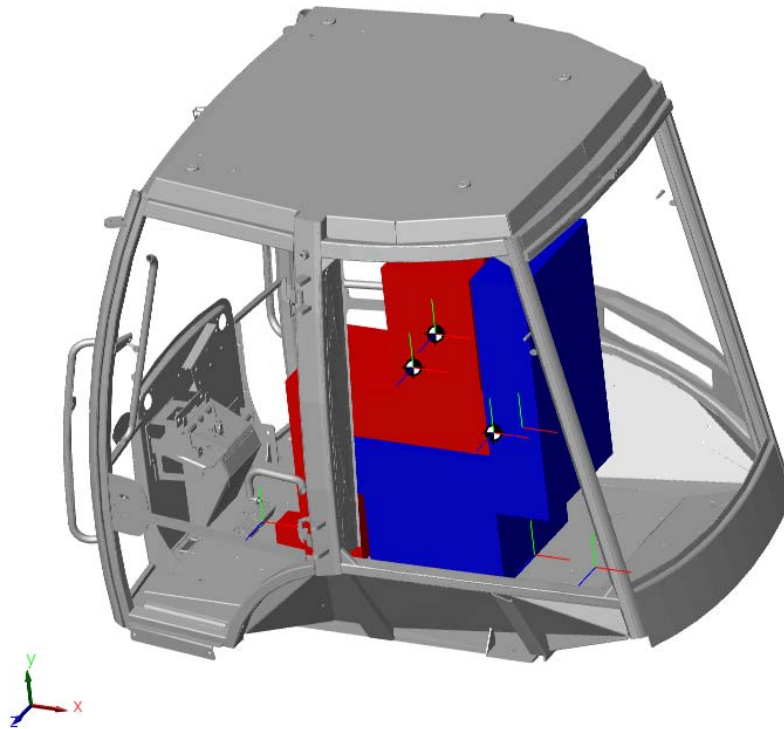


Figure 3.21 - Visualization of the Cab Model in SimMechanics

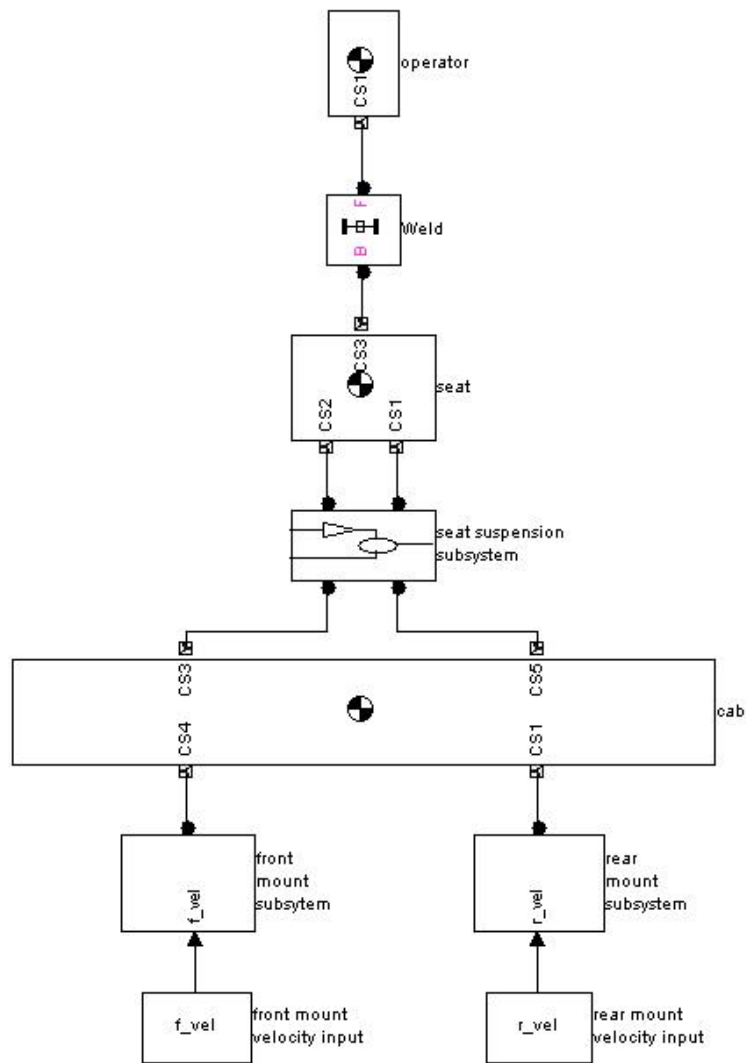


Figure 3.22 – SimMechanics Solution of the Cab

3.4.2 Extended Machine Model

Extended machine model in SimMechanics is obtained by inserting machine body and tire parameters to the cab model. Machine body seen in Figure 3.3 is not modeled with a single “Body Block” in SimMechanics. Parts that are assembled to

the machine like engine, transmission, axles, backhoe and loader mechanisms are assumed to be rigidly connected to the chassis. These parts are defined with separate body blocks in a subsystem and they are connected to the chassis with “Weld” blocks (Figure 3.23). Defining parts in this way allows calculating the inertia and mass properties of the each part separately by the help of a CAD program like ProEngineer. Calculation of the mass and inertia properties of the parts are done by applying the same procedure explained in Section 3.2.

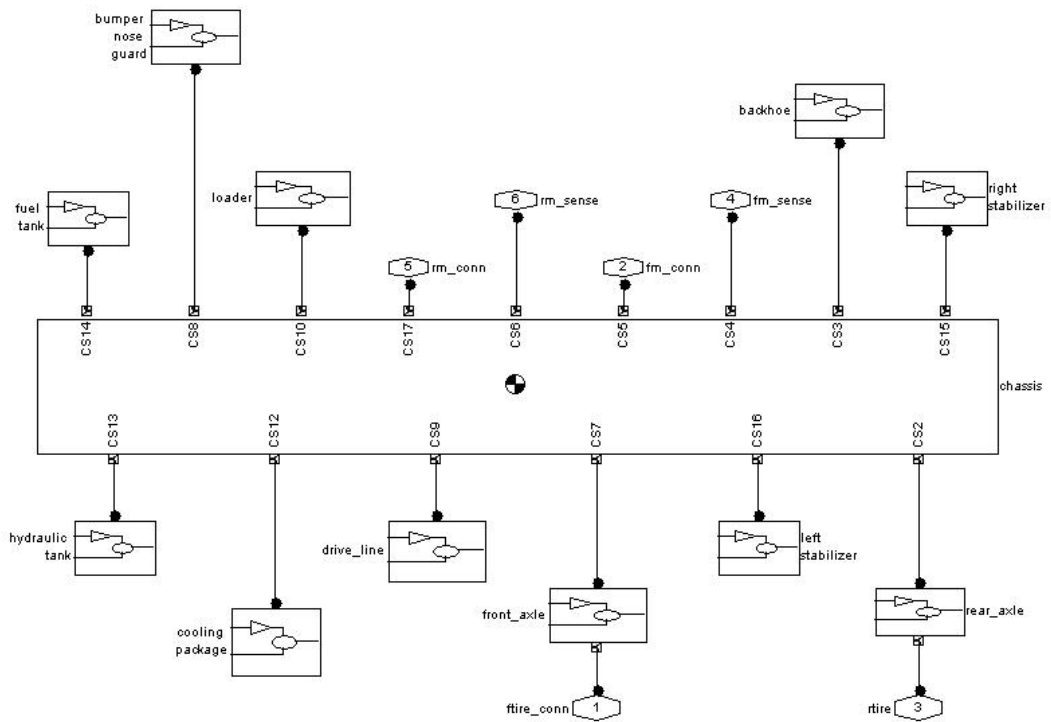


Figure 3.23 – Machine Body Subsystem

For the extended model, “Ground” blocks, which represent the stationary points throughout the simulation, are defined at the connection points of the front and rear

tires with the road surface. “Ground” blocks are defined with respect to the absolute reference frame. Front and rear axles positions are determined with respect to these blocks and the body coordinate systems of the chassis are determined with respect to the axles. “Body” blocks that describe the components assembled to the chassis are rigidly connected to the proper body coordinate system of the chassis defined in SimMechanics. However, the cab is connected to the chassis with “Custom Joint” blocks which represent the mounts. Visualization of the extended model is provided by importing the external graphic files to the “Body” blocks composing the machine body. Importing procedure described for the cab model in Section 3.4.1 is followed in order to obtain accurate model visualization. Visualization of the extended machine model in SimMechanics is demonstrated in Figure 3.24.

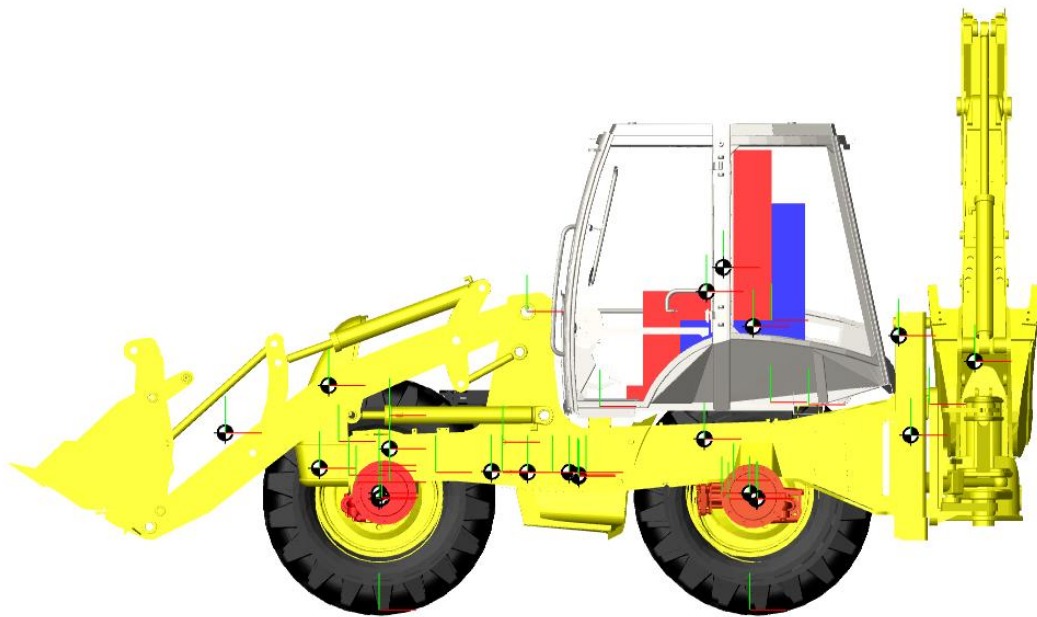


Figure 3.24 – Visualization of the Machine Model in SimMechanics

Similar to the mounts, tires are also defined with the “Custom Joint” blocks positioned between the “Ground” blocks and the axles. These blocks allow angular and vertical motion of the machine body relative to the road surface. Model developed for the whole machine is illustrated in Figure 3.25.

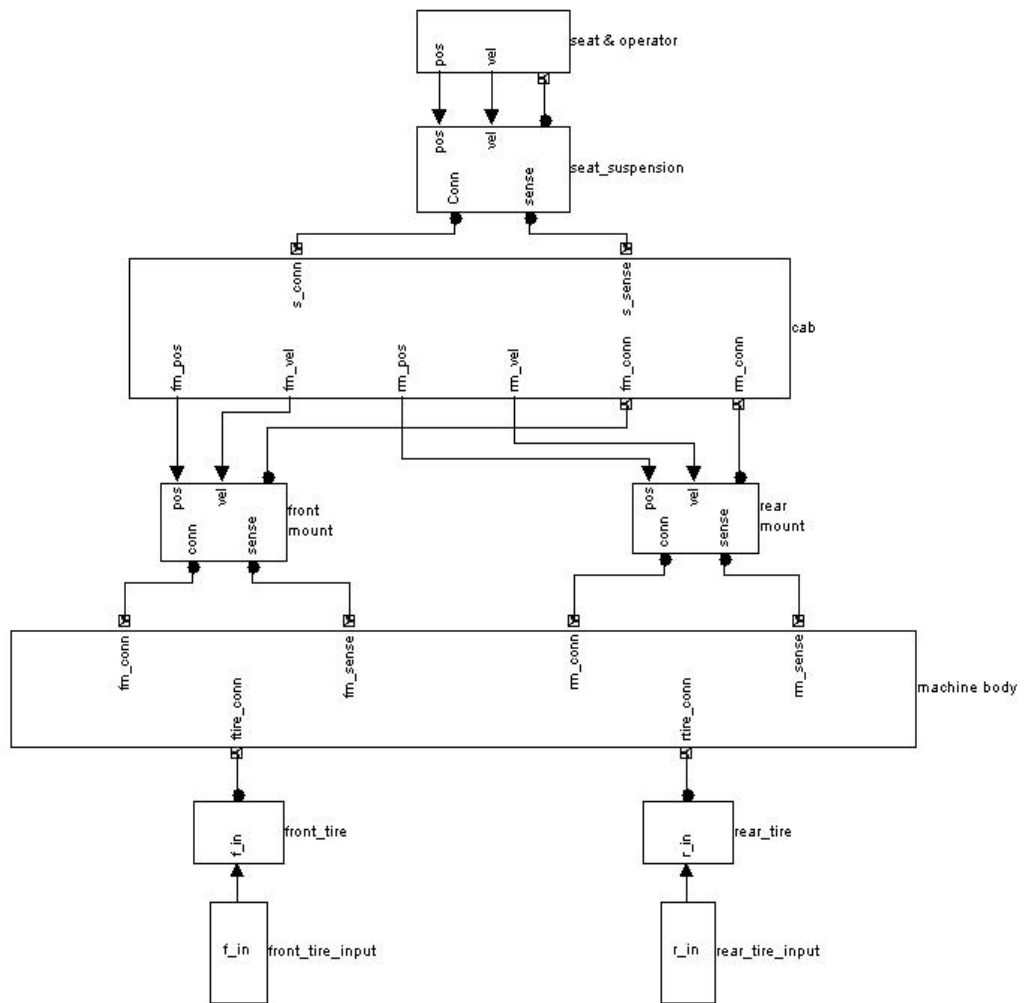


Figure 3.25 – SimMechanics Solution of the Whole Machine

CHAPTER 4

EXPERIMENTAL PROCEDURE FOR THE VALIDATION

For the experimental validation of the cab model and extended machine model, acceleration measurements are taken on a backhoe loader. Measurements are conducted for three different cases, namely,

- Bump test with a 10 km/h forward speed
- Rough road test with 10 km/h forward speed
- Rough road test with 15 km/h forward speed

In the selection of test conditions, the rigidity constraint between the seat and operator is taken into consideration. Test conditions that are not violating the rigid connection assumption between the seat and operator are selected for the validation of the models. In other words, the operator and the seat are required to behave like a single mass in the experiments.

Seat suspension is adjusted to the weight value that is used to identify the seat suspension stiffness and damping before starting the tests. The operator is required to sit in a position that he does not in contact with any part of the cab except the steering wheel during the measurements. The speed of the machine is adjusted with hand throttle and the braking pedal is not used unless it is necessary. Measured parameters to use in the validation process are as follows:

- Vertical acceleration of the front mount connection point of the chassis
- Vertical acceleration of the rear mount connection point of the chassis
- Vertical acceleration of the operator seat

Among these values, accelerations of the front and rear mount connection points are used as the input for the simulation of the cab models and the acceleration value measured from the seat is used for the validation of the models.

In this chapter, firstly, instrumentation used in the measurements is described. Then, measurement points are illustrated. Finally, preliminary data processing performed on the measured sets of data values is explained.

4.1 Instrumentation

LMS SCADAS Mobile data acquisition system is used for the measurements in this study (Figure 4.1). It is a compact data acquisition system with 72 channels. 8 of these channels are dedicated for piezoelectric type sensors. Maximum sampling rate per channel value is 204.8 kHz. Using such a compact data acquisition system is advantageous for gathering simultaneous data and limiting the possible time shifts for synchronization of the data obtained from different measurement points.

Acceleration values are measured with Crossbow LP series capacitive type triaxial accelerometers (Figure 4.2). Acceleration of the mount connection points of the chassis are measured with $\pm 4g$ range accelerometers and acceleration of the seat is measured with a $\pm 10g$ range one. Although, the signal-to-noise ratio of the piezoelectric accelerometers is better, capacitive type accelerometers are preferred due to their ability to measure the frequency range down to 0 Hz or DC. Using capacitive type accelerometers allows to measure low frequency vibrations accurately which is an important issue in comfort analysis.



Figure 4.1 – LMS SCADAS Mobile Data Acquisition System



Figure 4.2 – Crossbow LP Series Triaxial Accelerometer

A special disc is used for the measurement of seat acceleration. It is manufactured according to the dimensions given in BS EN 1032 [24]. The accelerometer is screwed on the sheet plate seen on Figure 4.3 and this plate is mounted to the bottom of the disc with bolts. Moreover, a cable groove is machined on it.



Figure 4.3 – Disc Used for Seat Measurements

4.2 Measurement Points

In the measurements, acceleration values of the front and rear mount connection points of the chassis are measured from one side of the cab. These values are measured to obtain the velocity inputs that are required for the simulation of the cab models. Locations of the accelerometers mounted on the front and rear mount connection points of the chassis are given in Figure 4.4 and Figure 4.5, respectively.



Figure 4.4 – Location of the Accelerometer Used on the Front Mount Connection

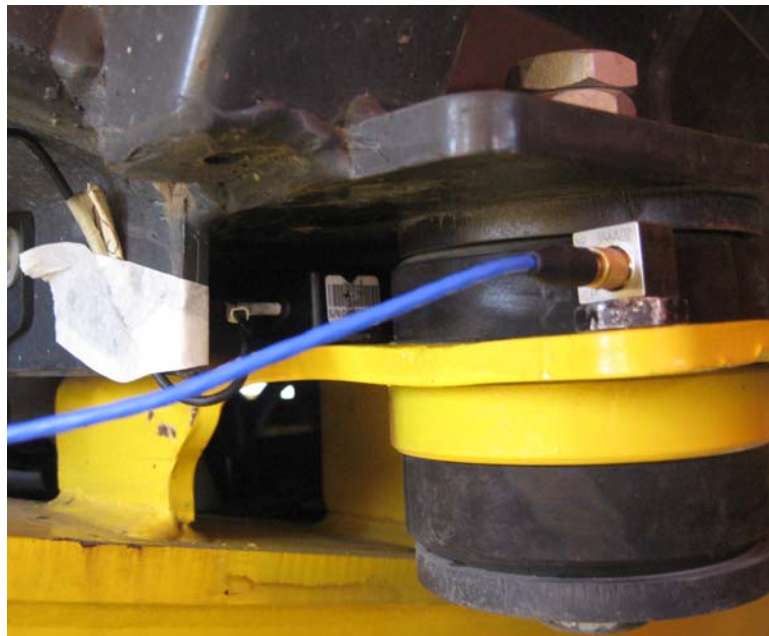


Figure 4.5 - Location of the Accelerometer Used on the Rear Mount Connection

Acceleration of the seat is measured on top of the seat cushion by using the disc described in instrumentation section. Disc is placed on the surface of the seat such that the transducer is located midway between the ischial tuberosities of the seated person [24]. Measurement point for the seat acceleration is shown in Figure 4.6.

In order to connect the accelerometers to the data acquisition system 9 pin connectors are used. Outputs for each measurement direction of the accelerometers, which are transmitted from a single cable, are separated by use of these connectors and recorded into the different channels of the data acquisition system. Installation of the data acquisition system is illustrated in Figure 4.7.



Figure 4.6 –Measurement Point for the Seat Acceleration



Figure 4.7 – Installation of the Data Acquisition System

4.3 Preliminary Data Processing

Velocities of the front and rear mount connection points of the chassis are used as the inputs for the cab models. Velocity values are obtained from the acceleration values measured from these points by integration. Therefore, it is required to process the data to overcome the problems caused by the integration and obtain usable input-output pairs for the simulation. One needs to make sure the signal-to-noise ratio in the data acquisition system to be sufficiently high for reliable results through integration. Signal-to-noise ratio is estimated around 52 dB in the measurements.

As the first step of the data processing, the acceleration values collected with 100 Hz sampling rate are filtered through a low-pass filter. A digital filtration is performed to

decompose the data from high frequency content which is generally not considered in ride comfort studies.

Due to the nature of the capacitive type accelerometers used in the measurements, DC offset is observed in the data. Since this offset causes formation of a linear trend after the integration, it is necessary to remove the offset from the acceleration values of the mount connection points. In addition, offset removal process is applied for the seat acceleration values in order to compare the simulation and measurement results accurately. In this way, initial conditions of the inputs and output are assigned to zero.

CHAPTER 5

COMPARATIVE EVALUTION OF THE CAB MODELS

Comparative evaluation of the analytical and SimMechanics solutions developed for the cab are made by employing the velocity input values obtained for the three different measurement cases. Velocity inputs obtained by integration of the acceleration values of the mount connection points of the chassis are given to the model for each validation case and the corresponding acceleration time histories measured from the seat and obtained from the SimMechanics solution are compared.

Moreover, comparison of the results is done in the frequency domain. In order to make a frequency domain comparison power spectral densities (PSD) of the vertical acceleration values measured from the seat and obtained from the simulations are used. PSD estimations are calculated with 4096 block size, %50 overlap and Hanning window. Frequency domain investigations are done up to 20 Hz with a frequency resolution of 0.2 Hz.

Simulations are done with the ode4 (Runge-Kutta) fixed-step solver. Simulation time is defined according to the each validation case test duration.

The first measurement case is driving through a bump with a 10 km/h forward speed. Before starting the test, engine rotational speed is adjusted with the hand throttle. Machine is started to travel from a certain distance to reach the desired speed before passing over the bump and continued to travel until it slows down after the bump. Velocity inputs, comparison of the acceleration time histories and PSD of the seat accelerations for the first case are shown in Figure 5.1, Figure 5.2, and Figure 5.3, respectively.

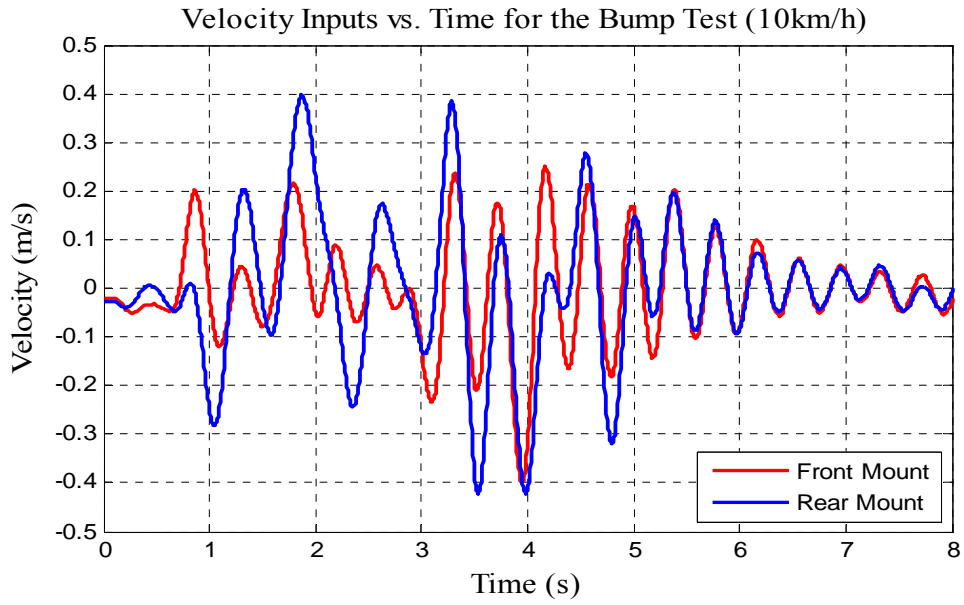


Figure 5.1 – Velocity Inputs for the First Case

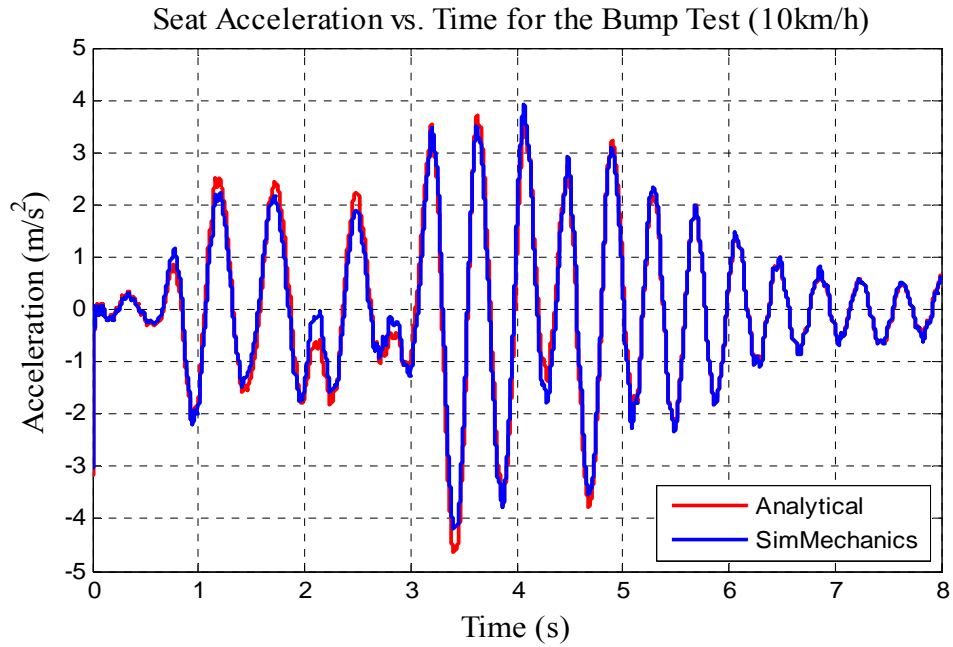


Figure 5.2 – Comparison of Analytical and SimMechanics Solution - (Seat Acceleration Time Histories for the First Case)

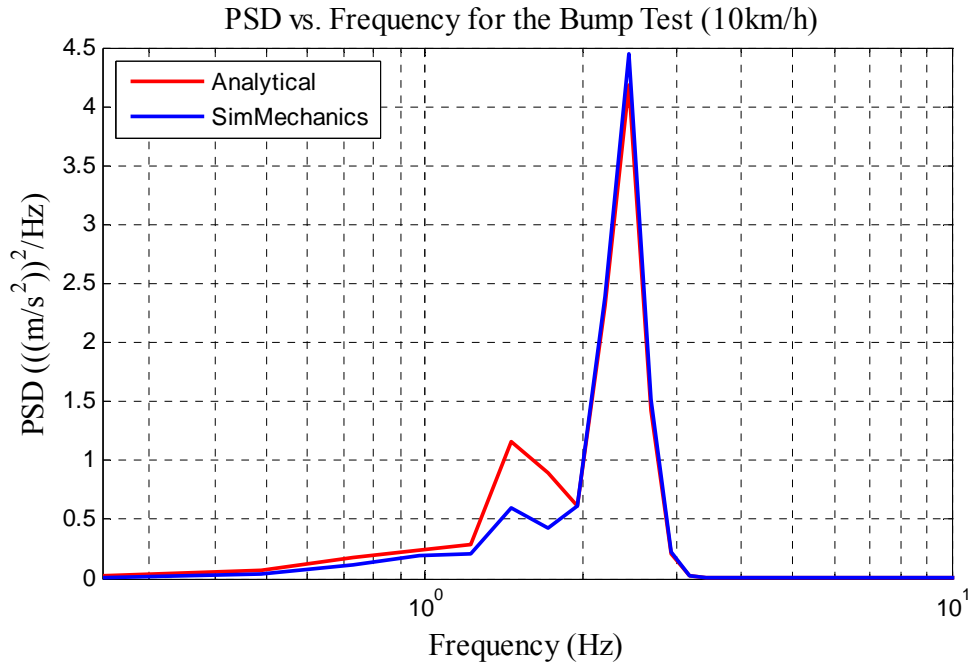


Figure 5.3 – Comparison of Analytical and SimMechanics Solution – (PSD of Seat Acceleration for the First Case)

The second measurement case is the rough road test with 10 km/h forward speed. Measurements are done on a gravel road which generates random excitation on the cab. Velocity inputs, comparison of the acceleration time histories and PSD of the seat accelerations for the second case are presented in Figure 5.4, Figure 5.5, and Figure 5.6, respectively.

The last measurement case is the rough road test with 15km/h forward speed. The same road which is used in the second case is also utilized in this case. However, machine speed is increased from 10km/h to 15km/h to generate different random excitation. In addition, machine is not followed the same path on the road. Therefore, the second and third measurement cases are totally different. Velocity inputs, comparison of the acceleration time histories and PSD of the seat accelerations for the third case are illustrated in Figure 5.7, Figure 5.8, and Figure 5.9, respectively.

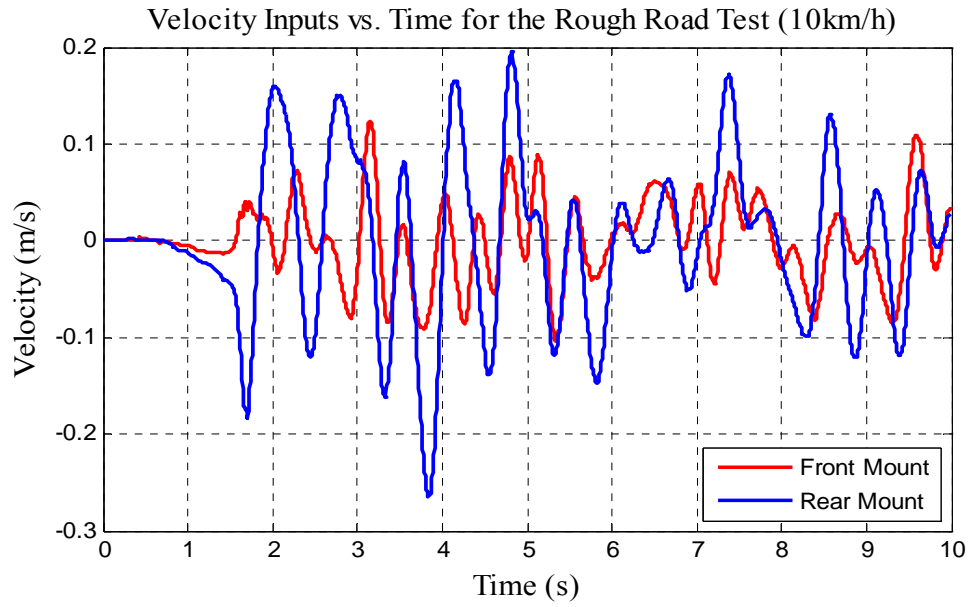


Figure 5.4 - Velocity Inputs for the Second Case

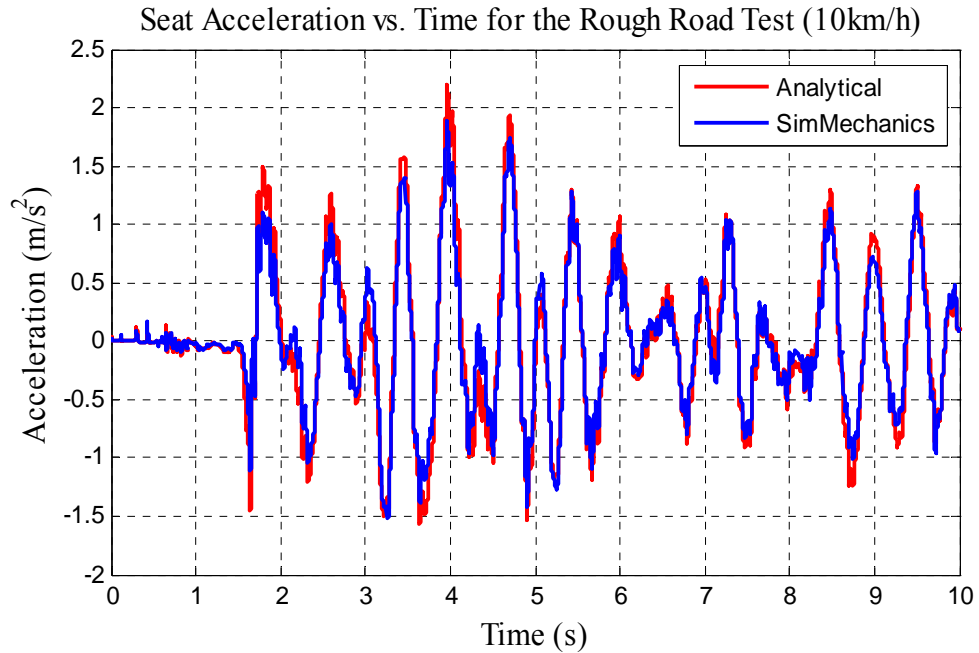


Figure 5.5 - Comparison of Analytical and SimMechanics Solution – (Seat Acceleration Time Histories for the Second Case)

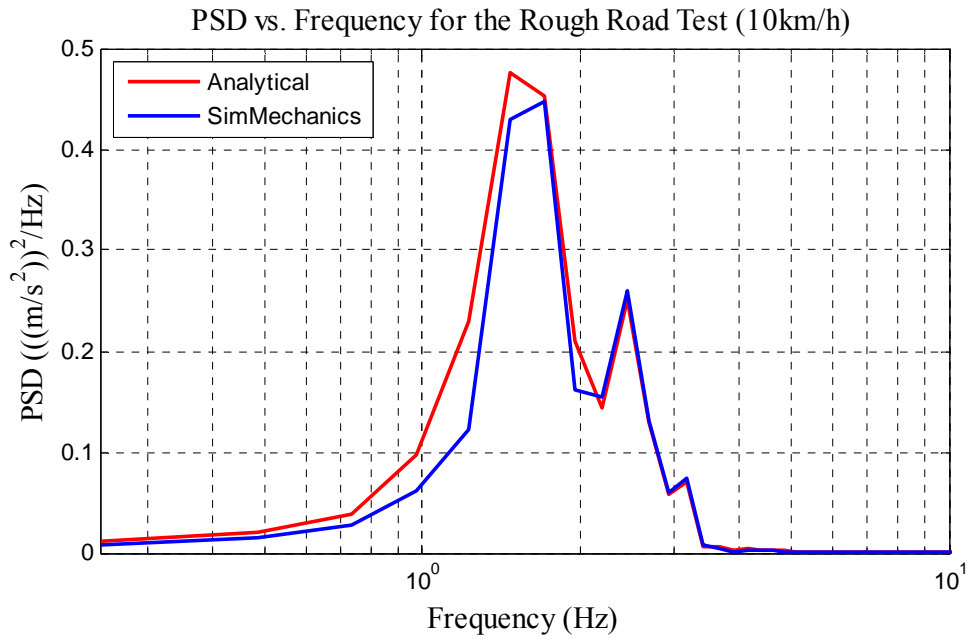


Figure 5.6 - Comparison of Analytical and SimMechanics Solution – (PSD of Seat Acceleration for the Second Case)

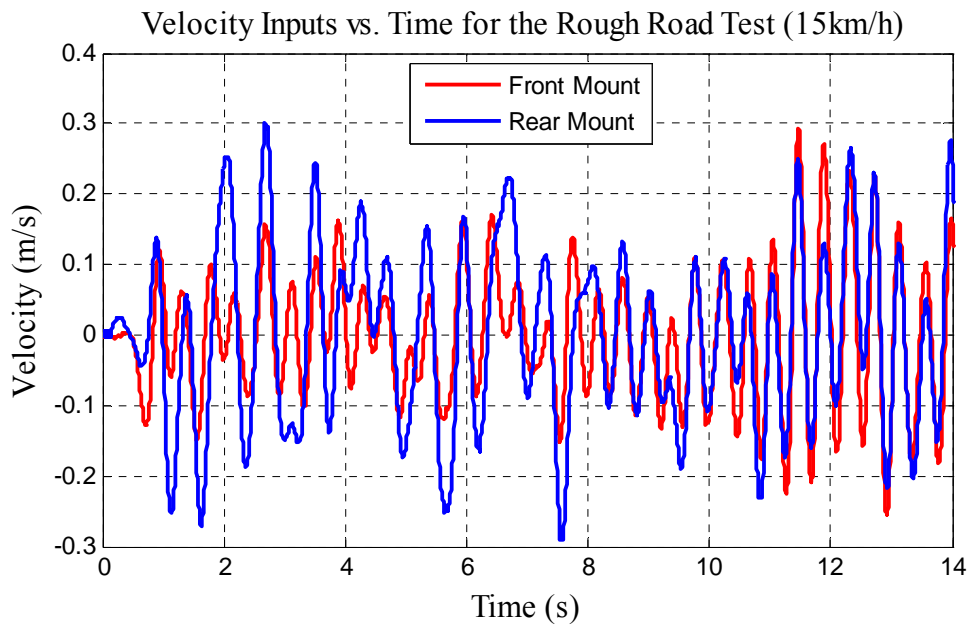


Figure 5.7 - Velocity Inputs for the Third Case

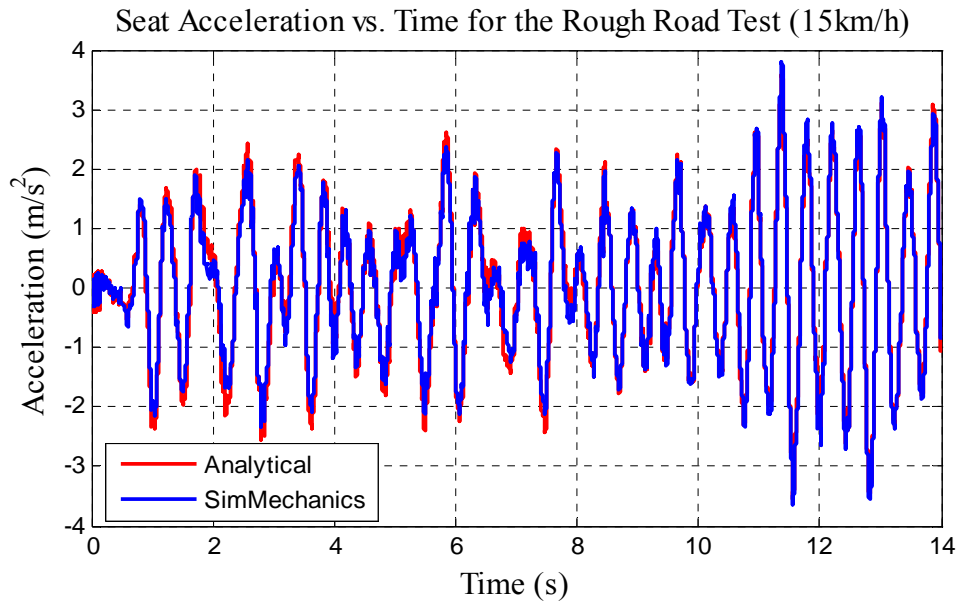


Figure 5.8 - Comparison of Analytical and SimMechanics Solution – (Seat Acceleration Time Histories for the Third Case)

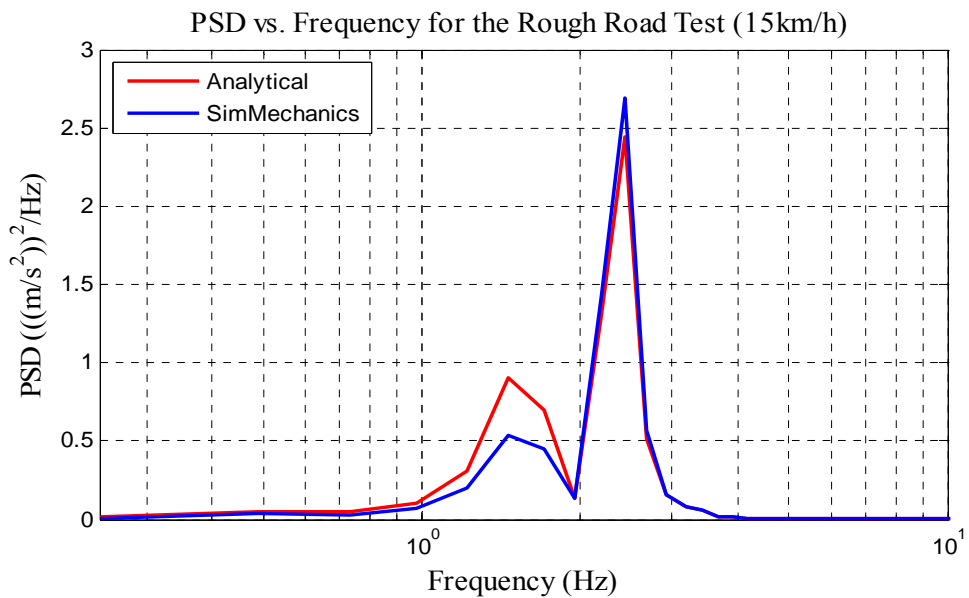


Figure 5.9 - Comparison of Analytical and SimMechanics Solution – (PSD of Seat Acceleration for the Third Case)

Time history and PSD comparisons of the seat accelerations reveals that the both analytical and SimMechanic solutions give similar results for the same inputs. Small deviations on the results may be due to fact that cab is assumed to make small oscillations in the analytical solution. However, this assumption is not valid for the SimMechanics solution.

In addition, comparison of the model results show that developed SimMechanics solution, which uses the physical modeling blocks instead of deriving system equations, will be employed for the simulation of dynamic behaviour of the cab and seat.

CHAPTER 6

RESULTS, DISCUSSION AND CONCLUSIONS

6.1 Comparison of the Measurement and Simulation Results

6.1.1 Comparison for the Cab Model

Physical test results are compared with the simulation results obtained from the cab model. Velocity inputs demonstrated for each measurement case in chapter five are used to simulate the model with the same solver settings. Therefore, inputs are not shown here. Only the acceleration time histories and PSD of the seat acceleration values for the simulations and measurements are given.

PSD estimations are calculated with 1024 block size, %50 overlap and Hanning window. Frequency domain investigations are done up to 20 Hz with a frequency resolution of 0.2 Hz.

Comparison of the measurement and simulation results for the first measurement case is shown in Figure 6.1 and Figure 6.2. For the second case, results are illustrated in Figure 6.3 and Figure 6.4, and they are presented in Figure 6.5 and Figure 6.6 for the third case.

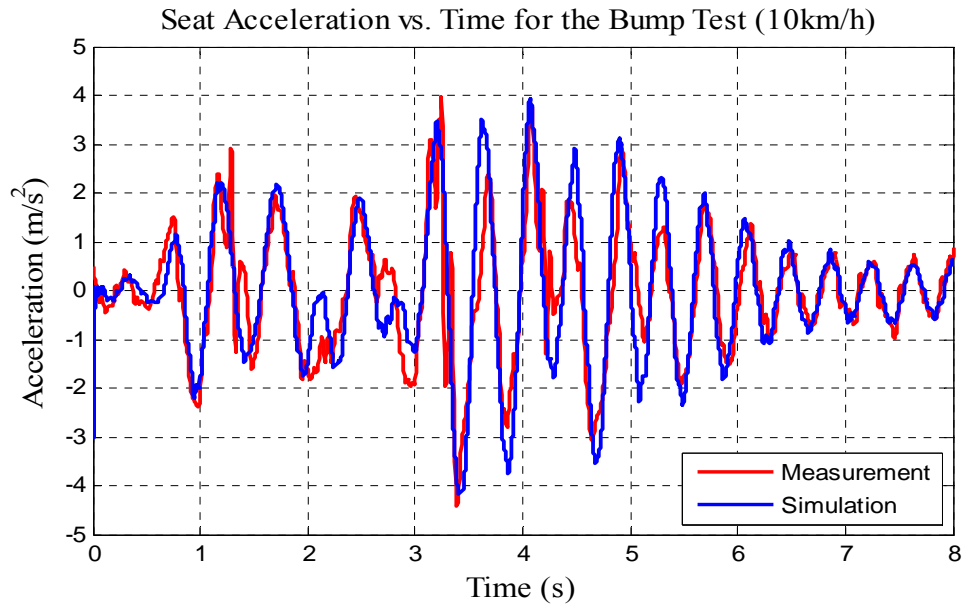


Figure 6.1 - Comparison of Measurement and Simulation – (Seat Acceleration Time Histories for the First Case)

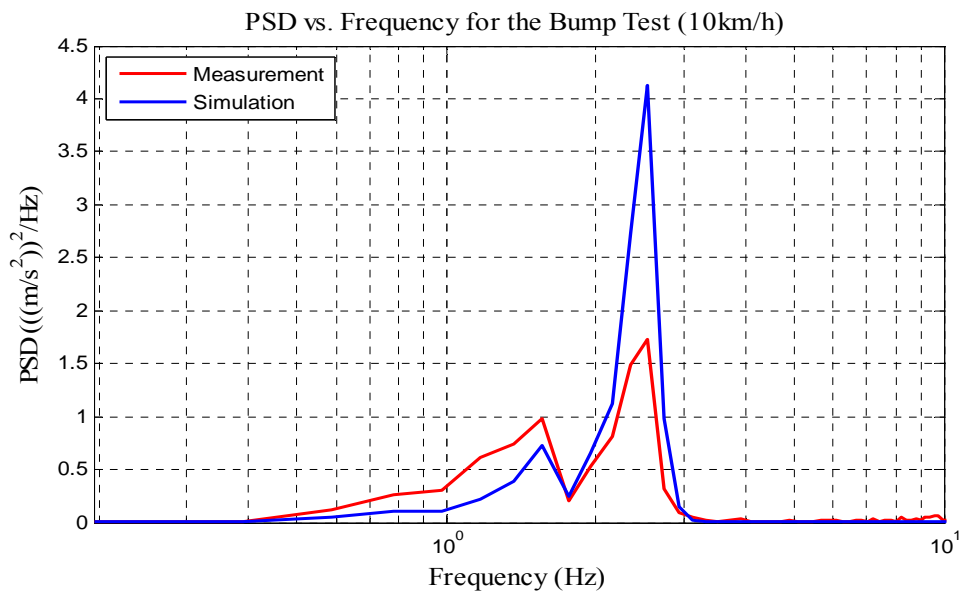


Figure 6.2 - Comparison of Measurement and Simulation – (PSD of Seat Acceleration for the First Case)

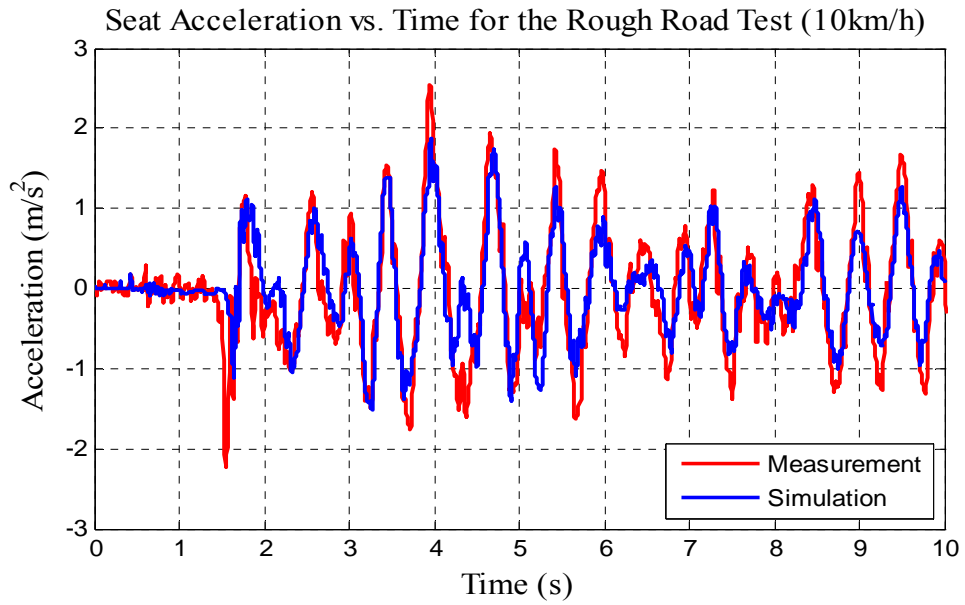


Figure 6.3 - Comparison of Measurement and Simulation – (Seat Acceleration Time Histories for the Second Case)

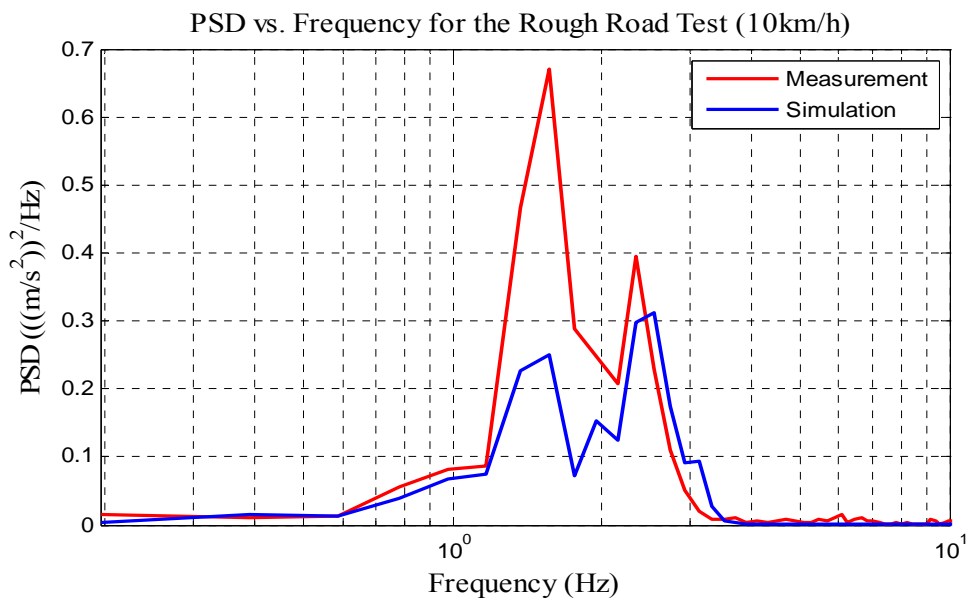


Figure 6.4 - Comparison of Measurement and Simulation – (PSD of Seat Acceleration for the Second Case)

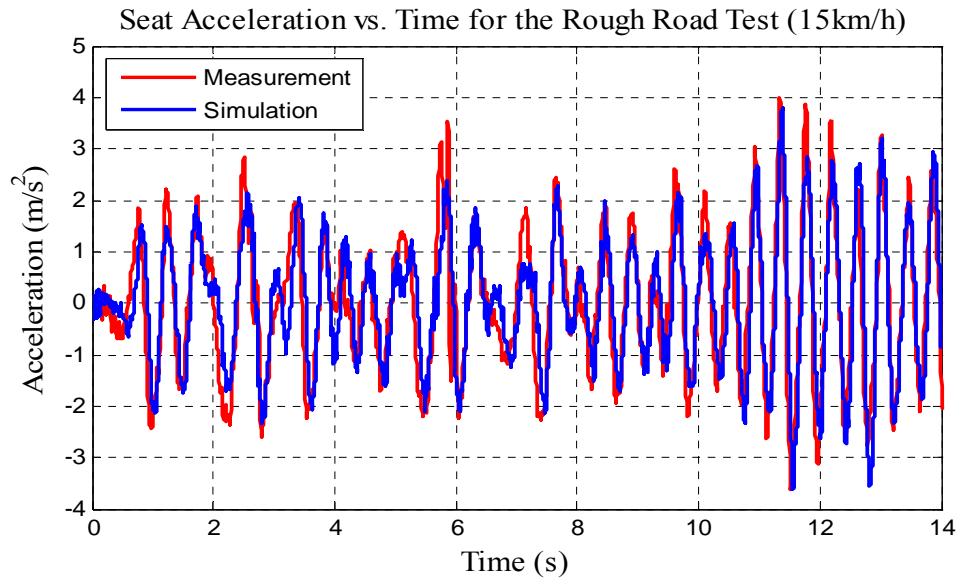


Figure 6.5 - Comparison of Measurement and Simulation – (Seat Acceleration Time Histories for the Third Case)

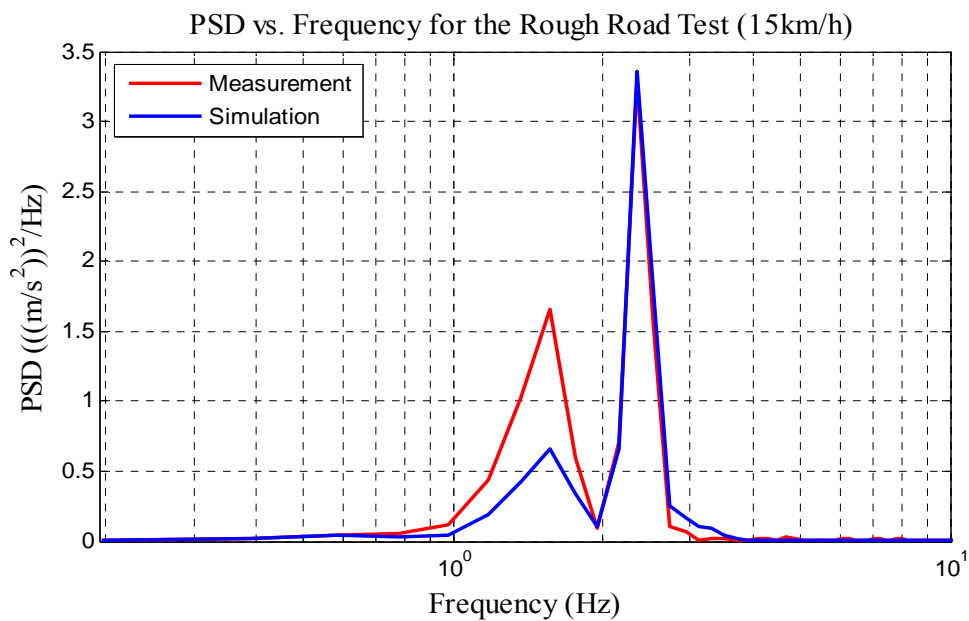


Figure 6.6 - Comparison of Measurement and Simulation – (PSD of Seat Acceleration for the Third Case)

Undamped natural frequencies of the system are calculated as to correspond to approximately 1.0 Hz, 4.5 Hz and 21.7 Hz. The PSD graphs display the peak frequencies approximately at 1.6 Hz and 2.4 Hz. As the system is expected to follow the input, these frequencies can be regarded as excitation frequencies associated with the input. For better explanation of the phenomenon fast Fourier transform (FFT) of the velocity inputs for the third measurement case is illustrated as an example in Figure 6.7.

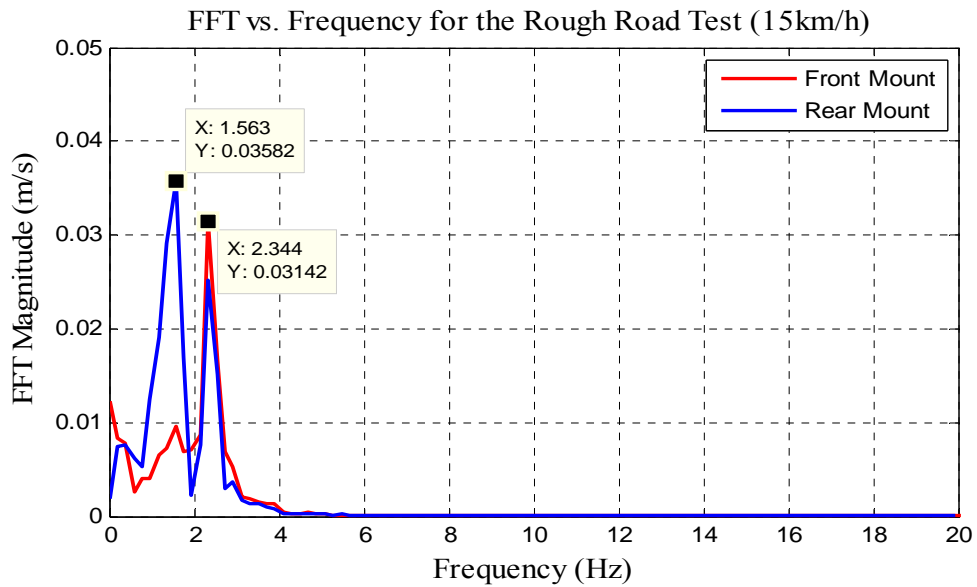


Figure 6.7 – FFT of the Velocity Inputs for the Third Case

6.1.2 Comparison for the Extended Machine Model

Measurement results are compared with the simulation results obtained from the extended machine model for the first measurement case involving drive through a

bump with a 10 km/h forward speed. Position inputs obtained from the bump profile are supplied to the extended machine model for simulation. Position input for the front tire is calculated by dividing the distance of the bump to the machine speed. Since the rear tires start to pass over the bump after a certain time, the input given to the rear tire is acquired by applying a specified delay to the front tire input signal. Amount of delay is estimated by dividing the wheelbase to the machine speed. Position inputs for the front and rear tires are shown in Figure 6.8.

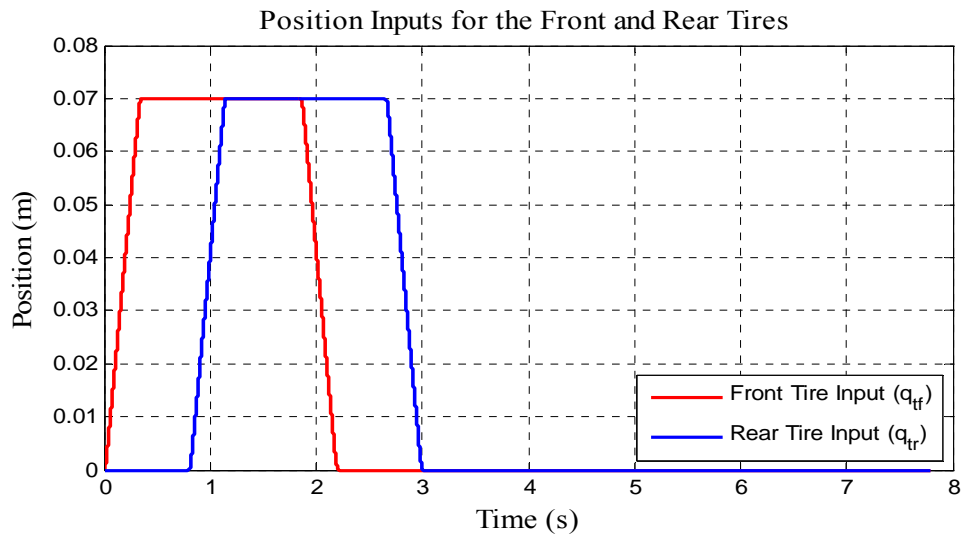


Figure 6.8 – Position Input for the Front and Rear Tires

Acceleration time histories measured from the seat and obtained from the model are compared in Figure 6.9 and comparison of the PSD estimations are illustrated in Figure 6.10.

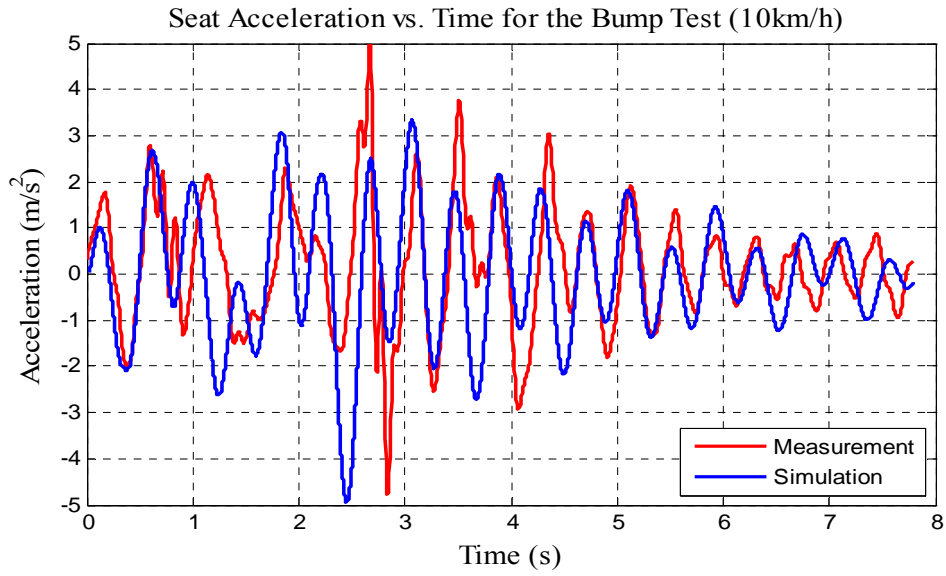


Figure 6.9 - Comparison of Measurement and Simulation for the Extended Machine Model – (Seat Acceleration Time Histories for the Bump Test)

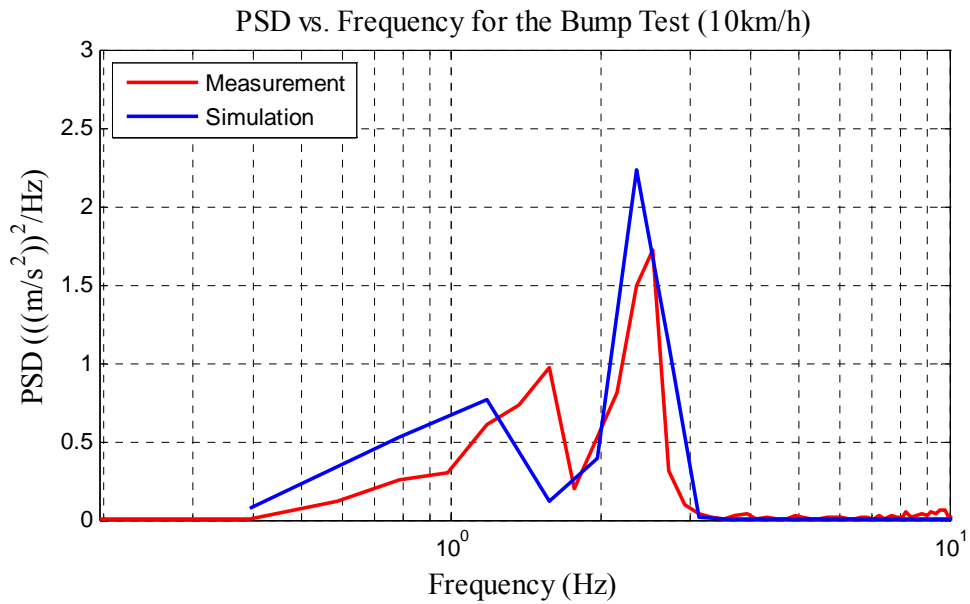


Figure 6.10 - Comparison of Measurement and Simulation for the Extended Machine Model – (PSD of Seat Acceleration for the Bump Test)

6.2 Discussion

Peak frequencies of the PSD estimations for seat accelerations obtained from the extended machine model and cab model for the bump test are demonstrated in detail in Figure 6.11 and Figure 6.12, respectively. It is observed from these PSD graphs that peak frequencies of the simulation and measurement for the cab model exactly match with each other. On the other hand, peak frequencies in the extended machine model are underestimated in simulations. It is anticipated that the possible errors in the identification of the machine body and tire parameters are the main reason for the discrepancy in the peak frequencies of the extended machine model.

PSD estimation of the tire input and the simulated frequency response function (FRF) between front tire input and seat acceleration are illustrated in Figure 6.13 and Figure 6.14, respectively.

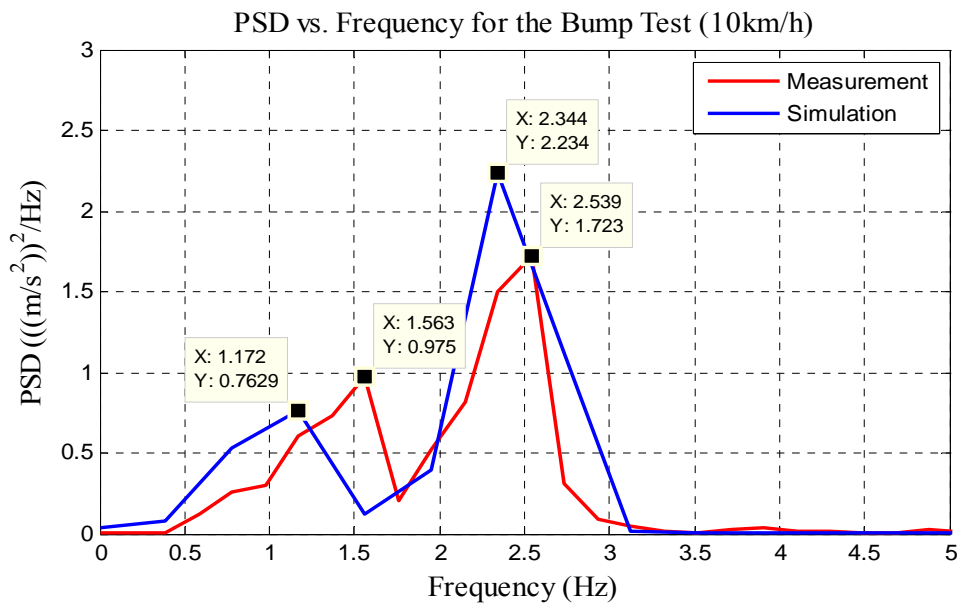


Figure 6.11 - Comparison of Measurement and Simulation for the Extended Machine Model for the Bump Test – (Peak Frequencies of the PSD Estimations)

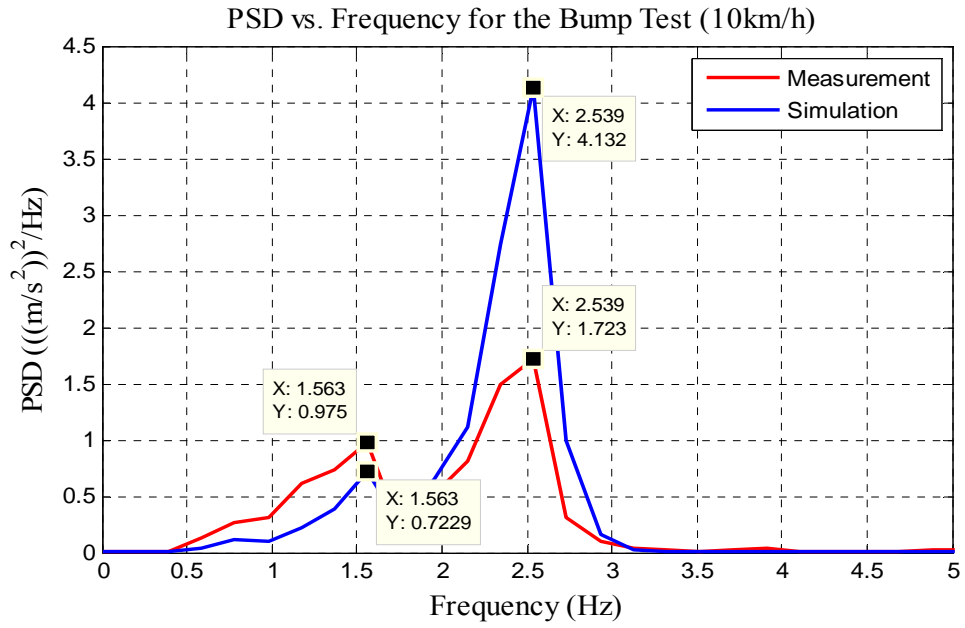


Figure 6.12 - Comparison of Measurement and Simulation for the Cab Model for the Bump Test – (Peak Frequencies of the PSD Estimations)

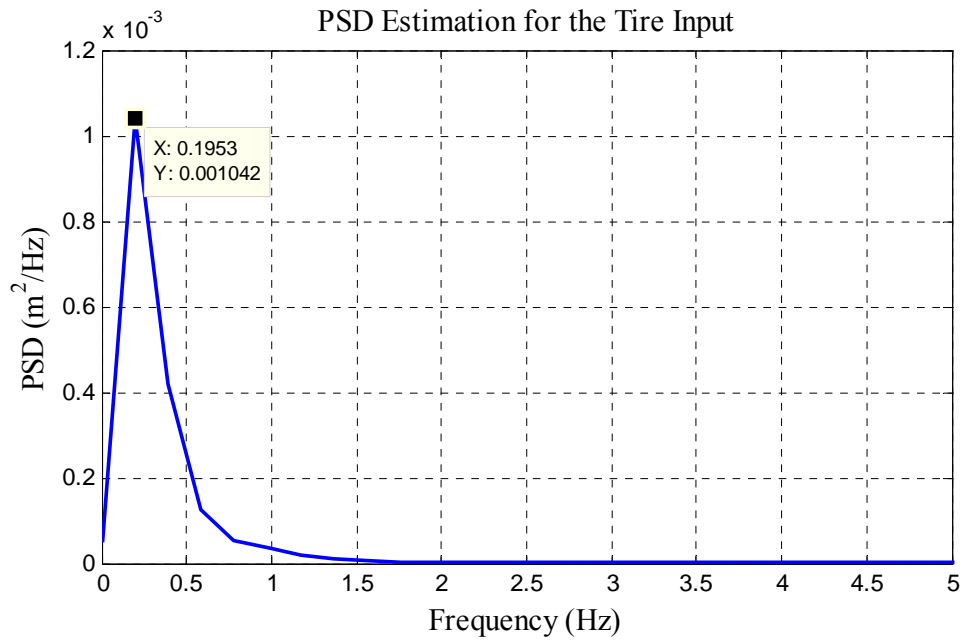


Figure 6.13 – PSD Estimation for the Tire Input

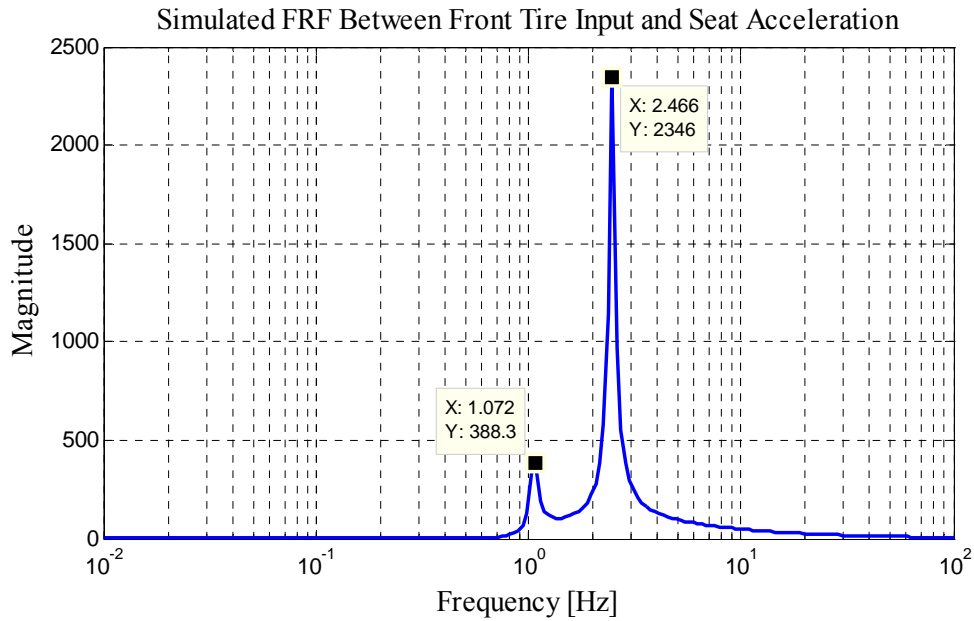


Figure 6.14 – Simulated FRF Between Front Tire Input and Seat Acceleration

It is observed from these PSD and FRF estimations, the fundamental excitation frequency of the bump input lies below resonant frequencies of the extended machine model. However, peak frequencies of the PSD estimations of the measured seat acceleration shown in Figure 6.11 are almost same with the resonant frequencies demonstrated in the simulated FRF function. Presence of the resonant frequencies in the PSD graph is interpreted that the free vibration behaviour of the machine after passing over the bump dominates the frequency content of the response of the seat and operator.

The resonant frequency calculated at 1.1 Hz does not exactly match with the peak frequency displayed at 1.5 Hz in the PSD estimation. This difference is also explained with the uncertainties in the identification procedure of the machine body and tire parameters which are used in the calculation of simulated FRF.

6.3 Summary and Conclusions

In this study, a dynamic model including the cab dynamics is developed to perform the simulation of the ride dynamics of a backhoe-loader. It is aimed to simulate vibration levels transmitted from chassis to the operator accurately and obtain the dynamic forces on the cab and on the machine from the models. Moreover, it is intended to implement a modeling methodology which is similar to the approach used in vehicle dynamics analyses and for use in further ride simulation studies of a backhoe-loader.

Dynamics of the cab is simulated with a planar 3 DOF model and dynamics of the whole machine is simulated with a planar 5 DOF model which is the adaptation of the half-car model used in vehicle ride comfort analyses. Analytical solutions of both systems are described by deriving the system equations and converting them into the state space form. State space solution is implemented into the Simulink environment for the simulation of the analytical solutions.

In addition to the analytical solutions, the cab model and the extended machine model are also constructed by using the physical simulation toolboxes inside SimMechanics.

Linear spring-dashpot units are used to realize the seat suspension, mounts and tires in the models. A methodology is proposed for the identification of the stiffness and damping values of these components in this study. For this purpose, force-displacement behaviour of the seat suspension and mounts obtained from the supplier at a certain velocity are used. Force-deflection tests and drop tests are performed in order to identify the tire parameters. Mass and inertia properties of the rigid parts are also identified by the help of the CAD program ProEngineer and inserted into the cab models.

Validation of the presented models is done by the acceleration measurements performed on the physical machine. Experimental validation process is performed for three cases with different road profiles and machine speeds for the cab model. The procedure is repeated with the bump test for the extended machine model.

Results obtained from the analytical and SimMechanics solution of the cab and results obtained from measurements and simulation of both models are compared separately. Vibration velocities obtained from the acceleration measurements of the front and rear mount connection points of the chassis are given as inputs to the cab models whereas position data obtained from the bump profile are given as inputs to the extended machine model. Acceleration time histories obtained from the seat surface and PSD estimation of these acceleration values are used for the comparison.

In conclusion, comparison of the analytical and SimMechanics solution of the cab show that SimMechanics solution constructed with physical blocks can be used to simulate the ride dynamics instead of deriving the system equations with less effort for the complicated models. In addition, consistency of the measurement and simulation results both in time and frequency domain reveals that the developed linear models can be used for the analyses of ride dynamics of cab and backhoe-loader. Furthermore, it is demonstrated that the free vibration behaviour of the machine after passing over the bump dominates the frequency content of the response of the seat and operator.

6.4 Future Work

For the extension of the present work in future, the following studies can be suggested:

Non-linear component models can be developed for the elastic parts like mounts and seat suspension which are modeled with linear spring-dashpot systems in this study.

Roll model can be added to the developed planar model to simulate the angular motion of the cab relative to the longitudinal axis of the machine for a further study on the cab dynamics.

Parameter identification procedures of the stiffness and damping values can be improved by performing measurements in various conditions for better understanding of the frequency and amplitude dependency of these parameters.

Moreover, identification procedure for the inertial parameters can also be refined and improved by employing more detailed drawings or by direct inertia measurements.

REFERENCES

- [1] SAE J1116 REV. NOV2004: *Categories of Off-Road Self-Propelled Work Machines*.
- [2] ISO 6165:2006: *Earth-moving machinery – Basic types – Identifications and terms and definitions*.
- [3] Scarlett A. J., Stayner R. M., *Whole-Body Vibration on Construction, Mining and Quarrying Machines: Evaluation of Emission and Estimated Exposure Levels*, Research Report 400, Silsoe Research Institute, 2005.
- [4] Directive 2002/44/EC of the European Parliament and of the Council, *on the minimum health and safety requirements regarding the exposure of workers to the risks arising from physical agents (vibration)*, 2002.
- [5] Rehnberg A., *Vehicle Dynamic Analysis of Wheel Loaders with Suspended Axles*, Licentiate thesis presented to Department of Aeronautical and Vehicle Engineering, Royal Institute of Technology, Stockholm, Sweden, 2008.
- [6] Van Boekel J. J. P., *Simmechanics, MapleSim and Dymola: A First Look on Three Multibody Packages*, Bachelor Final Project Report presented to Department of Mechanical Engineering, Technische Universiteit Eindhoven, Eindhoven, 2009.
- [7] De Temmerman J., Deprez K., Anthonis J., Ramon H., *Conceptual Cab Suspension System for a Self-propelled Agricultural Machine, Part 1:*

Development of a Linear Mathematical Model, Biosystems Engineering, 89(4), pp. 409-416, 2004.

- [8] De Temmerman J., Deprez K., Hostens I., Anthonis J., Ramon H., *Conceptual Cab Suspension System for a Self-propelled Agricultural Machine, Part 2: Operator Comfort Optimization*, Biosystems Engineering, 90(3), pp. 271-278, 2005.
- [9] Spelta C., Savaresi S. M., Previdi F., Galli F., Tremolada S., *Modeling and Identification of Vertical Dynamics of an Agricultural Machine*, Control Applications, (CCA) & Intelligent Control, (ISIC), pp. 101-106, 2009 IEEE.
- [10] Ahmed O. B., Goupillon J. F., *Predicting the Ride Vibration of an Agricultural Tractor*, Journal of Terramechanics, 34(1), pp. 1-11, 1997.
- [11] ElMadany M. M., *The Performance of Passive Cab Suspension Systems in Tractor-Semitrailer Vehicles*, Journal of King Saud University, Engineering Sciences, 2(1), 1990.
- [12] Evers W. J. E., Besselink I. J. M., Van der Knaap A. C. M., Nijmeijer H., *Development and Validation of a Modular Simulation Model for Commercial Vehicles*, International Journal of Heavy Vehicle Systems, 16(1-2), pp. 132-153, 2009.
- [13] Karlsson F., Persson A., *Modelling Non-linear Dynamics of Rubber Bushings – Parameter Identification and Validation*, Master's dissertation presented to Division of Structural Mechanics, Lund University, Lund, Sweden, 2003.
- [14] Ledesma R., Ma Z. D., Hulbert G., Wineman A., *A Nonlinear Viscoelastic Bushing Element in Multibody Dynamics*, Journal of Computational Mechanics, 17(5), pp. 287-296, 1996.

- [15] Sjöberg M. M., Kari L., *Non-linear Behavior of a Rubber Isolator System Using Fractional Derivatives*, *Vehicle System Dynamics*, 37(3), pp. 217-236, 2002.
- [16] Garcia M. J., *Engineering Rubber Bushing Stiffness Formulas Including Dynamic Amplitude Dependence*, Licentiate thesis presented to Department of Aeronautical and Vehicle Engineering, Royal Institute of Technology, Stockholm, Sweden, 2006.
- [17] Barber A. J., *Accurate Models for Bushings and Dampers Using the Empirical Dynamics Method*, 14th European ADAMS Users' Conference, Berlin, Germany, 1999.
- [18] Yoo W. S., Baek W. K., Sohn J. H., *A Practical Model for Bushing Components for Vehicle Dynamic Analysis*, *International Journal of Vehicle Design*, 36(4), pp. 345-364, 2004.
- [19] Gunston T. P., Rebelle J., Griffin M. J., *A Comparison of Two Methods of Simulating Seat Suspension Dynamic Performance*, *Journal of Sound and Vibration*, 278, pp. 117-134, 2004.
- [20] Stein G. J., Mucka P., Gunston T. P., *Simulation of Construction Machinery Performance in Realistic Operating Conditions*, *Proceedings of LMS Engineering Simulation Conference*, 2008.
- [21] Maciejewski I., Meyer L., Krzyzynski T., *Modelling and Multi-criteria Optimisation of Passive Seat Suspension Vibro-isolating Properties*, *Journal of Sound and Vibration*, 324, pp. 520-538, 2009.
- [22] Stein G. J., Mucka P., *Theoretical Investigation of a Linear Planar Model of a Passenger Car with Seated People*, *Proceedings of the Institution of*

Mechanical Engineers, Part D: Journal of Automobile Engineering, 217(4), pp. 257-268, 2003.

- [23] ISO 3164:1995: *Earth-moving machinery – Laboratory evaluations of Protective Structures – Specifications for Deflection-limiting Volume.*
- [24] BS EN 1032:2003+A1:2008: *Mechanical Vibration. Testing of Mobile Machinery in order to Determine the Vibration Emission Value.*